The characterization of changes in ground penetrating radar signal due to chloride induced corrosion of reinforcement in concrete

Tešić, Ksenija

Doctoral thesis / Disertacija

2024

Degree Grantor / Ustanova koja je dodijelila akademski / stručni stupanj: **University of Zagreb, Faculty of Civil Engineering / Sveučilište u Zagrebu, Građevinski fakultet**

Permanent link / Trajna poveznica: https://urn.nsk.hr/urn:nbn:hr:237:505235

Rights / Prava: In copyright/Zaštićeno autorskim pravom.

Download date / Datum preuzimanja: **2025-03-14**

Repository / Repozitorij:

Repository of the Faculty of Civil Engineering, University of Zagreb

University of Zagreb
Faculty of Civil Engineering

Ksenija Tešić

THE CHARACTERIZATION OF CHANGES IN GROUND PENETRATING RADAR SIGNAL DUE TO CHLORIDE-INDUCED CORROSION OF REINFORCEMENT IN CONCRETE

DOCTORAL DISSERTATION

Zagreb, 2024

University of Zagreb
Faculty of Civil Engineering

Ksenija Tešić

THE CHARACTERIZATION OF CHANGES IN GROUND PENETRATING RADAR SIGNAL DUE TO CHLORIDE-INDUCED CORROSION OF REINFORCEMENT IN CONCRETE

DOCTORAL DISSERTATION

Supervisors: Assoc. Prof. Ana Baričević, Ph.D.,
Full Prof. Nenad Gucunski, Ph.D.

Zagreb, 2024

Sveučilište u Zagrebu
Građevinski fakultet

Ksenija Tešić

KARAKTERIZACIJA PROMJENE SIGNALA GEORADARA ZBOG KOROZIJE ARMATURE PROUZROČENE KLORIDIMA U BETONU

DOKTORSKI RAD

Mentori: izv. prof. dr. sc. Ana Baričević,
prof. dr. sc. Nenad Gucunski

Zagreb, 2024

Statement of the originality

The work contained in this thesis has not been previously submitted for a degree or diploma at any other higher education institution. To the best of my knowledge and belief, the thesis contains no material previously published or written by another person except where due references are made.

Ksenija Tešić, MSc Civil Engineering

I would like to acknowledge the tenacious and exceptional support of my first mentor, Professor Baricevic, for her tireless guidance and understanding. My special thanks to her for pointing out the unseen directions when needed. I would also like to thank my co-mentor, Professor Gucunski, for his faithful guidance and support during the writing of this dissertation. His exceptional knowledge, as well as his clarity and calmness in imparting the knowledge are greatly appreciated. Finally, I would like to express my deepest gratitude to Professor Serdar for her unwavering dedication to science; her passion has been an exceptional source of inspiration and motivation throughout this journey and her exuberance and positivity is something I will never forget.

I would like to thank my mother Milada, my sister Aleksandra and my Ana for all their patient listening, understanding and encouragement. I would especially like to thank my father Dragan for his incredible commitment – my goal in life is to believe in myself as you believe in me.

Last but foremost, I would like to dedicate this dissertation to my partner Nemanja, who has walked very patiently, gently and tolerantly this journey with me, and to our daughter Kalina, who has brightened our lives.

"In all chaos there is a cosmos, in all disorder a secret order."
C. Jung

Ksenija Tešić

January 2024, Zagreb

Abstract

Corrosion of reinforcement in concrete, associated with consequent cracking, delamination, and spalling, is the greatest threat to the durability of reinforced concrete (RC). Timely detection of corrosion could be achieved using non-destructive testing (NDT) methods, which in turn could minimise, prolong, or avoid the serious consequences of corrosion. Ground penetrating radar (GPR) is proving to be one of the most beneficial NDT methods, especially due to its efficiency and versatility. Research activities in this field have increased, but uncertainties remain regarding the response of GPR in corrosive environments. In particular, the extent and even the sign of the amplitude change due to corrosion products is unresolved. This work addresses the observation and characterisation of GPR signal changes due to chloride-induced corrosion performed in the laboratory and with numerical simulations. It is expected that the findings of this work will contribute to a more accurate and detailed corrosion assessment procedure for RC structures.

Keywords: concrete, chloride-induced corrosion, non-destructive testing (NDT), ground penetrating radar (GPR), signal analysis.

Prošireni sažetak

Uzimajući u obzir potrebu čovječanstva za održivijim razvojem u odnosu na prethodni, racionalnije održavanje armiranobetonskih konstrukcija nameće se neophodnim. Najzahtjevniji problem u održavanju ovih konstrukcija je korozija armature koja uzrokuje pojavu pukotina, raslojavanja i odvajanja zaštitnog sloja betona, što dalje dovodi do narušavanja cjelovitosti konstrukcije i problema sa njezinom nosivošću. Održiviji način kontrole ovog procesa može biti njegovo rano otkrivanje, čime bi popravci bili manje složeni, a ujedno znatno isplativiji. U konačnici, time bi se mogao produžiti uporabni vijek, što je u skladu sa strategijama održivog razvoja.

Georadar je nerazorna metoda ispitivanja koja se temelji na emisiji elektromagnetskih valova u materijal. Informacije o položaju i geometriji objekta dobivaju se na osnovu refleksije valova o objekte koji se promatraju. U ovom radu karakteristike reflektiranog vala od armaturne šipke u betonu korištene su za analizu korozijskog stanja armature. Pregledom literature utvrđeno je da postoje nepoznanice o utjecaju produkata korozije na jačinu, ali i na predznak promjene amplitude vala. Međusobno neslaganje zaključaka pojedinih laboratorijskih istraživanja, zaključeno je, može potjecati od neadekvatnosti postavki eksperimentalnog sustava. Najveći broj provedenih laboratorijskih istraživanja o utjecaju procesa korozije na promjenu signala georadara proveden je na način da je korozija izazvana izlaganjem armaturne šipke vanjskom izvoru struje. U takvim postavkama korišten je elektrolit kako bi se u potpunosti simulirao galvanski članak, a koji je u najvećem broju studija bio takav da su betonski uzorci djelomično uronjeni u njega. To za posljedicu može imati potrošnju armature uslijed korozije na strani šipke koja je okrenuta prema elektrolitu. Ako je ispitivanje georadarom provedeno sa suprotne površine betona u odnosu na onu uronjenu u elektrolit, što je slučaj u većini postojećih radova, to može dati irelevantne rezultate s obzirom da tako nastali produkti korozije ne mogu uzrokovati promjene u jačini signala georadara. Razumijevanje mehanizama koji uzrokuju promjene signala uslijed kompleksnog procesa korozije se može dobiti kroz numeričko modeliranje. Ključno u numeričkom modeliranju jest adekvatan odabir svojstava materijala, uključujući i beton i korozijske produkte. Iako se mali broj studija bavio analizom amplitude signala georadara uslijed korozije armature, niti jedno istraživanje nije uključilo kompleksna dielektrična svojstva korozijskih produkata koja potječu od relaksacijskih mehanizama kojima

su izloženi željezovi oksidi u prisustvu elektromagnetskog polja.

Stoga, hipoteze ovog rada su da 1) parametri kloridima prouzročene korozije – vlaga, kloridi i korozijski produkti – izazivaju mjerljive promjene u amplitudi elektromagnetskog vala reflektiranog od armature u betonu, 2) raspodjela korozijskih produkata u zaštitnom sloju betona utječe na promjene materijala, što utječe na amplitudu elektromagnetskog vala reflektiranog od armature u betonu.

U prvom radu ove disertacije napravljen je pregled relevantne literature na temu procjene stanja korozije pomoću georadara. U radu su detaljno obrađena postojeća laboratorijskih ispitivanja kao i ispitivanja na terenu. Kao takav, rad je poslužio za utvrđivanje glavnih postavki sljedeća tri rada.

Drugi rad ove disertacije bavi se utjecajem različitog položaja elektrolita u ubrzanom procesu korozije na promjenu signala georadara. Laboratorijska ispitivanja provedena su na način da je kod jednog dijela uzoraka strana betona izložena elektrolitu bila suprotna od strane koja je ispitivana georadarom, dok je kod ostatka uzoraka strana izložena elektrolitu ujedno ispitana strana. Zaključak studije je da u prvom slučaju promjena amplitude ne prati jasan trend, te da amplituda uglavnom oscilira oko početne vrijednosti amplitude. Nasuprot tome, u drugom slučaju amplituda se smanjuje sa rastom stupnja korozije. Nakon otvaranja uzoraka po završetku ispitivanja, zaključeno je da se potrošnja metala i migracija korozijskih produkata odvila sa strane šipke okrenutoj prema elektrolitu. To dovodi do toga da se u prvom slučaju korozijski produkti ne mogu detektirati georadarom, dok se u drugom slučaju mogu detektirati što je ujedno uzrok pada amplitude.

U trećem radu promatra se utjecaj tri izolirana parametra korozije uzrokovane kloridima (vlaga, kloridi i produkti korozije) na promjenu jačine signala s ciljem kvantificiranja promjene amplitude izražene u *dB/cm*. Zaključeno je da sva tri izolirana faktora uzrokuju pad amplitude. Konkretno, zaključeno je da koncentracija klorida od 0.6% u odnosu na masu cementa na nivou armature, koja je srednja vrijednost beta raspodjele funkcije "kritične" vrijednosti klorida prema *fib Model Code*, uzrokuje promjenu amplitude od -0.7 *dB/cm*.

Numeričko modeliranje armiranobetonskih uzoraka u korozivnoj sredini provedeno je u četvrtom radu. Modeliranje je provedeno u softveru gprMax koji se temelji na rješavanju Maxwell-ovih diferencijalnih jednadžbi korištenjem principa konačnih razlika u vremenskoj domeni. Numeričkim simulacijama promatran je utjecaj vlage, klorida i produkata korozije. Dielektrična permitivnost betona modelirana je pomoću tzv. modela CRIM, koji na temelju

volumnih udjela heterogenih komponenti materijala i odgovarajućih permitivnosti daje jedinstvenu dielektričnu permitivnost betona. S obzirom da je jedna od sastavnih komponenti betona voda, koja ima disperzivna svojstva, dielektrična permitivnost betona se u konačnici modelira kao kompleksan broj. Također, dielektrična permitivnost proizvoda korozije modelirana je kao kompleksan broj, koji uzima u obzir relaksacijske mehanizme željeznih oksida. Usporedbe radi, provedeno je modeliranje uzoraka gdje su dielektrična svojstva uzeta kao realni brojevi. Nakon usporedbe rezultata numeričkog modeliranja s rezultatima laboratorijskih eksperimentalnih ispitivanja, zaključeno je da dielektrična svojstva treba modelirati kao kompleksna kako bi se dobili relevantni rezultati.

Ključne riječi: *beton, kloridima prouzročena korozija, nerazorna ispitivanja, georadar, analiza signala.*

Notations

Lower-case Latin characters

c	average chloride concentration in concrete cover
c_{crit}	critical chloride concentration
h	height of the concrete at which the pores are filled with corrosion products
m_c	mass of cement
t	time
w	saturation level
w/c	water to cement ratio
w_v	volumetric water content

Upper-case Latin characters

A, A_1	normalised amplitude
A_{35}	specimen stored at 35% r.h
A_c	amplitude in the observed corrosive condition
A_{Cl}	amplitude at a given chloride concentration
A_{CS}	amplitude on the control sample
$A_{DW,air}$	amplitude of the direct wave in air
A_{Dwi}	amplitude of the direct wave
A_i	amplitude of the reflected wave
A_m	amplitude at a given saturation level
A_{ref}	amplitude before the corrosive environment was created
A_s	amplitude in a saturated specimen
B	vector of magnetic flux density
C	label for the group of specimens in which the influence of corrosion products was observed
Cl	label for the group of specimens in which the influence of chlorides was observed
D	vector of electric flux density
E	vector of electric field strength

H	vector of magnetic field strength
J	vector of current density
M	label for the group of specimens in which the influence of moisture was observed
N_C	number of specimens in the *C* specimen group
N_{Cl}	number of specimens in the *Cl* specimen group
N_M	number of specimens in the *M* specimen group
R	receiving antenna
T	transmitting antenna
Q	quartile

Greek characters

Δm	mass loss due to corrosion
ε	dielectric permittivity of material
$\varepsilon_4(\omega)$	complex dielectric permittivity of corrosion products
$\varepsilon_I(\omega)$	complex dielectric permittivity of concrete in which pores are filled with air and pore solution
$\varepsilon_{II}(\omega)$	complex dielectric permittivity of concrete in which pores are 100% filled with corrosion products
$\varepsilon_{III}(\omega)$	complex dielectric permittivity of concrete in which pores are 60% filled with corrosion products
$\varepsilon_{IV}(\omega)$	complex dielectric permittivity of concrete in which pores are 30% filled with corrosion products
ε_r	real dielectric permittivity of concrete
μ	magnetic permeability
ρ	charge density
σ	electrical conductivity of material
Φ	porosity of concrete
ω	angular frequency

Acronyms

CRIM	Complex Refractive Index Model
EM	Electromagnetic
ER	Electrical Resistivity
FDTD	Finite-Difference Time-Domain

FHWA	Federal Highway Administration
GPR	Ground Penetrating Radar
H1	Hypothesis 1
H2	Hypothesis 2
HCP	Half-Cell Potential
IC	Impressed Current
IE	Impact Echo
JIF	Journal Impact Factor
NDT	Non-Destructive Testing
PEC	Perfect Electric Conductor
PR	Polarization Resistance
Q1	Quartile 1
Q2	Quartile 2
Q3	Quartile 3
RABIT	Robotics Assisted Bridge Inspection Tool
RC	Reinforced Concrete
USW	Ultrasonic Surface Waves

List of Tables

List of Figures

Content

Publications included in the thesis

Paper I

K. Tešić, A. Baričević, M. Serdar, Non-Destructive Corrosion Inspection of Reinforced Concrete Using Ground-Penetrating Radar: A Review, Materials (Basel). 14 (2021). https://doi.org/10.3390/ma14040975.

Paper II

K. Tesic, A. Baricevic, M. Serdar, N. Gucunski, Characterization of ground penetrating radar signal during simulated corrosion of concrete reinforcement, Autom. Constr. 143 (2022) 104548. https://doi.org/10.1016/j.autcon.2022.104548.

Paper III

K. Tesic, A. Baricevic, M. Serdar, N. Gucunski, Quantifying the impact of parameters of chloride-induced reinforcement corrosion on the GPR signal, Constr. Build. Mater. 399 (2023) 132594. https://doi.org/10.1016/j.conbuildmat.2023.132594.

Paper IV

K. Tesic, A. Baricevic, M. Serdar, N. Gucunski, Electromagnetic property selection for GPR modelling in corrosive concrete environments, Dev. Built Environ. (2023) 100302. https://doi.org/10.1016/j.dibe.2023.100302.

Chapter 1. Introduction

The 5th paragraph of the 12th Sustainable Development Goal of the United Nations 2030 Agenda [1] states, "By 2030, substantially reduce waste generation through *prevention*, reduction, recycling and reuse." Considering that concrete is the second most consumed material in the world after water [2], the waste generated at the end of the service life of concrete structures is a direct threat to the destruction of our planet. Therefore, one of the global goals of the research community is to extend the service life of concrete structures through certain strategies [3–5] in order to contribute to the well-being of the entire planet Earth. Finally, it is ultimately important to ensure the safety of concrete structures and reduce hazards during their service through maintenance, which is an obligation of the building owners.

1.1. Background

Extending service life could be achieved through *preventive* inspections and *preventive* repair work on concrete structures, rather than through subsequent repairs when deterioration is already advanced. Repeatable, comprehensive, and periodic inspection is attainable using non-destructive testing (NDT) methods.

The main durability concern that jeopardises the service life of reinforced concrete (RC) is the corrosion of the reinforcement [6,7]. Certain environmental conditions can favour the corrosion process. However, one of the harshest environments is chloride-rich, where the trigger of reinforcement corrosion is chloride ions from seawater or de-icing salts. Once the chloride concentration in the reinforcement level reaches a certain value, c_{crit}, sufficient to depassivate the protective steel layer [8,9], the chemical reactions that convert the iron into corrosion products begin [10,11]. Considering the reduced cross-section of the reinforcement and the fact that the corrosion products have a larger volume than the steel [12,13], the corrosion of the reinforcement can significantly affect the load-bearing capacity and lead to deterioration of the concrete, which manifests itself in the form of delamination, cracking and spalling. The duration of corrosion initiation and propagation depends on environmental conditions, concrete durability properties, and design characteristics (e.g., thickness of concrete cover), among other factors; however, appropriate inspections should be performed at regular intervals to control the corrosion process and minimise the need for repair.

The non-destructive testing methods used for corrosion evaluation of reinforcement in RC structures are half-cell potential (HCP) [14], electrical resistivity (ER) [15] and polarization resistance (PR) methods [6]. The main disadvantages of these methods are that they require a connection to the rebar (HCP and PR) or only provide information about the concrete (ER).

For the above reasons, ground penetrating radar (GPR) attracts the attention of civil engineers and researchers for the purpose of structural health assessment [16–25]. It is completely non-destructive and allows the investigation of very large areas in a short time. The GPR is based on the emission of electromagnetic (EM) waves, which fall in the radio wave range, into a structural element and the detection of reflected waves from the layers or objects embedded into material [26–28]. In the corrosion evaluation of reinforcement in RC structures, the wave reflected from the rebar is considered. In particular, the shape and the strength of the reflected wave are analysed to interpret the corrosion condition of the reinforcement.

The shape of the reflected wave changes due to the dispersive properties of the material [29–33]. Namely, due to certain mechanisms occurring in the material in the presence of an electromagnetic field, the frequency spectrum of the original electromagnetic wave changes. This means that, depending on the condition of the material, certain frequency components are attenuated, resulting in a general change in the waveform.

The second quantity that is commonly analysed and is the subject of this thesis, is the strength of the reflected electromagnetic waves. The strength of the reflected wave depends on 1) the reflection coefficient [34] and 2) the condition of the host material [35]. The first reason is related to the fact that the ratio between reflected and transmitted energy depends on the properties of the host material, i.e., the material through which the wave passes, and the material of the reflecting object or layer. The second reason is that electromagnetic waves propagate differently in different materials, and therefore different amounts of energy are lost during propagation.

If one examines chloride-induced corrosion of reinforcement in concrete, one should find different wave strengths in uncorroded and corroded rebar. This is due to both changes in the 1) reflection coefficient – the concrete-rebar interface has changed to concrete-corrosion products-rebar interfaces and 2) condition of the host material – concrete has changed into chloride-contaminated concrete.

In the last two decades, there has been increasing interest in monitoring the corrosion of reinforcing bars using ground penetrating radar, both in laboratory experiments [36–39] and in the field, as a stand-alone technique [21,40–42], or as part of integrated condition procedures in combination with other NDT methods [22,43–51]. However, after reviewing the studies that

investigated corrosion in the laboratory using GPR, it was found that the influence of the corrosive environment on the GPR signal was unresolved. This was the motivation for conducting a study to observe the influence of the entire corrosion process in reinforced concrete on the signal. This was done through both laboratory simulations and numerical modelling to uncover and understand the mechanisms that cause a change in the strength of the electromagnetic waves during chloride-induced corrosion of the reinforcement in concrete, which is also the expected scientific contribution of this work.

1.2. Objectives and hypothesis of the thesis

The overall objective of this research was to understand the behaviour of the change in the strength of electromagnetic waves during the corrosion of reinforcement in concrete. This should be a step towards a method for non-destructive corrosion assessment of RC structures using ground penetrating radar, which will help promote sustainable maintenance practices for RC structures.

The following specific objectives will be pursued:

1) reviewing laboratory and in-situ corrosion assessment studies using GPR and identifying knowledge gaps in the research field,

2) understanding and quantifying the effects of moisture on the change in strength of GPR waves reflected from reinforcement in laboratory simulations and numerical models,

3) understanding and quantifying the effects of chlorides on the change in strength of GPR waves reflected from reinforcement in laboratory simulations and numerical models,

4) understanding and quantifying the effects of corrosion product formation on the change in strength of GPR waves reflected from reinforcement in laboratory simulations and numerical models,

5) and understanding and quantifying the effects of the distribution of corrosion products in chloride-induced corrosion on the change in the strength of GPR waves reflected from the reinforcement in laboratory simulations.

The hypotheses of this doctoral dissertation are summarised in the following Table 1.

Table 1. The hypotheses of this work.

Hypotheses	
H1	The combined effects of corrosion products, moisture, and chlorides in the concrete cover affect measurable changes in the GPR wave reflected from the reinforcement.
H2	The distribution of corrosion products in the concrete cover resulting from corrosion affects material changes, which in turn affect amplitude changes in the GPR wave reflected from the reinforcement.

Table 2 gives an overview of the objectives, the journals and the corresponding category, the Journal Impact Factor (JIF) from the Web of Science database, the CiteScore from the Scopus database, and the quartiles (Q) at the time of publication (or the last available data) and the corresponding papers in this thesis. It is also indicated in which paper a particular hypothesis was investigated.

Table 2. An overview of objectives, journal, JIF/CiteScore, hypotheses and corresponding papers included within this thesis.

Paper	Journal/ Category	JIF (Q)/ CiteScore (Q)	Objectives	Hypothesis
Paper I. Non-Destructive Corrosion Inspection of Reinforced Concrete Using Ground-Penetrating Radar: A Review	Materials/ Materials Science, Multidisciplinary	3.748 (Q3) / 4.7 (Q2)	– reviewing laboratory corrosion assessment studies using GPR – reviewing in-situ corrosion assessment studies using GPR – identifying knowledge gaps in the research field	/
Paper II. Characterization of Ground Penetrating Radar Signal During Simulated Corrosion of Concrete Reinforcement	Automation in Construction/ Civil Engineering	10.3 (Q1) / 16.7 (Q1)	– understanding and quantifying the effects of the distribution of corrosion products in chloride-induced corrosion on the change in the strength of GPR waves reflected from the reinforcement in laboratory simulations	**H2**

Paper III. Quantifying the Impact of Parameters of Chloride-Induced Reinforcement Corrosion on the GPR Signal	Construction and Building Materials/ Civil Engineering	7.4 (Q1) / 12.4 (Q1)	– understanding and quantifying the effects of moisture, chlorides, and corrosion products on the change in strength of GPR waves reflected from reinforcement in laboratory simulations	**H1, H2**
Paper IV. Electromagnetic property selection for GPR modelling in corrosive concrete environments	Developments in the Built Environment/ Civil Engineering	8.2 (Q1) / 8.7 (Q1)	– revealing and understanding mechanisms changing the strength of GPR waves reflected from the reinforcement in numerical simulations due to moisture, chlorides, and corrosion products	**H1**

1.3. Outline of thesis

The thesis is based on the summary of the work and results of four papers, which are appended at the end.

The thesis is divided into several chapters:

- In Chapter 2, the main aspects of the theory of electromagnetic radiation and the fundamentals of ground penetrating radar principles are presented. In addition, Chapter 2 is mainly devoted to the review of studies on the influence of moisture, chlorides, and corrosion on ground penetrating radar. However, a detailed review of studies on the evaluation of corrosion in the laboratory and in-situ using GPR is given in Paper I, so this part is only summarised in Section 2.2.3. Therefore, an overview of the effects of moisture and chlorides on the GPR signal is added in Chapter 2, compared to Paper I. Furthermore, a brief overview of numerical modelling of GPR behaviour in a corrosive environment is given in Section 2.3.

- Chapter 3 contains a summary of the attached work. Section 3.1. presents the main methods, results, and discussions of each paper. The scientific contribution of this thesis is presented in section 3.2.

- Chapter 4 provides concluding remarks on the research conducted as part of this thesis. This chapter provides an overview of the conclusions, recommendations, and future work.

Chapter 2.   Assessment of Chloride-Induced Corrosion of Reinforcement Using GPR

This chapter summarises the studies conducted so far on the influence of the main parameters of chloride-induced corrosion of reinforcement on the changes in the strength of the GPR signal. These parameters are: 1) moisture, 2) chlorides, and 3) corrosion products. However, prior to the review, the underlying theory of electromagnetism and the principles of GPR are introduced to understand the features observed in this thesis. At the end of this chapter, a brief overview of the numerical modelling of corrosion assessment with GPR is given.

2.1. Electromagnetic Theory: Essential Aspects for GPR Signal Analysis

The differential equations describing the behaviour of electromagnetic waves in a homogeneous, isotropic medium are known as Maxwell's equations [35] and are presented in equations 1–4. The constitutive equations (equations 5–7) introduce the influence of material properties into Maxwell's equations.

$$\nabla \times E = -\partial B \big/ \partial t \qquad (1),$$

$$D = \varepsilon \cdot E \qquad (5),$$

$$\nabla \times H = -\partial D \big/ \partial t + J \qquad (2),$$

$$J = \sigma \cdot E \qquad (6),$$

$$\nabla \cdot D = \rho \qquad (3),$$

$$B = \mu \cdot H \qquad (7).$$

$$\nabla \cdot B = 0 \qquad (4),$$

In the above equations, E is the vector of electric field strength, H is the vector of magnetic field strength, B is the vector of magnetic flux density, D is the vector of electric flux density, J is the vector of current density, ρ is the charge density, ε is the dielectric permittivity of

material, σ is the electrical conductivity of material, μ is the magnetic permeability and t is time. The above equations show that the absorption of electromagnetic energy depends on the properties of the material through which the wave propagates. The dielectric permittivity ε is a frequency-dependent complex number [52], that describes the degree of polarisation of material particles in the presence of an electromagnetic field. In other words: when electromagnetic waves encounter the particles, they are displaced at the atomic level, resulting in the formation of dipole moments. When the electromagnetic wave passes, the particles return to their original position. In general, the degree of a material's ability to follow the incident electromagnetic wave in the form of dipole moments is described by the real part of the complex dielectric permittivity. When particles move, some energy is converted to heat because of the interaction of the particles, resulting in energy loss. The rate of loss is described by the imaginary part of the dielectric permittivity. In chloride-induced corrosion, both the real and imaginary parts of the dielectric permittivity depend most strongly on the water content of the concrete.

The electrical conductivity σ describes the degree of free charges in the material that can pass freely under the influence of an electromagnetic field [35]. In chloride-induced corrosion, the conductivity of concrete depends primarily on the amount of dissolved chloride ions in the pore solution.

The magnetic permeability μ describes the rate of magnetic polarisation of a material when exposed to an electromagnetic field [53]. This property is usually neglected when considering the propagation of EM waves in concrete. However, in cases where ferromagnetic materials, such as iron oxides, are the constituents of heterogeneous materials, this property can significantly affect the strength of the EM field [54]. Thus, if corrosion products migrate into concrete pores, this could also affect the strength of the EM field.

Ground penetrating radar is an electromagnetic technology that uses a transmitting antenna (labelled T in Figure 1) to emit waves and a receiving antenna (labelled R in Figure 1) to record the waves reflected from objects or layers. The travel time of the waves is on the order of nanoseconds (ns). When the wave encounters the reflecting surface, some of the energy is reflected and the rest is transmitted further into depth. The amount of reflected energy depends on the contrast between the dielectric permittivity of the host material and the material of the reflecting surface – the higher the contrast, the higher the reflected energy. This is expressed by the reflection coefficient [34]. If the wave encounters metallic objects, such as reinforcement in a concrete element, 100% of the energy is reflected.

The record of the received reflected wave, a so-called A-scan, is shown in Figure 1 on the right. When the transmitting antenna emits electromagnetic waves, a portion of them is transmitted

directly along the shortest path from the transmitting antenna to the receiving antenna. This is called a direct airwave. The second part of the energy is reflected from the air-ground surface and is called a direct ground wave. These two superimpose to form a direct wave (Figure 1). However, this work relies on the analysis of the amplitude of the reflected wave. In the literature, there are many parameters for analysing the reflected wave, such as the amplitude from the negative peak to the positive peak, called the peak-to-peak amplitude. In this work, only the positive peak of the reflected wave is analysed.
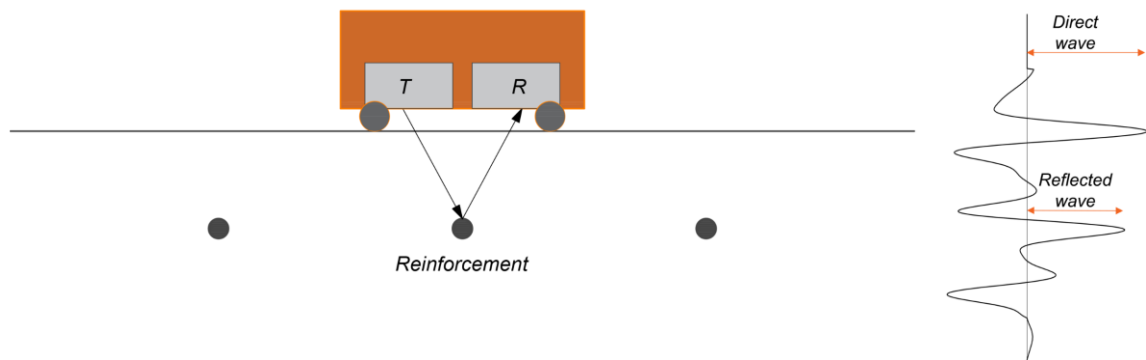
Figure 1. Illustration of ground penetrating radar (left) and the record of received signal (right).

From the above, it could be seen that the strength of the amplitude depends on 1) the reflection coefficient and 2) the material conditions. The objective of this thesis is to quantify the dependence of the strength of the reflected reinforcement wave on the parameters of chloride-induced corrosion. However, it is not based on the exact value of the strength, but rather on the change between the initial reference condition and the second, corrosive condition. First, this is because the excitation source is not uniform among manufacturers and the value of the amplitude in data units is not very meaningful when comparing different GPR devices. Second, when comparing waves reflected from the same object, many amplitude changes are annulled in this way due to normally neglected events, such as geometric imperfections.

Therefore, in this work, all observed effects are quantified in terms of the normalised amplitude A in dB, which is defined as follows:

$$A = 20 \cdot log(\frac{A_c}{A_{ref}})$$
(8),

where A_c is the amplitude of the wave reflected from the reinforcement in data units in the observed corrosive condition, while A_{ref} is the amplitude of the wave reflected from the reinforcement in data units in the reference condition measured before the corrosive environment was created.

The objective of this work is to show the magnitude of the amplitude change from the initial condition because of the mechanisms that occur in the concrete and reinforcement due to chloride-induced corrosion.

2.2. Laboratory assessment

2.2.1. Moisture

Ground penetrating radar is used to determine various water-related parameters in concrete to monitor hydration [55], setting time [56], the effect of curing on the pore system [57], and so on. Several parameters of the GPR signal can be observed to assess the moisture condition of the concrete, namely: amplitude of the direct wave [58–61], amplitude of the reflected wave [58–64], velocity or dielectric permittivity [65–68] in the time domain, or frequency spectra in the frequency domain [29–33,37].

The reason why the direct wave was used for moisture condition analysis is because the reflection coefficient at the air-concrete interface changes with the change in moisture content. This changes the dielectric permittivity of the concrete and thus the amplitude of the direct ground wave. Certain studies [69,70] have recommended the use of the direct wave for analysis because it does not require a specific reflector, such as reinforcement, and is therefore independent of reflector properties. The disadvantage, however, is that it provides information about the concrete moisture near the surface, whereas a more detailed corrosion assessment requires information about the moisture content deeper in the concrete element.

The velocity of the wave propagating from the transmitting antenna to the reflector and then to the receiving antenna is calculated based on the wave travel time. During the formation of dipole moments, the particles exhibit acceleration that leads to the formation of displacement currents [35] that are not in phase with the incident wave. Therefore, the wave is slowed down, and this deceleration increases with increasing moisture content. Since this effect is directly proportional to the polarisation of the material in an electromagnetic field, the velocity and dielectric permittivity are also related. Consequently, the electromagnetic wave velocity and the dielectric permittivity are used to evaluate the moisture content in concrete.

The review of studies on laboratory assessment of moisture using GPR is shown in Table 3.

Table 3. Overview of the studies on the influence of moisture on the GPR signal with the observations of the reflected waves.

Paper	Reflection/ Depth [cm]	w/c	Saturation degree [%]	Volumetric water content [%]	Attenuation formula/Function	Attenuation [dB or -]
Laurent et al. [58]	Slab bottom/7	0.6	15 – 83	-	$A = 20\ log\ (A_i/A_s)$ / -	8.5 – 3
Klysz et al. [59]	Slab bottom/12	0.48	19 – 78	-	$A = A_i/A_{DW,air}$ / $A = -0.0627w_v + 0.9$	0.75 – 0.35
		0.66	20 – 62	-		0.78 – 0.36
Sbartaï et al. [60]	Slab bottom/8	0.5	0 – 100	-	$A = A_i/A_{DW,air}$ / $A = -0.0442w_v + 0.9589$	0.98 – 0.36
		0.6	0 – 100			0.98 – 0.3
		0.7	0 – 100			0.93 – 0.33
		0.78	0 – 100			0.94 – 0.36
Senin et al. [61]	Slab bottom/7	0.7	-	0 – 10.1	$A = 20\ log\ (A_i/A_{CS})$ / $A = -12.695w_v - 11.51$	0 – -9.13
Kaplanvural et al. [71]	Rebar/10	0.48	-	3.91 – 7.2	$A = 20\ log\ (A_{DWi}/A_{RWi})$ / $A = 1.8587w_v^3 - 34.2589w_v^2 + 212.3947w_v - 405.8361$	9.65 – 45.55
Hugenschmidt et al. [63]	Slab bottom/8	0.5	35 – 90*	-	$A = A_i/A_{35}$	1 – 0.76

Note: A_i – amplitude of the reflected wave, A_s – amplitude in a saturated specimen, $A_{DW,air}$ – amplitude of direct wave in air, A_{CS} – amplitude on control sample, A_{DWi} – amplitude of direct wave, A_{35} – specimen stored at 35% r.h, w_v – volumetric water content (%).

* – the relative humidity of the storage chamber instead of saturation degree.

The increase in moisture content of concrete affects the decrease in amplitude. In most studies, a linear trend of the dependence of attenuation on moisture content is observed.

The conclusion after reviewing the studies on the effect of moisture on the change in the strength of the reflected wave is that most of the studies (except [71]), observed the reflection from the bottom of the slab, which indicates the lack of studies that investigated the reflection

from the reinforcement. The objective of this thesis is to evaluate the moisture content as a general method to evaluate corrosion.

2.2.2. Chlorides

Table 4 provides an overview of studies quantifying changes in the amplitude of the direct or reflected wave due to chlorides.

Table 4. Overview of the studies on the influence of chlorides on the GPR signal with the observations of the direct or reflected waves.

Paper	Reflection/ Depth [cm]	Saturation degree [%]	Volumetric water content [%]	Chloride content [g/l]	Chloride content [% of m_c]	Attenuation formula	Attenuation [dB or -]
Sbartaï et al. [69]	Direct wave	100	-	10	-	$A = -20\ log\ (A_{DW,i}/A_{DW,air})$	10.6 – 11
				20			10.2 – 11.9
				30			11.6 – 12.1
				40			11.7 – 13.4
				50			12.3 – 12.8
				60			12.8 – 14.2
Hugenschmidt et al. [63]	Slab bottom/8	35 – 90*	-	-	0.4 and 1	$A = A_i/A_0$	0.68 – 0.86
Senin et al. [61]	Slab bottom/7	1.7 – 10.1	-	10	-	$A = 20\ log\ (A_i/A_{CS})$	-2.4 – -9.13
		0 – 9.3		20			-6.87 – -10.39
		0 – 12.1		30			0.37 – -20.04
		0 – 9		40			-0.2 – -25.46
		5.5 – 10.2		50			-20.48 – -28

Note: $A_{DW,i}$ – amplitude of the direct wave, A_i – amplitude of the reflected wave, $A_{DW,air}$ – amplitude of direct wave in the air, A_{CS} – amplitude on control sample, A_0 – amplitude of reflected wave in the specimen without chlorides.

* – the relative humidity of the storage chamber instead of saturation degree.

After reviewing the studies, it was concluded that the only parameter observed was the change in the strength of the direct [69] or reflected wave from the bottom of the slab [61,63]. In [72],

the authors concluded that the wave velocity was more sensitive to moisture content than to chloride content. This was explained by a slight change in the real part of the dielectric permittivity due to the presence of chlorides, which does not further change the wave velocity. On the other hand, the chlorides affect the increase in conductivity, resulting in a loss of energy, which is manifested in a decrease in amplitude.

The effect of chlorides on electromagnetic properties is more pronounced the higher the moisture content, in contrast to dry conditions where this effect is insignificant [72]. Under dry conditions, the chlorides in the concrete pores are mainly in crystalline form, in contrast to the case where moisture is present in the pores and the chlorides are dissolved and in ionic form. Moreover, in [73], the effect of chlorides was compared with the effect of porosity and saturation of the specimens. It was shown that the GPR signal amplitude is the most sensitive to the chloride content. Similarly, in [61], the authors concluded that the amplitude is more attenuated by chlorides than by moisture.

2.2.3. Corrosion

Most of the unknowns in corrosion assessment using GPR arise from the influence of the corrosion products on the signal change. A clear answer to the question of whether corrosion products in concrete increase or decrease the strength of the electromagnetic field cannot yet be found in the existing literature. Table 5 gives an overview of the studies in which this phenomenon has been investigated in laboratory tests.

The inconsistency in the available literature could be due to a variety of reasons, the most important being inadequate experimental design. The inadequacy of the experimental design is evident in the physical conditions of the experiment and in the duration of the experiments. The first reason concerns the technique of accelerated corrosion testing. Namely, in most of the studies, the impressed current (IC) technique was used [36–38,74–79]. In most of the studies [37,38,75,76,78,79], sodium chloride solution was used as the electrolyte, while in the remaining studies, the tests were conducted under dry [36] or water-wetted conditions [74]. When sodium chloride is used as an electrolyte, it is of great importance to control or monitor the water and chloride concentration when the effects of corrosion products on the GPR signal are observed. In these cases, the environmental conditions prevent the isolation of the effects of corrosion products on the change in wave amplitude.

On the other hand, if the test is performed under dry conditions with IC, the specimens very often show extensive damage due to a sudden accumulation of corrosion products around the

rebar [80]. In this case, there is no change in the concrete as a material compared to the real scenario of corrosion of the reinforcement in concrete structures. This is more pronounced the higher the current used in IC and the shorter the time of the accelerated corrosion process [81]. However, the main drawback of the conducted experiments reported in the existing literature is the position of the electrolyte during the accelerated corrosion process. Namely, the specimens were immersed in a container of an electrolyte so that the exposed surface of the concrete specimen was the opposite one that was investigated with GPR. In this case, the onset of corrosion and thus the migration of the concrete products into the concrete pores takes place in the area where GPR could not detect the corrosion products [10] because the reinforcement blocks the penetration of the signal.

Table 5. Overview of the studies on the influence of corrosion products on the GPR signal (Original table was presented in Paper I).

Paper	Reflection	Depth [cm]	Trend of amplitude change
Hubbard et al. [74]		1.9 and 3.8	↓
Lai et al. [38]		2.5 and 7.5	↑
Hong et al. [77]		4.5 and 9	↑
Hong et al. [37]		7	↑
Zaki et al. [76]		7	↑↓
Raju et al. [75]	Rebar	2.5 and 5	↑
Wong et al. [36]		6	↑↓
Sossa et al. [82]		8 and 7	↓
Liu et al. [78]		3	↑
Zatar et al. [83]		6.4	↓
Fornasari et al. [79]		3	↑

Note: Cells shaded in grey are added compared to the Table in Paper I.

For the reasons explained in the previous sections, there is a lack of research to quantify the effects of corrosion products on the change in amplitude of waves reflected from reinforcement in concrete.

2.3.Numerical modelling

Numerical simulations of GPR signal propagation are mainly concerned with analysing the polarity, shape or velocity of the waves reflected from the modelled targets [84–92]. Thus, few studies have modelled concrete to observe the change in electromagnetic field strength due to a corrosive environment [93–96].

The essential thing in the analysis is the correct analysis of the materials, i.e., in the case of chloride-induced corrosion, the concrete containing moisture, chlorides and corrosion products in the pores, and the corroded reinforcement. There are numerous theoretical and empirical models of the electromagnetic properties of concrete [52,97–102], mainly dedicated to describing the frequency-dependent dielectric permittivity of concrete. Those include the influence of moisture and chlorides and their respective properties. However, there is insufficient research with the inclusion of the dispersive properties in numerical simulation, and to the author's knowledge, there is no research that included the complex, frequency-dependent properties of corrosion products in concrete in the analysis of electromagnetic field strength.

2.4. Identified knowledge gaps

In this brief overview of the studies, particular gaps in the research have been acknowledged. These are summarised in Table 6, together with the reference to the paper containing the study on the particular gap.

Table 6. Identified knowledge gaps from the literature review.

	Identified knowledge gap	Paper that considered the knowledge gap
1)	No review article on corrosion assessment with GPR	Paper I
2)	Inappropriate experimental design of the electrolyte in IC technique	Paper II
3)	The ambiguity about the trend of GPR amplitude change due to corrosion products	Papers II and III
4)	The lack of quantification of the amplitude change due to corrosion products	Paper III
5)	Modelling the properties of concrete and corrosion products as complex, frequency-dependent functions	Paper IV

Chapter 3.   Selected Results and Discussion

Section 3.1 summarises the methods and the most important results of the individual papers, while section 3.2 presents the contributions of the papers in the context of the thesis as a whole.

3.1. Discussion

The **existing reviews** on the condition assessment of reinforced concrete structures using GPR **focused** either **on a general overview** of the applications of GPR in construction [103,104] with a brief critique of corrosion assessment, **or** as part of a **review of** the general **use of NDT** methods [105]. The above studies did not include a comprehensive review of a specific topic – corrosion assessment of reinforcement in concrete using GPR (corresponding to **knowledge gap 1**). Therefore, the main objective of **Paper I** was to review all relevant work on laboratory and on-site inspection of reinforced concrete using GPR, with particular emphasis on the methods used to create a corrosive environment (laboratory studies), the methods used to analyse the results and comparison with other non-destructive techniques (on-site studies).

The relevant studies were searched in the Web of Science [106] and Scopus [107] databases. Studies included in the review were made between 1 January 2000 and 30 October 2020. The combination of the following terms was used to identify studies: – [(*ground penetrating radar* OR *GPR*) AND (*corrosion* OR *deterioration*) AND (*concrete*)]. After removing non-applicable, inaccessible, non-English, and duplicate papers, a total of 69 studies were finally included in the review analysis.

A summary of the work carried out to assess corrosion by GPR on concrete specimens produced and tested under laboratory conditions was summarised in a table similar to Table 4 of the present thesis. These were arranged according to the techniques used for the accelerated corrosion test, the methods used to acquire the GPR attributes, the current density, the dimensions of the specimens and the central frequencies of the GPR. The conclusion was that different results were reported on the trend of amplitude change due to corrosion products. In the studies where the amplitude was monitored during the accelerated corrosion process, it was reported that the amplitude increases with time and then decreases when the crack becomes "wide" [36].

The on-site investigations were predominantly carried out on the territory of the United States, probably due to the existence of relevant standards [108] that regulate the procedure for the inspection of asphaltic concrete bridge decks with GPR.

According to this standard, on-site inspections are based on the identification of zones of high attenuation indicating *deterioration* of the concrete. Deterioration is understood to be the ingress of moisture, chlorides, the formation of corrosion products, cracking, and delamination. This means that the on-site investigations do not directly mean the identification of the loss of mass of the reinforcement, but rather the identification of the corrosive agents, chlorides and moisture, and the consequences of the ongoing corrosion process, corrosion products, cracks, and delamination.

Qualitative or quantitative characterisation of corrosion based on GPR results relied on numerical analysis of GPR signal attributes or visual analysis of B-scans. In particular, the numerical analyses were based on equation 8 of this paper, where different reference amplitudes can be used: constant direct wave [109], varying direct wave [110], and arbitrary constant amplitude [111]. Some authors argued that observation and numerical analysis of the whole waveform are more appropriate instead of the specific amplitude [20,21]. In the numerical analyses, the thresholds indicating corrosion were derived based on the comparison with other NDT methods and their already established thresholds [112,113].

Visual analyses of B-scans [42,43,114], or combined visual and numerical analyses [25] mean that an analyst reviews the GPR B-scans, considering reflections from the reinforcement and concrete surfaces, and marks the boundaries of the damaged areas. This has the advantage over numerical analyses of detecting areas with disturbed signals due to geometric imperfections – different concrete cover thicknesses or reinforcement spacing, surface anomalies – that numerical analyses could not recognise.

Ground penetrating radar was often used in combination with other NDT methods to complement the results and compensate for the shortcomings of each other. One such achievement is the Robotics Assisted Bridge Inspection Tool (RABIT) [115,116], a robotic platform developed under the US Federal Highway Administration (FHWA) Long Term Bridge Performance programme. The robot is equipped with a GPR array with a total of 32 antennas. The GPR results are combined with electrical resistivity, impact echo (IE) and ultrasonic surface waves (USW) to provide a condition assessment of the concrete bridge decks throughout their service life.

In summary, the **conclusion** of **Paper I** was that **laboratory tests lead to opposite conclusions regarding the effects of corrosion products** and further research should be conducted to

increase knowledge in this field. On the other hand, ground penetrating radar showed promising performance in field investigations, especially when the analysis of the results is supported and combined with the results of other non-destructive techniques.

Most studies that investigated corrosion of reinforcement in the laboratory **used the IC** technique to accelerate corrosion and **placed the electrolyte to the surface opposite to that investigated with GPR** [37,38,75,76,78]. According to the [10], this leads to an accumulation of corrosion products on the side of the reinforcement that cannot be reached by the GPR signal. This is consistent with **knowledge gap 2**, Table 6.

The main objective of **Paper II** was to find out how different corrosion patterns caused by different positions of the electrolyte in the IC technique affect the amplitude of the GPR signal. For this purpose, two experimental setups were prepared that differ in the position of the electrolyte. The methodology is briefly explained in Figure 2.
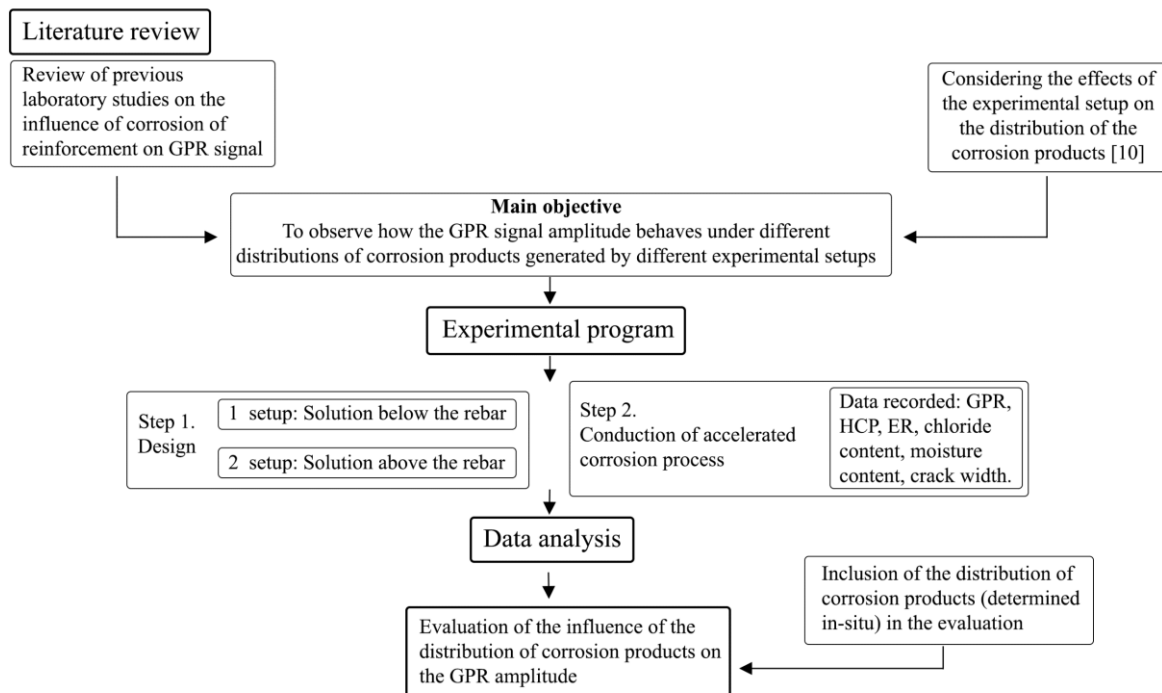

Figure 2. The research methodology (originally presented in Paper II).

The concrete specimens had dimensions 700 mm x 300 mm x 250 mm, with two reinforcing bars (20 mm diameter and 400 mm length) spaced 200 mm apart, which had a concrete cover of 50 mm. In the first experimental setup, the sodium chloride solution, which served as the electrolyte, was below the reinforcement level during the accelerated corrosion process. In the second experimental setup, however, the electrolyte was in a container above the concrete

specimens. In both setups, three specimens with different degrees of corrosion were produced. The specimens were exposed to the external current for up to 78 days.

During the accelerated corrosion process, the moisture and chloride content in the concrete cover as well as the half-cell potential, electrical resistivity, input voltage, and crack width were monitored. The GPR profiles perpendicular to the reinforcement were recorded every 7 days. A GPR device with a 2.7 GHz centre frequency antenna was used for this purpose. The normalised amplitude A in dB was calculated according to equation 8.

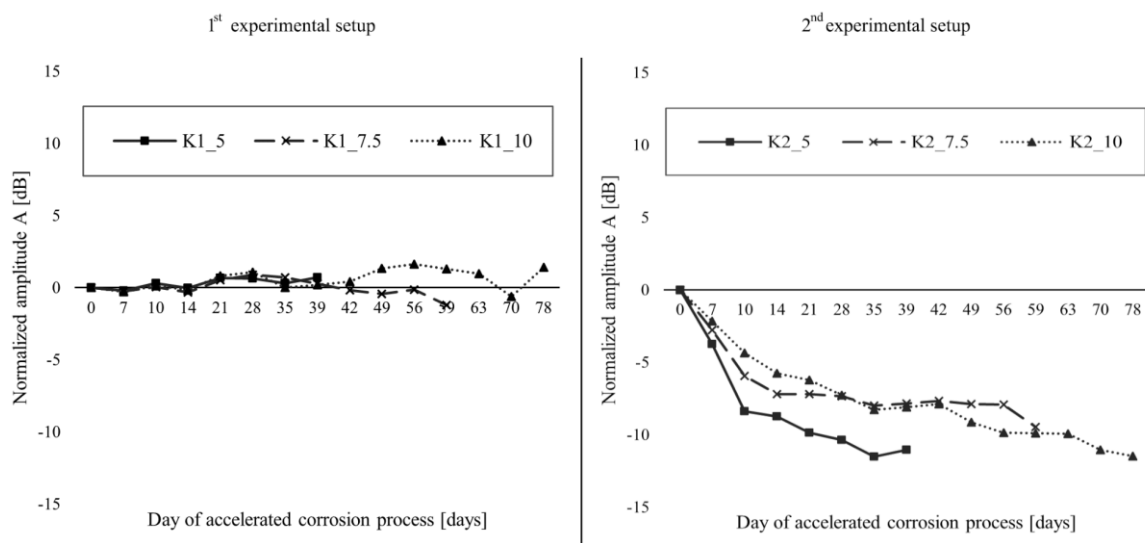The obtained normalised amplitude A in two different experimental setups is shown in Figure 3.

Figure 3. The normalised amplitude A in experimental setups 1 and 2 (originally presented in Paper II).

The normalised amplitude in the 1st experimental setup showed neither a consistent trend of change nor a significant deviation from its initial value. The value of A was between –1.2 dB and 1.6 dB. In contrast, the amplitude in the 2nd experimental arrangement decreased steadily. The strongest decrease was observed up to the 10th day, which is consistent with the higher current supplied by the external current source. The highest amplitude loss was –11.5 dB.

The moisture content was stable in both experimental setups, while the chloride content changed as the accelerated corrosion progressed. The change in chloride content in the concrete cover was more noticeable in the 2nd setup, which can be explained by the closer proximity of the sodium chloride solution than in the 1st setup. Similarly, the half-cell potential showed more negative values in the second test arrangement, while the electrical resistivity showed similar values in both test arrangements.

The corrosion pattern for both setups was analysed and the comparison for the two specimens with the same duration of the corrosion process but with different electrolyte positions is shown in Figure 4.

Figure 4. Comparison of the corrosion pattern in two experimental setups (originally presented in Paper II).

In the 1st setup, 94.3% of the total corrosion products were below the reinforcement, while 5.7% were above. In the 2nd test arrangement, on the other hand, 26.2% were below the reinforcement and 73.8% above. From the given, it is obvious that the distribution of the corrosion products is towards the electrolyte. When the corrosion products are below the reinforcement, the electromagnetic waves emitted with the GPR cannot penetrate deeper than the reinforcement. This is because the metal is considered to be a perfect reflector [117]. This explains the lack of amplitude change in the 1st experimental setup, which makes it unsuitable for considering the corrosion-induced change in the GPR signal.

On the other hand, the amplitude change in the 2nd test arrangement is because of 1) changes at the interface between concrete and reinforcement and 2) changes in the surrounding concrete. The former is related to the change from the concrete-reinforcement interface to the concrete-rust-reinforcement interface. The second change is related to the migration of corrosion products and chloride ions into the concrete pores.

The **main contribution** of **Paper II** was to show the mechanisms of **change in GPR signal** amplitude **due to different electrolyte positions** and thus to **clarify** whether they are **suitable for corrosion assessment with GPR**. This paper also showed that the distribution of corrosion products in the concrete cover influences material changes that alter the GPR signal, **confirming hypothesis 2**.

The **trend of change in GPR amplitude during corrosion** of reinforcement in concrete **is still not clearly understood**. **Paper III** focused on **isolating** three parameters of chloride-induced corrosion of reinforcement – **moisture, chlorides, and corrosion products** – to **observe** and **quantify** their effects on the GPR signal. Particular attention was paid to the experimental setup

of laboratory-induced corrosion in order to establish appropriate corrosion patterns. These are **knowledge gaps 3 and 4**.

The specimens were 300 mm x 200 mm x 90 mm, with a reinforcing bar (20 mm diameter and 300 mm length) and a concrete cover of 50 mm. Forty-two specimens were cast and divided into three groups: 1) group to observe the influence of moisture – M group (N_M, 9 specimens), 2) group to observe the influence of chlorides – Cl group (N_{Cl}, 27 specimens) and 3) group to observe the influence of corrosion products on the GPR signal – C group (N_C, 6 specimens). In the first group, the specimens were examined at the following saturation levels: 0% (dry), 15–20%, 45–50%, 75–80% or 100% (saturated). The degree of saturation w was determined by weighting. Chlorides were introduced by mixing them into the fresh concrete (internal chlorides) or by immersing the hardened specimens in sodium chloride solutions (external chlorides). The mixed chlorides were in the range of 0.24–3% of the cement mass, m_c, while the solutions had concentrations of 2–5%. The average chloride concentration in the concrete cover, c, was determined by potentiometric titration after performing the GPR measurements. The specimens of the second group were tested at saturation levels of 0% (dry), 15–20%, 45–50%, 75–80% and 100% (saturated). The six different degrees of corrosion were achieved using the IC technique. During the accelerated corrosion process, the container of water was placed on top of the specimens to keep the concrete cover partially dry and to ensure the gradual spreading of the corrosion products towards the upper concrete surface. After the GPR tests, the mass loss Δm due to corrosion was determined by weighing the cleaned reinforcing bars and compared with the mass of the non-corroded bars. The GPR profiles were recorded after stabilisation of the moisture content in the concrete under laboratory conditions, corresponding to a saturation level of 60–65%.

The GPR profiles were recorded using a GPR device with a 2.7 GHz centre frequency antenna perpendicular to the reinforcement. The normalised amplitude (A) was calculated according to equation 8, where the reference amplitude for the first group was the amplitude in the dry state, for the second group the amplitude of the specimen without chlorides at the same degree of saturation (for normalised amplitude A_1) or same specimen in a dry state (for normalised amplitude A), and for the third group the amplitude before corrosion.

The results are summarised in Table 7.

Moisture leads to amplitude loss – the loss is greater at saturation levels below 20% and above 80% (Table 7). Amplitude loss is the result of interactions between particles due to dipolar polarisation mechanisms. The energy is converted into heat and the overall strength of the electric field is reduced.

Table 7. Figures and normalised amplitudes for the observed parameters (data originally in Paper III, in other form).

Figure		Normalised amplitude [dB/cm]			
		Parameter	Trend of change	Saturation level	Value
Moisture		5% increase in saturation level	↓	20–80%	−0.1
				below 20% and above 80%	−0.2
Chlorides		0.4% (of m_c) increase in chloride content	↓	45–50%	−0.21
				75–80%	−0.26
				100%	−0.37
Corrosion		0.1% increase in mass loss due to reinforcement corrosion	↓	60–65%	−0.07

Amplitude loss increases with chloride concentration and degree of saturation. The loss of amplitude is mainly due to the increased conductivity of the concrete as a material, as the pore solution is now enriched with negative (chloride) ions dissolved in the water. In general, it has been found that the loss is less for internal chlorides than for external chlorides. It is assumed that the ratio of free to total chloride ions is higher for external chlorides [118] than for internal

chlorides. Since the energy loss for free ions is higher than for bound ions due to unhindered movement, the total energy loss for external chlorides is higher than for internal chlorides.

The corrosion products cause the amplitude loss – the greater the mass loss due to corrosion, the greater the loss of signal. After opening the specimens, it was found that the metal consumption was from the top half of the cylinder of the rebar facing the container of water. The loss of amplitude is due to two mechanisms. The first is related to the loss due to the presence of corrosion products in the concrete pores leading to the ferromagnetic relaxation mechanisms as the signal propagates through the concrete. The second mechanism is related to the change in the interface between the concrete and the reinforcement, between which there is now a layer of corrosion products that suddenly creates more reflective surfaces than in the case of non-corroded reinforcement.

The **main contribution** of **Paper III** was to show **the trend of the change in GPR amplitude** due to **the isolated effect of the corrosion products** and to **quantify** this change. It was shown that all three parameters influence the measurable decrease in amplitude (**proof for hypothesis 1**), including the distribution of corrosion products in the concrete cover (**proof for hypothesis 2**). Furthermore, it was found that a normalised amplitude of –0.7 dB/cm corresponds to the case when 0.6% of the m_c chloride concentration is at the depth of the reinforcement, which is a mean "critical" chloride concentration according to [119].

Indispensable for modelling the GPR response in a corrosive concrete environment is an adequate description of the material properties. There are a **limited number of studies** that have even **analysed the variation of signal strength in corrosive environments** [96]. Nevertheless, there is **no study in which the magnetic properties of corrosion products in concrete have been included in numerical simulations**. Considering this **knowledge gap 5**, **Paper IV** dealt with the analysis of the change of GPR signal amplitude due to moisture, chlorides, and corrosion products, incorporating the real and imaginary parts of the concrete and corrosion product properties in the modelling of the materials. The results were compared with the corresponding laboratory specimens analysed in Paper III.

The numerical simulations were performed using the open-source software gprMax, which is based on solving Maxwell's equations with finite difference algorithms in the time domain (finite-difference time-domain (FDTD)). The geometry of the numerical models entirely corresponded to the laboratory specimens analysed in the previous Paper III. The normalised amplitude was calculated in the same way as in Paper III. The dimensions of the finite elements were 0.001 m x 0.001 m and 0.001 m for the *M* and *Cl* specimen groups, while they were 0.0001 m in the *x* and *y* plane for the *C* group. The dielectric permittivity of the concrete was modelled

using the Complex Refractive Index Model (CRIM). This model considers the dielectric properties of constituents of a heterogeneous material based on their volumetric fractions to obtain a unique dielectric permittivity. The dielectric permittivity of concrete is thus represented by its real and imaginary parts. The dielectric permittivity of concrete for *M* and *Cl* specimen group ($\varepsilon_I(\omega)$) included the dielectric permittivity of a solid phase – cement paste and aggregates –, a liquid phase – pore solution in the concrete pores – and a gaseous phase – air in the concrete pores. The imaginary part comes from the complex permittivity of water, which is described by the Debye function [53]. Considering that the Debye function describes the behaviour of free water, the parameters of the function were changed to take into account the behaviour of capillary water in concrete, which is not a free liquid [120,121]. In the current version of gprMax, it is not possible to include the dielectric permittivity formulated by CRIM in the calculation. In this study, the algorithm presented in [99] was used to fit $\varepsilon_I(\omega)$ to the multi-Debye model currently available in gprMax. The conductivity of concrete was calculated as the reciprocal of the electrical resistivity measured on laboratory specimens with the Wenner probe [15]. In addition, the corresponding numerical models in which only the real part of the dielectric permittivity of concrete is included were modelled. The dielectric permittivity was also calculated with CRIM and the only difference to the previously described models was that the water was modelled with a real, frequency-independent dielectric permittivity.
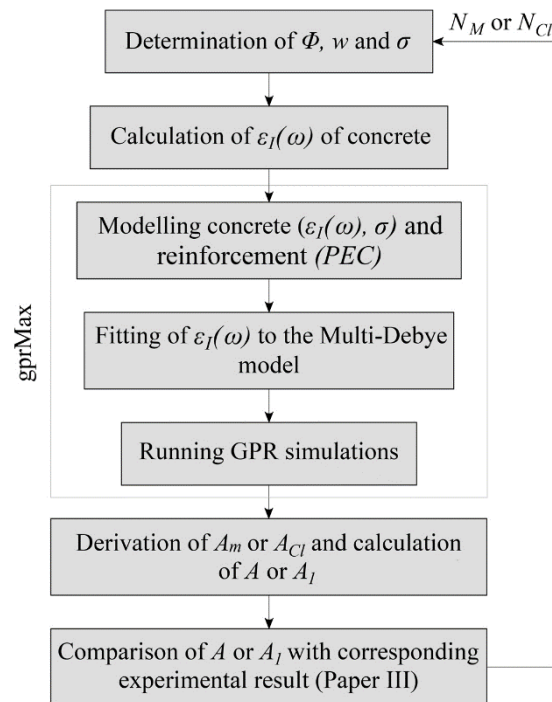

Figure 5. Flowchart of the modelling *M* and *Cl* groups (originally presented in Paper IV).

The specimens from *C* group were modelled using two approaches: 1) uniformly and 2) nonuniformly distributed corrosion products around the rebar, Figure 6. In the first "uniform" corrosion approach, it was assumed that the concrete pores are filled with corrosion products up to an experimentally determined height *h*. In the second approach, referred to as the "non-uniform" distribution of corrosion products, three different layers of *h*/3 thickness of concrete filled with corrosion products were modelled. The layer closest to the rebar was a concrete whose pores were filled with corrosion products, the layer next to it was 60% filled, while the layer furthest from the rebar was 30% filled.
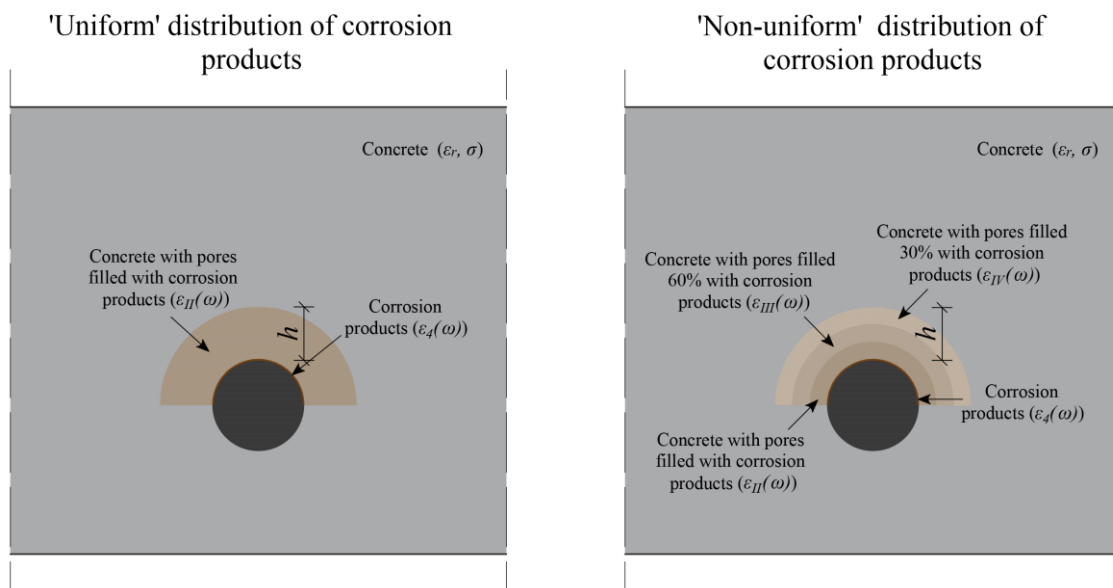

Figure 6. Concepts for modelling 1) uniformly (left) and 2) non-uniformly distributed corrosion products (right), (originally presented in Paper IV).

The dielectric permittivity of the concrete was calculated using CRIM, while the complex dielectric permittivity of the corrosion products was taken from [54] as a tool that takes into account the ferromagnetic relaxation of iron oxides. The layers of concrete and corrosion products were modelled only from the side of the rebar facing the concrete cover, as this corresponds to the case found in Paper III. The dielectric permittivity of the concrete filled with corrosion products was also fitted to the multi-Debye function.

The specimen with the highest degree of corrosion (Paper III) showed a crack at the end of the test. The crack was modelled with a width of 1 mm and was modelled as a crack filled with I) corrosion products at height *h* and with air for the rest of the crack, II) air and III) corrosion products. The flow charts for modelling the specimen groups *M*, *Cl*, and *C* are shown in Figures 5 and 7, respectively.

For the comparison, all specimens of group *C* were modelled with real, frequency-independent properties of the corrosion products. The properties of the corrosion products were the same as in [96]. The other features related to the modelling concepts (uniform and non-uniform) were the same as in Figure 7. The results of the numerical simulations are summarised in Table 8.
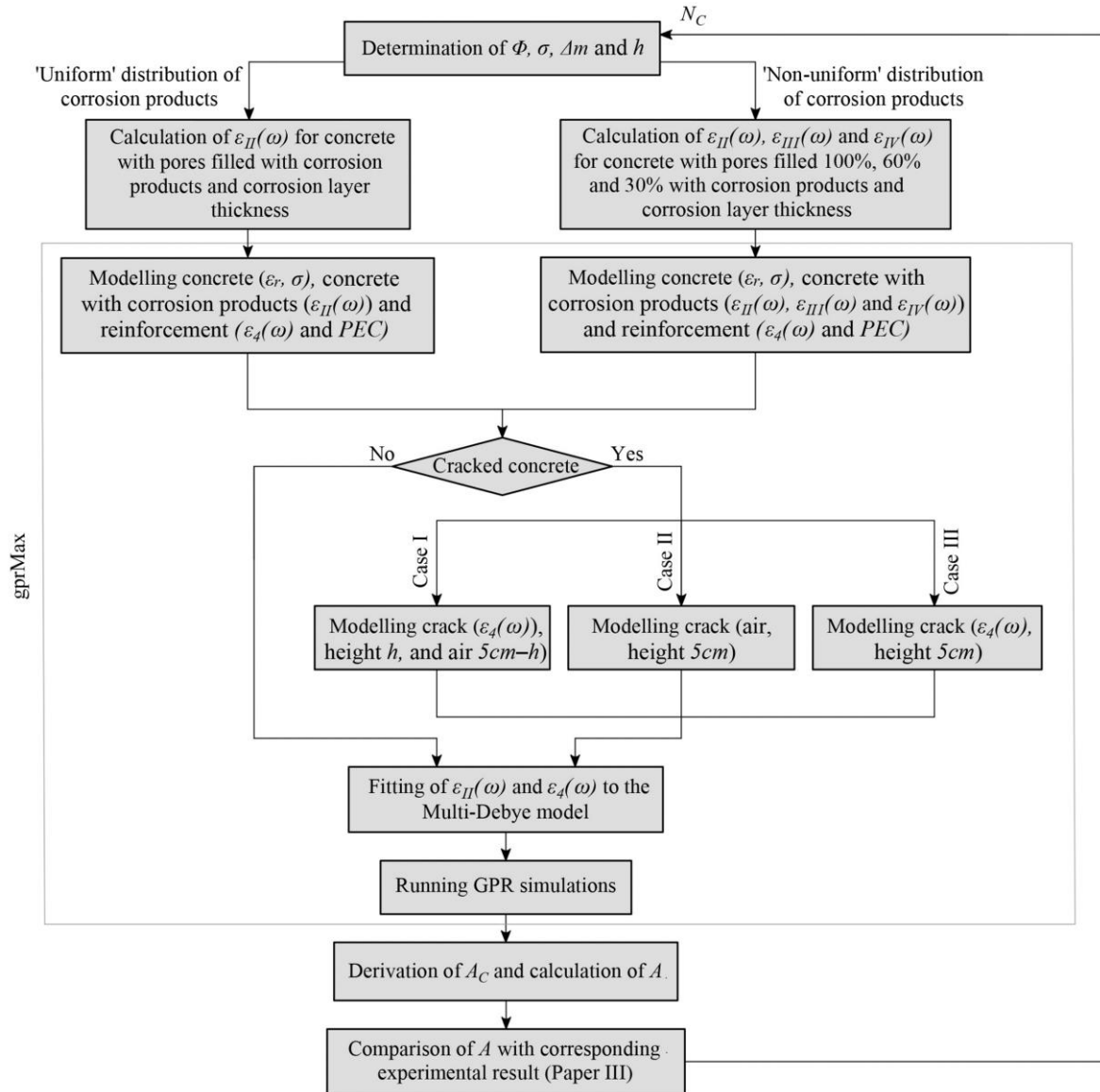

Figure 7. Flowchart of the modelling *C* group of specimens (originally presented in Paper IV).

The results of the models that only consider the real part of the dielectric permittivity of the concrete (*M*, *Cl* and *C* group) and the corrosion products (*C* group) are marked in grey as "numerical models (real)". The models that take into account the complex dielectric permittivity are marked in magenta as "numerical models (complex)". The experimental data are shaded grey, with the upper and lower limits corresponding to the added/subtracted two standard deviations of the residuals from the linear regression of the experimental results. while linear regression of results is shown in black.

Table 8. Summary of results obtained in Paper IV (data originally in Paper IV, in other form).
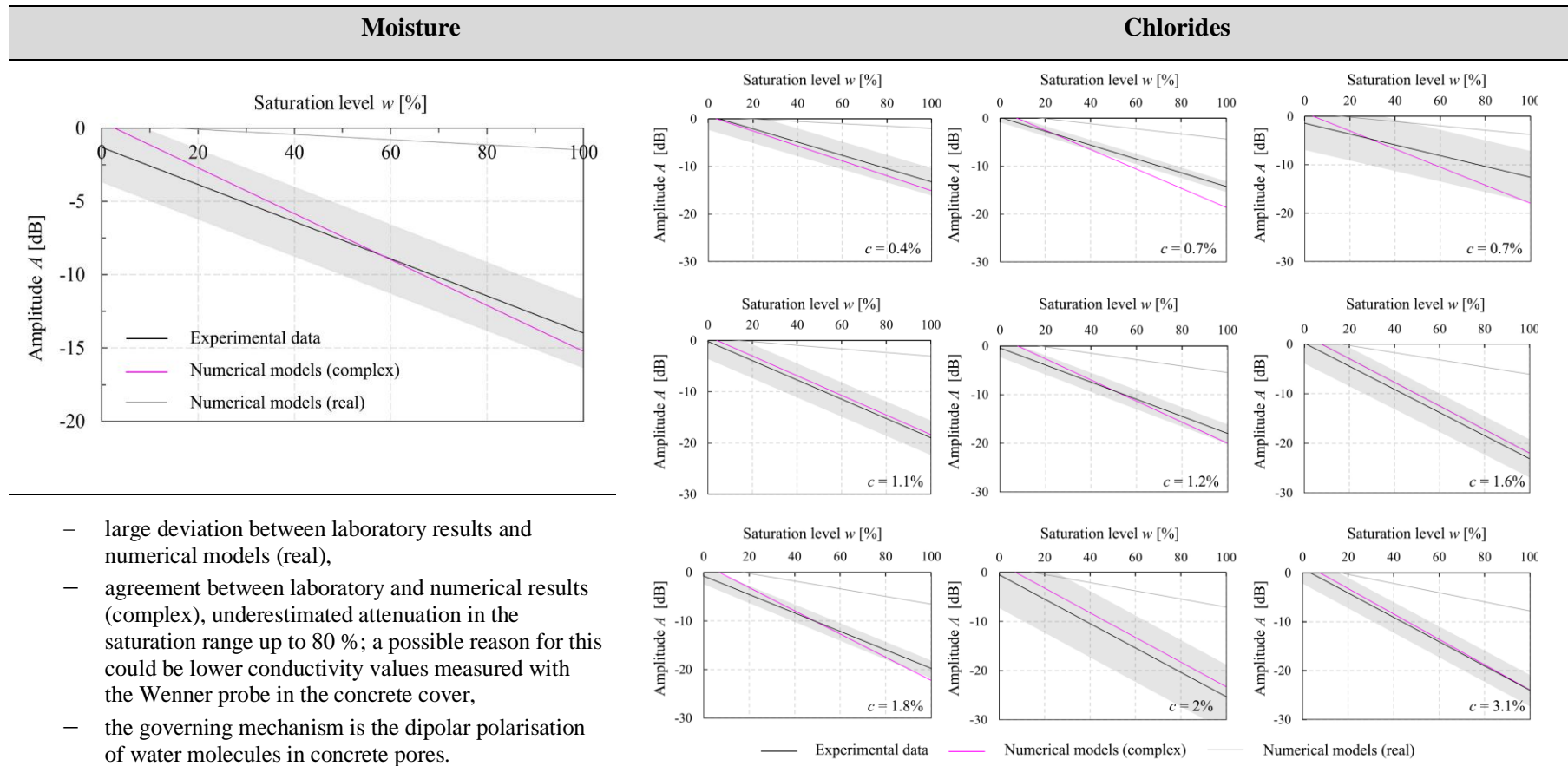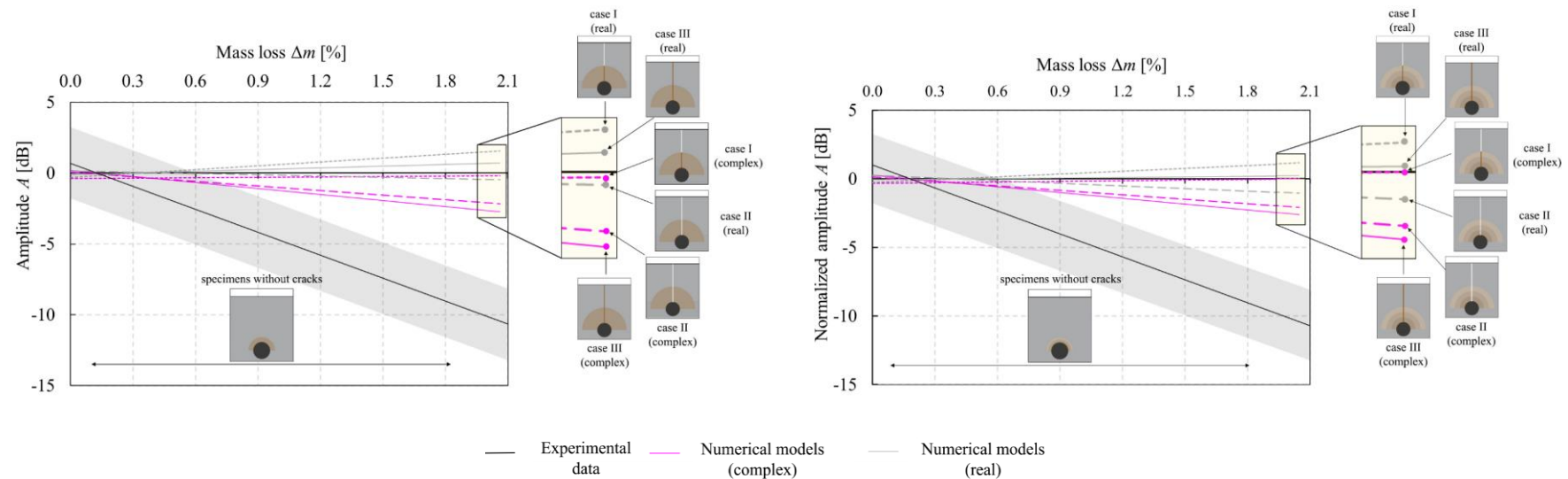

– large deviation between laboratory results and numerical models (real),

– agreement between laboratory and numerical results (complex), underestimated attenuation in the saturation range up to 80 %; a possible reason for this could be lower conductivity values measured with the Wenner probe in the concrete cover,

– the governing mechanism is the dipolar polarisation of water molecules in concrete pores.

– approximate agreement between laboratory and numerical results (complex) at higher saturation levels (above 75 %), while attenuation is underestimated at lower ranges (same reason as for the *M* models),

– mechanisms that change the strength of the electromagnetic field are the dipolar polarisation of the water molecules and the conduction of the dissolved chloride ions.

- opposite trend of change between laboratory results and numerical models (real),
- decreasing trend of amplitude change with increasing degree of corrosion in specimens without cracks (numerical models (complex)), which is in agreement with laboratory results
- generally, very little variation between results for uniform and non-uniform models; most likely due to the small volumetric contribution of corrosion products to the total volume of concrete,
- cracks filled with corrosion products and air lead to a loss of amplitude,
- the mechanism causing the amplitude loss is mainly related to the magnetic properties of iron oxides, deviations between laboratory and numerical results could be due to inappropriate modelling of the distribution of the corrosion products in the concrete or to the complex magnetic properties of the specific composition of the corrosion products.

The **conclusion** from **Paper IV** was that **not taking into account the complex dielectric properties of water and corrosion products**, i.e., the properties of the concrete, leads to an **underestimation of the attenuation**. When considering the strength of the GPR signal in a corrosive environment, the **imaginary part of the dielectric permittivity and magnetic permeability** was a **crucial** factor in the **magnitude of the losses**. The deeper understanding of the change in GPR amplitude due to chloride-induced parameters gained through numerical simulations provided an explanation for **hypotheses 1 and 2**

3.2. Scientific contribution

The main scientific contributions of this thesis are:

1. *Clarification of the influence of the corrosion process on the data recorded with ground penetrating radar*,

    – In Papers II, III and IV the influence of the corrosion process on the data recorded with ground penetrating radar was analysed. In Papers II and III, the tendency of the amplitude change of the ground penetrating radar wave and the magnitude of the change were determined based on the results of experimental investigations. In Paper IV, based on the results of numerical modelling and comparison with the results of experimental investigations, it was clarified what mechanisms cause the changes in the amplitude of the GPR wave reflected from the reinforcement.

2. *Determination of the influence of the distribution of corrosion products in the concrete cover on the amplitude of the GPR wave reflected from the reinforcement*,

    – Papers II, III and IV show, among other things, the influence of the distribution of corrosion products in the concrete cover on the amplitude of the GPR wave reflected by the reinforcement, which is considered a special contribution, as it was shown in Paper I that contradictory results regarding the trend of the amplitude change were reported in the literature.

3. *Quantification of corrosion-related parameters on the change of GPR amplitude and identifying the dominant causes as a basis for developing the corrosion assessment procedure using ground penetrating radar,*

    – The result of Paper III are the functions of the amplitude change of the GPR signal depending on moisture, chloride, and corrosion product content. Three main parameters of chloride-induced corrosion were isolated and analysed. Based on

the results, recommendations were given for the assessment of corrosion of reinforced concrete structures both in the initiation phase and in the corrosion propagation phase.

Chapter 4.   Concluding Remarks

In this thesis, the feasibility of ground penetrating radar to detect parameters of chloride-induced corrosion is analysed. This chapter summarises the conclusions in Section 4.1, while recommendations for future work are given in Section 4.2.

4.1. Conclusions

The characterisation of the ground penetrating radar signal in an environment favourable to corrosion initiation and during corrosion propagation is presented in this thesis. For this purpose, an overview of studies on this topic was given following the laboratory experiments and numerical modelling. Laboratory experiments were first conducted to investigate the suitability of the IC technique in terms of the location of the electrolyte for the GPR studies. Based on the conclusions, the experimental laboratory study was designed to observe and quantify the effects of isolated parameters, moisture, chlorides, and corrosion products on the changes in amplitude strength. The specimens were replicated in the gprMax software to analyse the mechanisms that change the signal, regarding the inclusion of dispersive and non-dispersive material properties. The specific conclusions on each topic can be found in Papers I – IV. The main conclusions from the research are:

- From the review of the existing literature, it is concluded that there is lack of studies comprehensively observing and quantifying the effect of corrosion-related parameters, moisture, and chlorides, on the GPR signal based on the observation of waves reflected from reinforcement as part of the integrated corrosion assessment of RC structures. It was also noted that it is not clear whether corrosion products cause an increase or decrease in amplitude. Furthermore, no study takes into account the complex, frequency-dependent properties of concrete due to the migration of corrosion products into concrete pores.

- The migration of the corrosion products during the simulated corrosion process with the impressed current technique develops towards the electrolyte (if used). Since the emitted electromagnetic waves cannot penetrate metal objects and are therefore completely reflected by them, the examination of concrete elements from the surface

not exposed to the electrolyte is unreliable. The corrosion products hidden by the reinforcement could not be detected with the GPR. It was found that the amplitude in this case does not show a clear trend of change and fluctuates around the initial amplitude before corrosion. When the surface exposed to the electrolyte solution is examined with GPR, the amplitude shows a decreasing trend during the corrosion progress.

- For all isolated parameters – moisture, chlorides, and corrosion products – the amplitude decreased with increasing observed impact (increase in the degree of saturation, chloride concentration or mass loss due to corrosion). Increasing the degree of saturation by 5% affects the attenuation by –0.1 dB/cm in the 20–80% saturation range, increasing the chloride content by 0.4% m_c affects the attenuation by –0.26 dB/cm (at 75–80% saturation), and increasing the mass loss due to corrosion by 0.1% affects the attenuation by –0.07 dB/cm.

- An increase in the degree of saturation in the range of 0–20% and 80–100% causes twice as much attenuation as in the range of 20–80% with the same degree of increase.

- The same chloride concentration for chlorides mixed into the fresh concrete compared to chlorides diffused into the hardened specimen has a slightly lower effect on attenuation. The lower ratio of free to total chlorides in the specimens where chlorides were mixed into the fresh concrete is believed to be responsible for this.

- The attenuation value of –0.7 dB/cm of normalised amplitude is obtained for the case where 0.6% of the chloride concentration is reached in the depth of the reinforcement, which corresponds to the mean value of the beta distribution of the "critical" chloride content according to the *fib Model Code*. This value was determined at an ambient relative humidity of 60%.

- The comparison of the results of numerical simulations, in which the dielectric permittivity of concrete and corrosion products is modelled firstly as a complex frequency-dependent and secondly as a real frequency-independent number, with the laboratory results led to the following conclusion: The exclusion of the imaginary part of the dielectric permittivity results in several times less attenuation compared to the case in which it is included. If the magnetic properties for corrosion products are not included, even the trend of the change could be wrong.

- Through numerical modelling and comparison of the results from the laboratory experiments and the numerical simulation, it was found that the presence of moisture, chloride and corrosion products leads to a loss of amplitude, i.e., signal attenuation. The attenuation of the electromagnetic wave at these three parameters of chloride-induced corrosion is due to three different processes. The dipolar polarisation of water molecules in the presence of an electromagnetic field is mainly responsible for the attenuation when moisture is present in the concrete pores. In the case of chlorides, this is the conduction of charged ions. Finally, the ferromagnetic relaxation of iron oxides, which occurs when corrosion products are exposed to the electromagnetic field, is the most influential mechanism that changes the strength of the signal when corrosion products migrate into the concrete pores.

- No significant differences were found between the results of modelling a uniform and a non-uniform distribution of corrosion products in the concrete cover. It is assumed that this is due to the generally low volumetric proportion of corrosion products in the total volume of concrete.

The scientific contribution of this thesis lies in the clarification of the influence of the parameters of chloride-induced corrosion on the change in GPR amplitude. This was done through laboratory tests, in which the extent and the sign of the change were determined, and through numerical simulations, which provided a deeper understanding of the material mechanisms that cause the amplitude change.

4.2. Further research

This research has raised some questions for further investigation of corrosion assessment using ground penetrating radar. In the following text, recommendations for further research are given, one relating to laboratory investigation and the other to numerical modelling.

The following recommendations refer to the laboratory investigations:

- Even though the conclusion from this study is that the signal changes due to moisture, chlorides, and corrosion products with three different mechanisms, quantification of the combined effect of the three parameters should be investigated.

- The data should be enlarged regarding the isolated effect of corrosion products for higher corrosion degrees than in this study.

- The data should be extended to samples with different properties, such as water-cement ratio, to test the applicability of the results regardless of the concrete type.

- As the investigation was carried out with a GPR device at 2.7 GHz, the deviation of the results should be investigated as a function of the centre device frequency. However, this frequency range should be 2–3 GHz as it is not expected that the results of this study can be used for GPR devices that are not intended for the investigation of reinforced concrete structures.

- The limitation in corrosion assessment with GPR is that normally only one parameter is observed, namely the amplitude of the signal, whereas in chloride-induced corrosion more than one parameter varies – moisture, chlorides, temperature, or reinforcement loss. Considering the recommendation from Paper III, which suggests that the investigations can be carried out when the temperature and moisture content are close to the values measured during the baseline measurement, the remaining parameters that could be related to the signal are chlorides and reinforcement loss. During corrosion propagation, the combined application could be performed with another NDT method, such as electrical resistivity, to obtain a more accurate corrosion assessment. It is suggested to consider a combined two-parameter two-method assessment procedure.

Regarding the numerical modelling, the following suggestions are given:

- The models for observing the influence of corrosion products on the GPR signal should be improved concerning geometric changes as corrosion propagates (e.g., including the influence of microcracks).

- The dielectric properties of corrosion products should be determined experimentally, which are then used as input parameters for more accurate modelling.

Literature

[1]   United Nations, Transforming Our World: The 2030 Agenda for Sustaniable Development, United Nations, 2016. https://doi.org/10.1201/b20466-7.

[2]   K.L. Scrivener, V.M. John, E.M. Gartner, Eco-efficient cements: Potential economically viable solutions for a low-CO2 cement-based materials industry, Cem. Concr. Res. 114 (2018) 2–26. https://doi.org/10.1016/j.cemconres.2018.03.015.

[3]   J. Li, Z. Wu, C. Shi, Q. Yuan, Z. Zhang, Durability of ultra-high performance concrete – A review, Constr. Build. Mater. 255 (2020) 119296. https://doi.org/10.1016/j.conbuildmat.2020.119296.

[4]   M. Alexander, H. Beushausen, Durability, service life prediction, and modelling for reinforced concrete structures – review and critique, Cem. Concr. Res. 122 (2019) 17–29. https://doi.org/10.1016/j.cemconres.2019.04.018.

[5]   H. Beushausen, R. Torrent, M.G. Alexander, Performance-based approaches for concrete durability: State of the art and future research needs, Cem. Concr. Res. 119 (2019) 11–20. https://doi.org/10.1016/j.cemconres.2019.01.003.

[6]   L. Bertolini, B. Elsener, P. Pedeferri, E. Redaelli, R. Polder, Corrosion of Steel in Concrete: Prevention, Diagnosis, Repair, 2nd ed., Wiley, Weinheim, 2003. ISBN: 9783527308002.

[7]   U. Nürnberger, Corrosion of metals in contact with mineral building materials, in: M. Raupach, B. Elsener, R. Polder, J. Mietz (Eds.), Corros. Reinf. Concr. Struct. Mech. Monit. Inhib. Rehabil. Tech., CRC Press LLC, Boca Raton, FL, USA, 2007.

[8]   U. Angst, B. Elsener, C.K. Larsen, Ø. Vennesland, Critical chloride content in reinforced concrete - A review, Cem. Concr. Res. 39 (2009) 1122–1138. https://doi.org/10.1016/j.cemconres.2009.08.006.

[9]   R. Wassermann, A. Katz, A. Bentur, Minimum cement content requirements: A must or a myth?, Mater. Struct. Constr. 42 (2009) 973–982. https://doi.org/10.1617/s11527-008-9436-0.

[10] J. Chen, C. Fu, H. Ye, X. Jin, Corrosion of steel embedded in mortar and concrete under different electrolytic accelerated corrosion methods, Constr. Build. Mater. 241 (2020) 117971. https://doi.org/10.1016/j.conbuildmat.2019.117971.

[11] A. Poursaee, C.M. Hansson, Potential pitfalls in assessing chloride-induced corrosion of steel in concrete, Cem. Concr. Res. 39 (2009) 391–400. https://doi.org/10.1016/j.cemconres.2009.01.015.

[12] Y. Zhao, H. Ren, H. Dai, W. Jin, Composition and expansion coefficient of rust based on X-ray diffraction and thermal analysis, Corros. Sci. 53 (2011) 1646–1658. https://doi.org/10.1016/j.corsci.2011.01.007.

[13] Y. Zhao, J. Dong, Y. Wu, W. Jin, Corrosion-induced concrete cracking model considering corrosion product-filled paste at the concrete/steel interface, Constr. Build. Mater. 116 (2016) 273–280. https://doi.org/10.1016/j.conbuildmat.2016.04.097.

[14] B. Elsener, C. Andrade, J. Gulikers, R. Polder, M. Raupach, Half-cell potential measurements - Potential mapping on reinforced concrete structures, Mater. Struct. 36 (2003) 461–471. https://doi.org/10.1007/BF02481526.

[15] R. Polder, C. Andrade, B. Elsener, Ø. Vennesland, J. Gulikers, R. Weidert, M. Raupach, Test methods for on site measurement of resistivity of concrete, Mater. Struct. 33 (2000) 603–611, https://doi.org/10.1007/BF02480599.

[16] H. Ahmed, H.M. La, N. Gucunski, Review of non-destructive civil infrastructure evaluation for bridges: State-of-the-art robotic platforms, sensors and algorithms, Sensors (Switzerland). 20 (2020) 1–38. https://doi.org/10.3390/s20143954.

[17] C.L. Barnes, J.F. Trottier, Phenomena and conditions in bridge decks that confound ground-penetrating radar data analysis, Transp. Res. Rec. (2002) 57–61. https://doi.org/10.3141/1795-07.

[18] C.L. Barnes, J.F. Trottier, D. Forgeron, Improved concrete bridge deck evaluation using GPR by accounting for signal depth-amplitude effects, NDT E Int. 41 (2008) 427–433. https://doi.org/10.1016/j.ndteint.2008.03.005.

[19] C.L. Barnes, J.F. Trottier, Effectiveness of Ground Penetrating Radar in Predicting Deck Repair Quantities, J. Infrastruct. Syst. 10 (2004) 69–76. https://doi.org/10.1061/(asce)1076-0342(2004)10:2(69).

[20] K. Dinh, N. Gucunski, J. Kim, T.H. Duong, Method for attenuation assessment of GPR

data from concrete bridge decks, NDT E Int. 92 (2017) 50–58. https://doi.org/10.1016/j.ndteint.2017.07.016.

[21] K. Dinh, T. Zayed, F. Romero, A. Tarussov, Method for analyzing time-series GPR data of concrete bridge decks, J. Bridg. Eng. 20 (2015). https://doi.org/10.1061/(ASCE)BE.1943-5592.0000679.

[22] K. Dinh, N. Gucunski, T. Zayed, Automated visualization of concrete bridge deck condition from GPR data, NDT&E Int. 102 (2019) 120–128. https://doi.org/10.1016/j.ndteint.2018.11.015.

[23] K. Dinh, N. Gucunski, K. Tran, A. Novo, T. Nguyen, Full-resolution 3D imaging for concrete structures with dual-polarization GPR, Autom. Constr. 125 (2021) 103652. https://doi.org/10.1016/j.autcon.2021.103652.

[24] K. Dinh, N. Gucunski, Factors affecting the detectability of concrete delamination in GPR images, Constr. Build. Mater. 274 (2021). https://doi.org/10.1016/j.conbuildmat.2020.121837.

[25] K. Dinh, T. Zayed, S. Moufti, A. Shami, A. Jabri, M. Abouhamad, T. Dawood, Clustering-Based Threshold Model for Condition Assessment of Concrete Bridge Decks with Ground-Penetrating Radar, Transp. Res. Rec. (2015) 81–89. https://doi.org/10.3141/2522-08.

[26] D.J. Daniels, Ground Penetrating Radar, second ed., The Institution of Electrical Engineers, London, 2004. ISBN: 9780863413605.

[27] A.P. Annan, Electromagnetic Principles of Ground Penetrating Radar, in: M.H. Jol (Ed.), Gr. Penetrating Radar Theory Appl., Elsevier B.V, Amsterdam, The Netherlands, 2009: pp. 1–40. https://doi.org/https://doi.org/10.1016/B978-0-444-53348-7.X0001-4.

[28] G. Manacorda, R. Persico, H. F. Scott, Design of Advanced GPR Equipment for Civil Engineering Applications, in: A. Benedetto, L. Pajewski (Eds.), Civil Engineering Applications of Ground Penetrating Radar, Springer, New York, USA, 2014: pp. 3–40. https://doi.org/10.1007/978-3-319-04813-0_1.

[29] W.L. Lai, T. Kind, S. Kruschwitz, J. Wöstmann, H. Wiggenhauser, Spectral absorption of spatial and temporal ground penetrating radar signals by water in construction materials, NDT E Int. 67 (2014) 55–63. https://doi.org/10.1016/j.ndteint.2014.06.009.

[30] W.L. Lai, T. Kind, H. Wiggenhauser, Frequency-dependent dispersion of high-

frequency ground penetrating radar wave in concrete, NDT E Int. 44 (2011) 267–273. https://doi.org/10.1016/j.ndteint.2010.12.004.

[31] T. Klewe, C. Strangfeld, S. Kruschwitz, Review of moisture measurements in civil engineering with ground penetrating radar – Applied methods and signal features, Constr. Build. Mater. 278 (2021) 122250. https://doi.org/10.1016/j.conbuildmat.2021.122250.

[32] F. Tosti, E. Slob, Determination, by Using GPR, of the Volumetric Water Content in Structures, Substructures, Foundations and Soil, in: A. Benedetto, L. Pajewski (Eds.), Civil Engineering Applications of Ground Penetrating Radar, Springer, New York, USA, 2014: pp. 163–196. https://doi.org/10.1007/978-3-319-04813-0_7.

[33] W.L. Lai, T. Kind, H. Wiggenhauser, Using ground penetrating radar and time-frequency analysis to characterize construction materials, NDT&E Int. 44 (2011) 111–120. https://doi.org/10.1016/j.ndteint.2010.10.002.

[34] ACI Committee 228, Nondestructive Test Methods for Evaluation of Concrete in Structures, American Concrete Institute, Farmington Hills, MI, 1998. https://www.concrete.org/publications/internationalconcreteabstractsportal/m/details/id/5119. (Accessed 18 July 2023).

[35] N.J. Cassidy, Electrical and Magnetic Properties of Rocks, Soils and Fluids, in: H.M. Jol (Ed.), Gr. Penetrating Radar Theory Appl., Elsevier, Amsterdam, 2009: pp. 41–72. https://doi.org/10.1016/B978-0-444-53348-7.00002-8.

[36] P.T.W. Wong, W.L. Lai, J.F.C. Sham, C. Poon, Hybrid non-destructive evaluation methods for characterizing chloride-induced corrosion in concrete, NDT E Int. 107 (2019). https://doi.org/10.1016/j.ndteint.2019.05.008.

[37] S. Hong, W.L. Lai, G. Wilsch, R. Helmerich, R. Helmerich, T. Günther, H. Wiggenhauser, Periodic mapping of reinforcement corrosion in intrusive chloride contaminated concrete with GPR, Constr. Build. Mater. 66 (2014) 671–684. https://doi.org/10.1016/j.conbuildmat.2014.06.019.

[38] W.L. Lai, T. Kind, M. Stoppel, H. Wiggenhauser, Measurement of Accelerated Steel Corrosion in Concrete Using Ground-Penetrating Radar and a Modified Half-Cell Potential Method, J. Infrastruct. Syst. 19 (2013) 205–220. https://doi.org/10.1061/(ASCE)IS.1943-555X.0000083.

[39] B.J. Zhan, W.L. Lai, S.C. Kou, C.S. Poon, W.F. Tsang, Correlation between accelerated steel corrosion in concrete and ground penetrating radar parameters, in: C. Leung, K.T. Wan (Eds.), Int. RILEM Conf. Adv. Constr. Mater. Through Sci. Eng., RILEM Publications SARL, Hong Kong, China, 2011.

[40] N. Diamanti, A.P. Annan, J.D. Redman, Concrete Bridge Deck Deterioration Assessment Using Ground Penetrating Radar (GPR), J. Environ. Eng. Geophys. 22 (2017). https://doi.org/10.2113/JEEG22.2.121.

[41] K. Dinh, T. Zayed, A. Tarussov, GPR image analysis for corrosion mapping in concrete slabs, in: In Proceedings of the Canadian Society of Civil Engineering 2013 Conference, Montreal, QC, Canada, 29 May–1 June 2013.

[42] A. Tarussov, M. Vandry, A. De La Haza, Condition assessment of concrete structures using a new analysis method: Ground-penetrating radar computer-assisted visual interpretation, Constr. Build. Mater. 38 (2013) 1246–1254. https://doi.org/10.1016/j.conbuildmat.2012.05.026.

[43] M. Abouhamad, T. Dawood, A. Jabri, M. Alsharqawi, T. Zayed, Corrosiveness mapping of bridge decks using image-based analysis of GPR data, Autom. Constr. 80 (2017) 104–117. https://doi.org/10.1016/j.autcon.2017.03.004.

[44] M. Solla, S. Lagüela, N. Fernández, I. Garrido, Assessing rebar corrosion through the combination of nondestructive GPR and IRT methodologies, Remote Sens. 11 (2019). https://doi.org/10.3390/rs11141705.

[45] S. Abu Dabous, S. Yaghi, S. Alkass, O. Moselhi, Concrete bridge deck condition assessment using IR Thermography and Ground Penetrating Radar technologies, Autom. Constr. 81 (2017) 340–354. https://doi.org/10.1016/j.autcon.2017.04.006.

[46] T. Omar, M.L. Nehdi, T. Zayed, Performance of NDT Techniques in Appraising Condition of Reinforced Concrete Bridge Decks, J. Perform. Constr. Facil. 31 (2017). https://doi.org/10.1061/(asce)cf.1943-5509.0001098.

[47] B.M. Pailes, N. Gucunski, Understanding Multi-modal Non-destructive Testing Data Through the Evaluation of Twelve Deteriorating Reinforced Concrete Bridge Decks, J. Nondestruct. Eval. 34 (2015) 1–14. https://doi.org/10.1007/s10921-015-0308-6.

[48] N. Gucunski, J. Kim, K. Dinh, J. Gong, F. Liu, Innovative Ways in Condition Assessment of Concrete Bridge Decks: Data Collection Using Robotics, and Advanced

Data Interpretation and Visualization, in: SynerCrete'18 Int. Conf. Interdiscip. Approaches Cem. Mater. Struct. Concr., Funchal, 2018: pp. 21–28.

[49] N. Gucunski, B. Basily, J. Kim, J. Yi, T. Duong, K. Dinh, S.H. Kee, A. Maher, RABIT: implementation, performance validation and integration with other robotic platforms for improved management of bridge decks, Int. J. Intell. Robot. Appl. 1 (2017) 271–286. https://doi.org/10.1007/s41315-017-0027-5.

[50] G. Kilic, A. Caner, Augmented reality for bridge condition assessment using advanced non-destructive techniques, Struct. Infrastruct. Eng. (2020). https://doi.org/10.1080/15732479.2020.1782947.

[51] M. Rashidi, H. Azari, J. Nehme, Assessment of the overall condition of bridge decks using the Jensen-Shannon divergence of NDE data, NDT&E Int. 110 (2020). https://doi.org/10.1016/j.ndteint.2019.102204.

[52] U.B. Halabe, A. Sotoodehnia, K.R. Maser, E.A. Kausel, Modeling of the Electromagnetic Properties of Concrete, ACI Mater. J. 90 (1993) 552–563. https://doi.org/10.14359/4495.

[53] C.A. Balanis, Advanced Engineering Electromagnetics, second ed. Wiley, Hoboken, NJ, USA. https://www.wiley.com/en-cn/Advanced+Engineering+Electromagnetics,+2nd+Edition-p-9781118213483.

[54] N.J. Cassidy, Frequency-dependent attenuation and velocity characteristics of nano-to-micro scale, lossy, magnetite-rich materials, Near Surf. Geophys. 6 (2008) 341–354. https://doi.org/10.3997/1873-0604.2008023.

[55] W.L. Lai, T. Kind, H. Wiggenhauser, A Study of Concrete Hydration and Dielectric Relaxation Mechanism Using Ground Penetrating Radar and Short-Time Fourier Transform, EURASIP J. Adv. Signal Process. 2010 (2010). https://doi.org/10.1155/2010/317216.

[56] L. Xie, Z. Xia, S. Xue, X. Fu, Detection of setting time during cement hydration using ground penetrating radar, J. Build. Eng. 60 (2022) 105166. https://doi.org/10.1016/j.jobe.2022.105166.

[57] W.L. Lai, W.F. Tsang, Characterization of pore systems of air/water-cured concrete using ground penetrating radar (GPR) through continuous water injection, Constr. Build. Mater. 22 (2008) 250–256. https://doi.org/10.1016/j.conbuildmat.2006.08.021.

[58] S. Laurens, J.P. Balayssac, J. Rhazi, G. Klysz, G. Arliguie, Non-destructive evaluation of concrete moisture by GPR: Experimental study and direct modeling, Mater. Struct. 38 (2005) 827–832. https://doi.org/10.1007/BF02481655.

[59] G. Klysz, J.P. Balayssac, Determination of volumetric water content of concrete using ground-penetrating radar, Cem. Concr. Res. 37 (2007) 1164–1171. https://doi.org/10.1016/j.cemconres.2007.04.010.

[60] Z.M. Sbartaï, S. Laurens, J.P. Balayssac, G. Ballivy, G. Arliguie, Effect of concrete moisture on radar signal amplitude, ACI Mater. J. 103 (2006) 419–426. https://doi.org/10.14359/18219.

[61] S.F. Senin, R. Hamid, Ground penetrating radar wave attenuation models for estimation of moisture and chloride content in concrete slab, Constr. Build. Mater. 106 (2016) 659–669. https://doi.org/10.1016/j.conbuildmat.2015.12.156.

[62] Kaplanvural, E. Pekşen, K. Özkap, Volumetric water content estimation of C-30 concrete using GPR, Constr. Build. Mater. 166 (2018) 141–146. https://doi.org/10.1016/j.conbuildmat.2018.01.132.

[63] J. Hugenschmidt, R. Loser, Detection of chlorides and moisture in concrete structures with ground penetrating radar, Mater. Struct. 41 (2008) 785–792. https://doi.org/10.1617/s11527-007-9282-5.

[64] Z.W. Coleman, A.K. Schindler, Investigation of ground-penetrating radar defect detection capabilities, influence of moisture content, and optimal data collection orientation in condition assessments of concrete bridge decks, J. Appl. Geophys. 202 (2022) 104655. https://doi.org/10.1016/j.jappgeo.2022.104655.

[65] K. Agred, G. Klysz, J.P. Balayssac, Location of reinforcement and moisture assessment in reinforced concrete with a double receiver GPR antenna, Constr. Build. Mater. 188 (2018) 1119–1127. https://doi.org/10.1016/j.conbuildmat.2018.08.190.

[66] X. Dérobert, J. Iaquinta, G. Klysz, J.P. Balayssac, Use of capacitive and GPR techniques for the non-destructive evaluation of cover concrete, NDT E Int. 41 (2008) 44–52. https://doi.org/10.1016/j.ndteint.2007.06.004.

[67] W. Chen, P. Shen, Z. Shui, Determination of water content in fresh concrete mix based on relative dielectric constant measurement, Constr. Build. Mater. 34 (2012) 306–312. https://doi.org/10.1016/j.conbuildmat.2012.02.073.

[68]   K. Viriyametanont, S. Laurens, G. Klysz, J.P. Balayssac, G. Arliguie, Radar survey of concrete elements: Effect of concrete properties on propagation velocity and time zero, NDT E Int. 41 (2008) 198–207. https://doi.org/10.1016/j.ndteint.2007.10.001.

[69]   Z.M. Sbartaï, S. Laurens, J. Rhazi, J.P. Balayssac, G. Arliguie, Using radar direct wave for concrete condition assessment: Correlation with electrical resistivity, J. Appl. Geophys. 62 (2007) 361–374. https://doi.org/10.1016/j.jappgeo.2007.02.003.

[70]   Z.M. Sbartaï, S. Laurens, J. Balayssac, G. Arliguie, G. Ballivy, Ability of the direct wave of radar ground-coupled antenna for NDT of concrete structures, NDT E Int. 39 (2006) 400–407. https://doi.org/10.1016/j.ndteint.2005.11.003.

[71]   İ. Kaplanvural, K. Özkap, E. Pekşen, Influence of water content investigation on GPR wave attenuation for early age concrete in natural air-drying condition, Constr. Build. Mater. 297 (2021). https://doi.org/10.1016/j.conbuildmat.2021.123783.

[72]   X. Dérobert, G. Villain, Effect of water and chloride contents and carbonation on the electromagnetic characterization of concretes on the GPR frequency band through designs of experiment, NDT E Int. 92 (2017) 187–198. https://doi.org/10.1016/j.ndteint.2017.09.001.

[73]   X. Dérobert, J.F. Lataste, J.P. Balayssac, S. Laurens, Evaluation of chloride contamination in concrete using electromagnetic non-destructive testing methods, NDT E Int. 89 (2017) 19–29. https://doi.org/10.1016/j.ndteint.2017.03.006.

[74]   S.S. Hubbard, J. Zhang, P.J.M. Monteiro, J.E. Peterson, Y. Rubin, Experimental Detection of Reinforcing Bar Corrosion Using Nondestructive Geophysical Techniques, ACI Mater. J. 100 (2003) 501–510. https://doi.org/10.14359/12957.

[75]   R.K. Raju, M.I. Hasan, N. Yazdani, Quantitative relationship involving reinforcing bar corrosion and ground-penetrating radar amplitude, ACI Mater. J. 115 (2018) 449–457. https://doi.org/10.14359/51702187.

[76]   A. Zaki, M.A.M. Johari, W.M.A.W. Hussin, Y. Jusman, Experimental Assessment of Rebar Corrosion in Concrete Slab Using Ground Penetrating Radar (GPR), Int. J. Corros. 2018 (2018). https://doi.org/10.1155/2018/5389829.

[77]   S. Hong, W.L. Lai, R. Helmerich, Experimental monitoring of chloride-induced reinforcement corrosion and chloride contamination in concrete with ground-penetrating radar, Struct. Infrastruct. Eng. 11 (2015) 15–26.

https://doi.org/10.1080/15732479.2013.879321.

[78]   H. Liu, J. Zhong, F. Ding, X. Meng, C. Liu, J. Cui, Detection of early-stage rebar corrosion using a polarimetric ground penetrating radar system, Constr. Build. Mater. 317 (2022) 125768. https://doi.org/10.1016/j.conbuildmat.2021.125768.

[79]   G. Fornasari, L. Capozzoli, E. Rizzo, Combined GPR and Self-Potential Techniques for Monitoring Steel Rebar Corrosion in Reinforced Concrete Structures: A Laboratory Study, Remote Sens. 15 (2023). https://doi.org/10.3390/rs15082206.

[80]   M.E. Said, A.A. Hussein, Induced Corrosion Techniques for Two-Way Slabs, J. Perform. Constr. Facil. 33 (2019). https://doi.org/10.1061/(ASCE)CF.1943-5509.0001299.

[81]   T.A. El Maaddawy, K.A. Soudki, Effectiveness of Impressed Current Technique to Simulate Corrosion of Steel Reinforcement in Concrete, J. Mater. Civ. Eng. 15 (2003) 41–47. https://doi.org/10.1061/(ASCE)0899-1561(2003)15:1(41).

[82]   V. Sossa, V. Pérez-Gracia, R. González-Drigo, M.A. Rasol, Lab non destructive test to analyze the effect of corrosion on ground penetrating radar scans, Remote Sens. 11 (2019). https://doi.org/10.3390/rs11232814.

[83]   W. Zatar, T.T. Nguyen, H. Nguyen, Environmental effects on condition assessments of concrete structures with ground penetrating radar, J. Appl. Geophys. 203 (2022) 104713. https://doi.org/10.1016/j.jappgeo.2022.104713.

[84]   R.M. Jaufer, A. Ihamouten, Y. Goyat, S.S. Todkar, D. Guilbert, A. Assaf, X. Dérobert, A Preliminary Numerical Study to Compare the Physical Method and Machine Learning Methods Applied to GPR Data for Underground Utility Network Characterization, Remote Sens. 14 (2022). https://doi.org/10.3390/rs14041047.

[85]   Q. Cao, L. Abufares, I. Al-Qadi, Development of a Simulation-Based Approach for Cold In-Place Recycled Pavement Moisture-Content Prediction Using Ground-Penetrating Radar, Transp. Res. Rec. 2676 (2022) 682–694. https://doi.org/10.1177/03611981221090933.

[86]   J. Lei, B. Xue, H. Fang, Y. Li, M. Yang, Forward analysis of GPR for underground pipes using CUDA-implemented conformal symplectic euler algorithm, IEEE Access. 8 (2020) 205590–205599. https://doi.org/10.1109/ACCESS.2020.3037811.

[87]   J. Lachowicz, M. Rucka, A novel heterogeneous model of concrete for numerical

modelling of ground penetrating radar, Constr. Build. Mater. 227 (2019) 116703. https://doi.org/10.1016/j.conbuildmat.2019.116703.

[88] J. Lachowicz, M. Rucka, A concept of heterogeneous numerical model of concrete for GPR simulations, 2017 9th Int. Work. Adv. Gr. Penetrating Radar, IWAGPR 2017 - Proc. (2017) 4–7. https://doi.org/10.1109/IWAGPR.2017.7996032.

[89] D. Feng, X. Wang, B. Zhang, Specific evaluation of tunnel lining multi-defects by all-refined GPR simulation method using hybrid algorithm of FETD and FDTD, Constr. Build. Mater. 185 (2018) 220–229. https://doi.org/10.1016/j.conbuildmat.2018.07.039.

[90] Y. Liu, L.X. Guo, FDTD investigation on GPR detecting of underground subsurface layers and buried objects, 2016 IEEE MTT-S Int. Conf. Numer. Electromagn. Multiphysics Model. Optim. NEMO 2016. (2016) 1–2. https://doi.org/10.1109/NEMO.2016.7561622.

[91] C. Warren, A. Giannopoulos, I. Giannakis, gprMax: Open source software to simulate electromagnetic wave propagation for Ground Penetrating Radar, Comput. Phys. Commun. 209 (2016) 163–170. https://doi.org/10.1016/j.cpc.2016.08.020.

[92] A. Giannopoulos, Modelling ground penetrating radar by GprMax, Constr. Build. Mater. 19 (2005) 755–762. https://doi.org/10.1016/j.conbuildmat.2005.06.007.

[93] G. Klysz, J.P. Balayssac, X. Ferrières, Evaluation of dielectric properties of concrete by a numerical FDTD model of a GPR coupled antenna-Parametric study, NDT E Int. 41 (2008) 621–631. https://doi.org/10.1016/j.ndteint.2008.03.011.

[94] X. Núñez-Nieto, M. Solla, A. Novo, H. Lorenzo, Three-dimensional ground-penetrating radar methodologies for the characterization and volumetric reconstruction of underground tunneling, Comput. Chem. Eng. 71 (2014) 551–560. https://doi.org/10.1016/j.conbuildmat.2014.08.083.

[95] P.T.W. Wong, W.L. Lai, Characterization of Complex Dielectric Permittivity of Concrete by GPR Numerical Simulation and Spectral Analysis, J. Nondestruct. Eval. 41 (2022) 1–15. https://doi.org/10.1007/s10921-021-00836-z.

[96] S. Hong, D. Chen, B. Dong, Numerical simulation and mechanism analysis of GPR-based reinforcement corrosion detection, Constr. Build. Mater. 317 (2022). https://doi.org/10.1016/j.conbuildmat.2021.125913.

[97] T. Bourdi, J.E. Rhazi, F. Boone, G. Ballivy, Modelling dielectric-constant values of

concrete: An aid to shielding effectiveness prediction and ground-penetrating radar wave technique interpretation, J. Phys. D. Appl. Phys. 45 (2012). https://doi.org/10.1088/0022-3727/45/40/405401.

[98] T. Bourdi, J.E. Rhazi, F. Boone, G. Ballivy, Application of Jonscher model for the characterization of the dielectric permittivity of concrete, J. Phys. D. Appl. Phys. 41 (2008). https://doi.org/10.1088/0022-3727/41/20/205410.

[99] S. Majchrowska, I. Giannakis, C. Warren, A. Giannopoulos, Modelling Arbitrary Complex Dielectric Properties -- an automated implementation for gprMax, In: 11th Int Work Adv Gr. Penetrating Radar, vol. 10. IWAGPR, Valleta, Malta.

[100] K. Chahine, A. Ihamouten, V. Baltazart, G. Villain, X. Derobert, On the variants of Jonscher's model for the electromagnetic characterization of concrete, in: Proc. XIII Internarional Conf. Gr. Penetrating Radar, IEEE, 2010: pp. 9–14.

[101] H. Zadhoush, A. Giannopoulos, I. Giannakis, Optimising the complex refractive index model for estimating the permittivity of heterogeneous concrete models, Remote Sens. 13 (2021) 1–15. https://doi.org/10.3390/rs13040723.

[102] F. Tsui, S.L. Matthews, Analytical modelling of the dielectric properties of concrete for subsurface radar applications, Constr. Build. Mater. 11 (1997) 149–161. https://doi.org/10.1016/S0950-0618(97)00033-0.

[103] W.L. Lai, X. Dérobert, P. Annan, A review of Ground Penetrating Radar application in civil engineering: A 30-year journey from Locating and Testing to Imaging and Diagnosis, NDT E Int. 96 (2018) 58–78. https://doi.org/10.1016/j.ndteint.2017.04.002.

[104] F. Tosti, C. Ferrante, Using Ground Penetrating Radar Methods to Investigate Reinforced Concrete Structures, Surv. Geophys. 41 (2020) 485–530. https://doi.org/10.1007/s10712-019-09565-5.

[105] S. Abu Dabous, S. Feroz, Condition monitoring of bridges with non-contact testing technologies, Autom. Constr. 116 (2020). https://doi.org/10.1016/j.autcon.2020.103224.

[106] Clarivate Analytics Web of Science. Available online: www.webofknowledge.com (accessed on 30 October 2020).

[107] Science Direct Scopus. Available online: https://www.scopus.com (accessed on 30 October 2020).

[108] ASTM D6087-08, Standard Test Method for Evaluating Asphalt-Covered Concrete Bridge Decks Using Ground Penetrating Radar, (2008) 1790–1793. https://doi.org/10.1520/D6087-08.1.

[109] K. Dinh, N. Gucunski, J. Kim, T.H. Duong, Understanding depth-amplitude effects in assessment of GPR data from concrete bridge decks, NDT E Int. 83 (2016) 48–58. https://doi.org/10.1016/j.ndteint.2016.06.004.

[110] S. Pashoutani, J. Zhu, Ground Penetrating Radar Data Processing for Concrete Bridge Deck Evaluation, J. Bridg. Eng. 25 (2020). https://doi.org/10.1061/(ASCE)BE.1943-5592.0001566.

[111] I. Geophysical Survey Systems, RADAN 7 Manual, Geophysical Survey Systems, Inc., New Hampshire.

[112] N. Martino, K. Maser, R. Birken, M. Wang, Determining ground penetrating radar amplitude thresholds for the corrosion state of reinforced concrete bridge decks, J. Environ. Eng. Geophys. 19 (2014) 175–181. https://doi.org/10.2113/JEEG19.3.175.

[113] N. Martino, K. Maser, R. Birken, M. Wang, Quantifying Bridge Deck Corrosion Using Ground Penetrating Radar, Res. Nondestruct. Eval. 27 (2016) 112–124. https://doi.org/10.1080/09349847.2015.1067342.

[114] T. Dawood, Z. Zhu, T. Zayed, Deterioration mapping in subway infrastructure using sensory data of GPR, Tunneling Undergr. Sp. Technol. 103 (2020). https://doi.org/10.1016/j.tust.2020.103487.

[115] N. Gucunski, B. Basily, J. Kim, T. Duong, A. Maher, K. Dinh, H. Azari, H. Ghasemi, Assessing Condition of Concrete Bridge Decks by Robotic Platform RABIT for Development of Deterioration and Predictive Models, in: 8th Int. Conf. Bridg. Maintenance, Saf. Manag., Foz do Iguacu, Brazil, 2016.

[116] H.M. La, N. Gucunski, S.H. Kee, L. Van Nguyen, Data analysis and visualization for the bridge deck inspection and evaluation robotic system, Vis. Eng. 3 (2015). https://doi.org/10.1186/s40327-015-0017-3.

[117] D.J. Clem, T. Schumacher, J.P. Deshon, A consistent approach for processing and interpretation of data from concrete bridge members collected with a hand-held GPR device, Constr. Build. Mater. 86 (2015) 140–148. https://doi.org/10.1016/j.conbuildmat.2015.03.105.

[118] J. Xu, L. Jiang, W. Wang, Y. Jiang, Influence of CaCl2 and NaCl from different sources on chloride threshold value for the corrosion of steel reinforcement in concrete, Constr. Build. Mater. 25 (2011) 663–669. https://doi.org/10.1016/j.conbuildmat.2010.07.023.

[119] International Federation for Structural Concrete (fib), Model Code for Service Life Design, Lausanne, 2010.

[120] B. Minasny, Microwave dielectric behavior of wet soils, 2006. https://doi.org/10.1016/j.geoderma.2005.08.001.

[121] S. Soldatov, M. Umminger, A. Heinzel, G. Link, B. Lepers, J. Jelonnek, Dielectric characterization of concrete at high temperatures, Cem. Concr. Compos. 73 (2016) 54–61. https://doi.org/10.1016/j.cemconcomp.2016.01.006.

Biography

Ksenija Tešić was born on 27 November 1995 in Užice, Republic of Serbia. She graduated from the primary school "Petar Leković" in Požega in 2010 and enrolled in the science and mathematics module of the secondary school "Sveti Sava" in Požega in the same year.

In the academic year 2014/2015, she enrolled in undergraduate studies at the Faculty of Civil Engineering at the University of Belgrade, majoring in Civil Engineering, Structural Engineering module. In 2018, she obtained the academic title of Civil Engineer and defended her thesis entitled "Reinforced concrete structure project of a multi-storey residential and commercial building (P0 + Pr + 8)" under the supervision of Assoc. Prof. Branko Milosavljević at the Department of Concrete Structures. In the same year, she enrolled for a Master's degree at the Faculty of Civil Engineering, University of Belgrade, majoring in Civil Engineering, Structural Engineering module. She obtained the academic title of Master Civil Engineer in 2020 by defending her Master's thesis entitled "The influence of cement replacement with limestone filler on the properties of concrete" under the supervision of Full Prof. Snežana Marinković at the Department of Concrete Structures.

On 16 October 2020, she enrolled in a PhD programme at the Faculty of Civil Engineering, University of Zagreb, specialising in Materials in Civil Engineering (student ID 494, researcher ID: 384973), under the supervision of Assoc. Prof. Ana Baričević, and Full Prof. Nenad Gucunski.

In the period from October 2018 to June 2019, she worked as a student assistant at the Department of Concrete Structures, Faculty of Civil Engineering University of Belgrade. She participated in teaching the courses Concrete Structures 1 and Theory of Concrete Structures 2. From July 2020 to the present she has been employed as an assistant at the Department of Materials, Faculty of Civil Engineering, University of Zagreb.

Within her scientific work, she published independently and in co-authorship six scientific papers in journals, one chapter in a university monograph, nine scientific papers and five abstracts in conference proceedings.

Journal Publications

1) K. Tešić, A. Baričević, M. Serdar, Non-Destructive Corrosion Inspection of Reinforced Concrete Using Ground-Penetrating Radar: A Review, Materials (Basel). 14 (2021). https://doi.org/10.3390/ma14040975.

2) K. Tešić, A. Baričević, M. Serdar, Comparison of cover meter and ground penetrating radar performance in structural health assessment: case studies, Građevinar. 73 (2021) 11, pp. 1131-1144. https://doi.org/10.14256/JCE.3323.2021.

3) K. Tešić, S. Marinković, A. Savić, Influence of cement replacement with limestone filler on the properties of concrete, Building Materials and Structures. 64 (2021), 3; pp. 165-170. https://doi.org/0.5937/GRMK2103165T.

4) K. Tesic, A. Baricevic, M. Serdar, N. Gucunski, Characterization of ground penetrating radar signal during simulated corrosion of concrete reinforcement, Autom. Constr. 143 (2022) 104548. https://doi.org/10.1016/j.autcon.2022.104548.

5) K. Tesic, A. Baricevic, M. Serdar, N. Gucunski, Quantifying the impact of parameters of chloride-induced reinforcement corrosion on the GPR signal, Constr. Build. Mater. 399 (2023) 132594. https://doi.org/10.1016/j.conbuildmat.2023.132594.

6) K. Tesic, A. Baricevic, M. Serdar, N. Gucunski, Electromagnetic property selection for GPR modelling in corrosive concrete environments, Dev. Built Environ. (2023) 100302. https://doi.org/10.1016/j.dibe.2023.100302.

Conference Publications

1) K. Tešić, A. Baričević, M. Serdar, Condition assessment of concrete structures using ground penetrating radar (GPR). 6th Symposium on Doctoral Studies in Civil Engineering, Štirmer, Nina (ed.). Zagreb, 2020. pp. 197-207.

2) K. Tešić, A. Baričević, M. Serdar, Case Study on Application of Ground-Penetrating Radar for Non-Destructive Assessment of Historical Building. 1st Croatian Conference on Earthquake Engineering 1CroCEE Zagreb, Hrvatska, 2021. pp. 763-772.

3) K. Tešić, S. Marinković, A. Savić, Uticaj zamene cementa krečnjačkim filerom na svojstva betona. Zbornik radova sa nacionalnog simpozijuma DGKS Aranđelovac, Srbija, 2021. str. 218-227.

4) K. Tešić, S. Ereiz, A. Baričević, M. Serdar, M. Bartolac, I. Duvnjak, Autonomni sistemi za pregled mostova. Zbornik radova sa nacionalnog simpozijuma DGKS Aranđelovac, Srbija, 2021. str. 250-258.

5) K. Tešić, A. Baričević, M. Serdar, Influence of corrosion-induced damage in reinforced concrete on GPR signal parameters. 7th Symposium on Doctoral Studies in Civil Engineering, Štirmer, Nina (ed.). Zagreb, 2021. pp. 35-44.

6) K. Tešić, A. Baričević, M. Serdar, I. B. Pečur, Ground Robotic Systems for the Inspection of Concrete Bridges. MIPRO 2021 44th International Convention Proceedings Rijeka, 2021. pp. 1301-1305.

7) K. Tešić, M. Božić, M. Švaco, A. Baričević, B. Jerbić, M. Serdar, Prototyping of a Wall-climbing Robot for the Inspection of Concrete Bridges. 15th International Scientific Conference iNDiS Planning, Design, Construction and Building Renewal Proceedings. Radonjanin, V; Vukobratović, V; Lukić, I (eds.). Novi Sad, 2021. pp. 347-352.

8) K. Tešić, A. Baričević, M. Serdar, Identifying the capitabilities of ground penetraing radar in structural condition assessment. X. skup mladih istraživača iz područja građevinarstva i srodnih tehničkih znanosti: Zajednički temelji 2023 – uniSTem. Split, 2023. doi: 10.31534/10.ZT.2023.05.

9) K. Tešić, A. Baričević, M. Serdar, Assessment of concrete structures using ground penetrating radar (GPR): Main findings of the ASAP project. 16th International Scientific Conference iNDiS Planning, Design, Construction and Building Renewal Proceedings. Novi Sad, 2023.

Publications

Paper I

K. Tešić, A. Baričević, M. Serdar, Non-Destructive Corrosion Inspection of Reinforced Concrete Using Ground-Penetrating Radar: A Review, Materials (Basel). 14 (2021). https://doi.org/10.3390/ma14040975

Review

Non-Destructive Corrosion Inspection of Reinforced Concrete Using Ground-Penetrating Radar: A Review

Ksenija Tešić, Ana Baričević * and **Marijana Serdar**

Department of Materials, Faculty of Civil Engineering, University of Zagreb, 10000 Zagreb, Croatia;
ksenija.tesic@grad.unizg.hr (K.T.); marijana.serdar@grad.unizg.hr (M.S.)
***** Correspondence: ana.baricevic@grad.unizg.hr

Abstract: Reduced maintenance costs of concrete structures can be ensured by efficient and comprehensive condition assessment. Ground-penetrating radar (GPR) has been widely used in the condition assessment of reinforced concrete structures and it provides completely non-destructive results in real-time. It is mainly used for locating reinforcement and determining concrete cover thickness. More recently, research has focused on the possibility of using GPR for reinforcement corrosion assessment. In this paper, an overview of the application of GPR in corrosion assessment of concrete is presented. A literature search and study selection methodology were used to identify the relevant studies. First, the laboratory studies are shown. After that, the studies for the application on real structures are presented. The results have shown that the laboratory studies have not fully illuminated the influence of the corrosion process on the GPR signal. Also, no clear relationship was reported between the results of the laboratory studies and the on-site inspection. Although the GPR has a long history in the condition assessment of structures, it needs more laboratory investigations to clarify the influence of the corrosion process on the GPR signal.

1. Introduction

Every structure, depending on its intended purpose, must be designed and constructed so that during its lifecycle it fulfils the basic requirements for structures and other requirements, namely, the conditions prescribed by the Building Act [1]. Unfortunately, experience has shown that a large number of concrete structures show significant signs of degradation after only 20 to 30 years due to the joint action of mechanical and environmental effects [2]. The causes of degradation are mainly the consequence of corrosion, which on a global scale increases the annual maintenance costs to more than 3% of the world's Gross Domestic Product (GDP) [3]. The maintenance and strengthening of bridges in Europe alone require £215 million, not including the costs of redirection and organization of traffic [4]. The unsystematic approach to maintenance, especially of infrastructure, contributes to its premature deterioration and has a negative impact on safety and reliability. Particularly worrying is the fact that today, the resources invested in maintenance and repair are higher than the cost of construction [5]. The question therefore arises: how to stop or delay the degradation of global infrastructure?

The concern resulting from the problems outlined led to the development of strategies to mitigate the consequences of the corrosion process. At the design level, strategies are mainly aimed at improving the durability properties of the concrete cover in terms of its thickness and quality [6]. Other strategies aim at the preventive use of corrosion inhibitors, corrosion-resistant steel or other surface treatments [7–9]. However, these have limited ability to solve the corrosion problem of existing structures.

One of the most promising approaches to delay the degradation of existing structures is the extensive use of non-destructive techniques (NDT). Increased inspection frequency

and coverage of larger inspection areas could lead to timely detection of deterioration and, in sum, better decisions in the maintenance of the structure. In this regard, the progress in the development of NDT methods towards visualization of results leads to the increased use of advanced NDT methods in the future [10]. Many NDT methods are currently available; however, this paper focuses on the application of ground-penetrating radar (GPR) for corrosion inspection of reinforced concrete structures.

Originally, the radar was designed for military use [11]. Today, its application has expanded to various disciplines, such as civil engineering, hydrogeology, archaeology, etc. [12,13]. When combined with other non-destructive methods, it is feasible for evaluating the condition assessment of the concrete structures [14,15] with increased effectiveness and speed of inspection. The laboratory investigations have shown that the corrosion process could be monitored based on observing the changes in the GPR signal [16–20]. Moreover, GPR has a history in the assessment of corrosion and corrosion-related pathologies for on-site inspection [21–25]. The main difference between these two approaches is that the laboratory investigation was mainly focused on discrete corrosion characterization. The on-site investigation is based on the observation of several simultaneous effects, namely the variation of moisture, chlorides, and the formation of corrosion products and cracks.

Previous studies have focused on reviewing the general application of GPR in civil engineering [26,27] or have focused on on-site inspection for a specific type of construction [28]. To date, there is no comprehensive critical study that evaluates the use of GPR for corrosion assessment of reinforced concrete. The main objective of this review paper is to identify all relevant publications on corrosion assessment of reinforced concrete using ground-penetrating radar. The authors have attempted to gain more understanding of the relationship between laboratory testing and the application of GPR on-site. This prompted the authors to organize the paper into the following sections. Section 2 presents the details of the literature search in terms of the databases used, the search terms and the rationale for the publication screening. Section 3 deals with the main topic. It is introduced with the corrosion process and the main principles of GPR, presenting the characteristics for corrosion monitoring. Furthermore, it is divided into sections dealing with laboratory and on-site inspections, with each section ending with conclusions. Finally, Section 4 summarizes the work with recommendations for future studies.

2. Methodology

As a first step, a systematic literature search was conducted. Relevant studies were searched in the databases of Web of Science [29] and Scopus [30] over a period between 1 January 2000 and 30 October 2020. Initially, the authors began the search with the terms [(ground penetrating radar OR GPR) AND (corrosion) AND (concrete)]. The authors found that a number of studies for on-site assessment of concrete structures using GPR were excluded. They suggest that this is because some of the studies looked at the causes and consequences of corrosion (e.g., delamination), and it appears that the term corrosion was not appropriate in this case. For this reason, the term deterioration was included in the database search. The authors found that the terms [(ground penetrating radar OR GPR) AND (corrosion OR deterioration) AND (concrete)] expanded the number of studies so that a better overview of GPR application could be created. Duplicates were then removed, and the authors briefly reviewed titles and abstracts and excluded studies that did not meet the following criteria: (a) the study is published in English, (b) the full version of the study is available to the authors and (c) GPR was used to evaluate reinforcement corrosion and corrosion consequences (e.g., studies in which GPR was used only to determine cover thickness were excluded). Full-text articles were obtained, and further selection excluded studies that were not relevant or were beyond the scope. The final selection included 69 studies. Figure 1 shows the steps described.
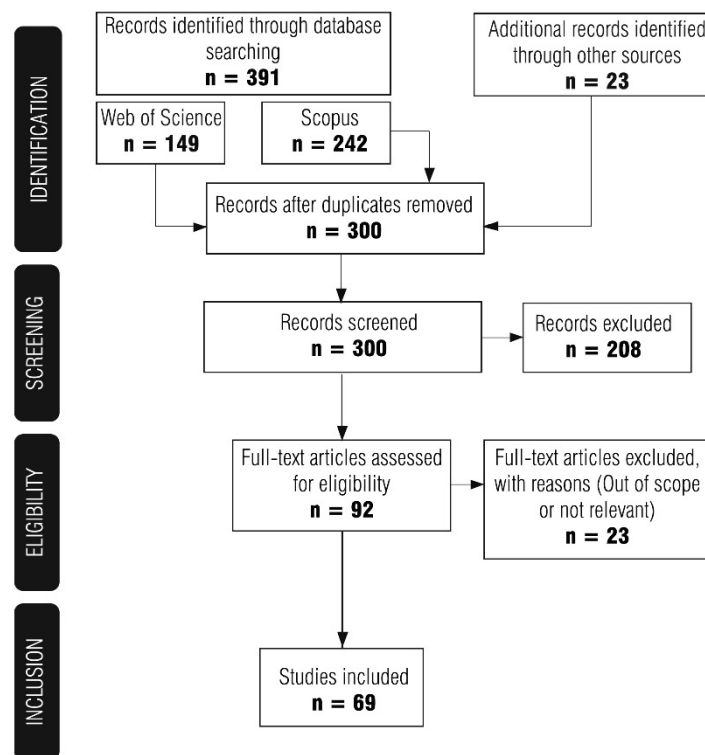
Figure 1. Steps in the review process for the selection of articles.

3. Corrosion Monitoring Using Ground-Penetrating Radar

As mentioned earlier, the main causes of degradation are mainly the result of corrosion of reinforcement [31]. The corrosion of steel in concrete is a balanced electrochemical mechanism [32] between anodic and cathodic reactions that occur on the surface of the reinforcing steel. The anodic reaction, the oxidation of iron, occurs in an environment where the protective passive film of steel is not stable. The instability of the protective layer is related to the changes in the surrounding concrete and the main cause of these changes are processes such as chloride penetration or carbonation [32,33]. The time required for the breakdown of the passive film is called the initiation period in Tuutti's corrosion model [34]. The further development of corrosion is called the propagation period and involves crack initiation, as a result of expansive stresses around the bar induced by rust formation. The progressive corrosion leads to spalling of the concrete and reduction of the cross-section of the reinforcement, which may compromise the load-bearing capacity of the structure [35]. Most corrosion assessment techniques are electrochemical-based [36,37]. In the field assessment of corrosion probability, the half-cell potential (HCP) and electrical resistivity (ER) are most used.

The description of the half-cell method and interpretation of the results are given in ASTM C876 [38] and RILEM recommendations [37]. The Wenner probe is commonly used to determine the electrical resistivity [39,40]. The resistivity values can be used to estimate the corrosion risk [41]. Although these methods have long been used successfully in the condition assessment of concrete structures, they have some drawbacks. The half-cell potential is a semi-destructive technique, so it requires a connection to the reinforcement. This is a limitation when a large area is to be inspected. Measuring electrical resistivity does not provide information about the reinforcement, only about the corrosive environment. Also, large areas require a lot of time for inspection. These issues can be overcome by using GPR.

Ground-penetrating radar is a non-destructive technique that emits electromagnetic waves into the material, with the main objective of locating the buried objects underneath the surface [12]. Nowadays, its scope broadens to a wide range of materials, and among

others is concrete [26]. The emitted electromagnetic wave propagates through the host material, as far as it encounters an interface between different materials, whereupon it is reflected back. The predominant types of GPR antennas used for civil engineering investigations are air-coupled and ground-coupled. The second type implies contact of the antenna with the ground and has a better penetration depth. The reflected wave is recorded with the receiving antenna and the recording is called an A-scan (Figure 2, right). When a wave is transmitted, the receiver first records a direct wave propagating through the air from the transmitter to the receiver. Then, a portion of the electromagnetic wave is reflected off the surface of the material. In a ground-coupled system, these two components superimpose to form the wave, called direct coupling, Figure 2. The rest of the wave energy passes through the material until it reaches the material with different dielectric properties. The electromagnetic wave is then reflected, and the receiver records it as a reflected wave. Therefore, the attributes of the A-scan that provide information about the target are the amplitude of the reflected wave and the travel time from the transmitter to the receiver. In addition, the most common representation of the results obtained with GPR is a B-scan, the two-dimensional slice that represents the area under investigation along the line.
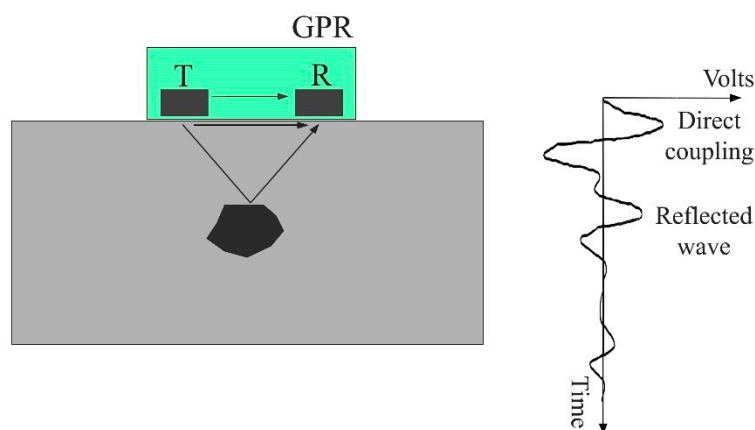

Figure 2. Recorded signals for ground-coupled antenna.

The strength of the reflected wave depends on the properties of the host material. The properties that determine the behavior of electromagnetic waves in the material are its dielectric properties—dielectric permittivity (ε) and electrical conductivity (σ) [42]. Signal losses are mainly due to electrical conduction and dielectric relaxation [43]. Electrical conduction arises from the motion of free charges, while dielectric relaxation arises from the rotation of polar molecules. At the microscopic scale, friction occurs between particles due to these motions, resulting in energy dissipation. In summary, the propagation behavior of electromagnetic waves strongly depends on the composition of the pore solution. Changes in dielectric properties can be expected in the presence of moisture and/or chlorides in the concrete. The presence of water molecules and chlorides in pores results in an overall loss of energy and signal [43–45]. However, this attenuation is primarily caused by the presence of chlorides in the pore solution [46] as a result of the increased electrical conductivity of concrete. Changes in the concrete microstructure caused by carbonation can also affect the GPR response. The most noticeable ones are due to a reduction in porosity and ion exchange in the pore solution. It has been reported that carbonation causes a decrease in the dielectric permittivity, resulting in reduced attenuation [47].

3.1. Laboratory Simulated Corrosion Inspection

Corrosion assessment using ground-penetrating radar is still a novel approach, therefore only a limited number of studies have been conducted under laboratory conditions (Table 1). There are many challenges to ensure a suitable experimental setup for such a study, starting with the criteria for corrosion initiation, corrosion monitoring and corrosion

probability assessment. In order to simulate natural corrosion under laboratory conditions, various techniques are often used to accelerate the process, such as impressed current technique, artificial climatic environment, accelerated migration tests, etc. [48]. The most commonly used method for corrosion acceleration is the impressed current technique, which is based on exposing the embedded reinforcement to the electric current provided by an external power supply. The current density and exposure time are controlled to achieve different degrees of corrosion [49,50]. Besides, corrosion can be enhanced by creating favorable conditions such as high temperature, high humidity and cycles of wetting–drying [51]. Even if these methods tend to simulate corrosion well, it is inevitable that the artificial conditions for corrosion to occur will differ from natural conditions. Recognition of these limitations is important to ensure adequate correlation between accelerated corrosion investigations and on-site corrosion assessments using GPR. Therefore, Table 1 summarizes the corrosion probability studies conducted to date that consider both corrosion acceleration methods and GPR signal attributes analysis. Two experimental setups were found: (a) GPR attributes acquired before and after the corrosion process, and (b) GPR attributes monitored during the corrosion acceleration process. The second setup is more significant as it ensures information about the different stages of corrosion, starting from the depassivation of the steel to the appearance of cracks.

Table 1. Previous laboratory investigations on the influence of corrosion on the ground-penetrating radar (GPR) attributes.

Study	Year	Technique for Accelerated Corrosion Test	Method of Acquiring GPR Attributes	Current Density, i ($\mu A/cm^2$)	Dimension of Specimens (m)	GPR (GHz) [1]
Hubbard et al. [16]	2003	Impressed current technique	Before and after corrosion acceleration	-	$1.25 \times 1 \times 0.25$	1.2
Raju et al. [53]	2018			-	$0.76 \times 0.38 \times 0.203$	2.6
Zaki et al. [54]	2018			-	$1 \times 0.5 \times 0.2$	2
Lai et al. [56]	2010		Monitoring during corrosion acceleration	-	$1.5 \times 0.5 \times 0.5$	1.5 and 2.6
Zhan et al. [57]	2011			165,000	$0.45 \times 0.14 \times 0.135$	1
Lai et al. [58]	2011			340	-	1.5 and 2.6
Lai et al. [17]	2013			260 and 760	$1.5 \times 0.5 \times 0.5$	1.5 and 2.6
Hong et al. [18]	2014			424	$1.5 \times 1.5 \times 0.3$	2.6
Hong et al. [19]	2015			125	$0.8 \times 0.8 \times 0.24$	2.6
Wong et al. [20]	2019			650 [2]	$0.548 \times 0.4 \times 0.15$	2
Hasan et al. [55]	2016	Corroded rebars immersed in emulsion	Before and after corrosion acceleration	-	Water oil emulsions	2.6
Sossa et al. [52]	2019	Corroded rebars cast in concrete		-	$0.3 \times 0.08 \times 0.08$	1.6
		Curing chamber		-	$0.3 \times 0.2 \times 0.07$	

[1.] All of the antennas are ground-coupled. [2.] Level of current density was lowered in the latter stage of experiment.

One of the first studies to have acknowledged the GPR potential for corrosion detection was published in 2003 by Hubbard et al. [16]. The rebar was subjected to an accelerated corrosion process for 10 days. The results showed that corrosion causes a reduction in amplitude, which they attributed to the scattering and attenuation of waves due to the

roughness at the corroded interface between concrete and rebar. This was also confirmed in Reference [52], where the amplitude of the signal was also reduced in specimens where the previously corroded bar was cast in concrete. To extend these observations, additional specimens were subjected to an accelerated corrosion process in an environmental chamber at different corrosion levels. It was found that corrosion causes a decrease in amplitude for each corrosion level. This is explained by the signal scattering in the concrete cover zone caused by the presence of cracks, corrosion products and the roughness of the corroded bar. In Reference [53], the influence of the diameter of the anode bar on the signal reflection was also observed. The increase in amplitude was associated with corrosion development but was also increased with the increase in diameter. In contrast, Reference [54] attributed lower amplitudes to the presence of corrosion products, but also indicated that the decrease could be influenced by the accumulation of chlorides in the concrete cover zone.

In Reference [55], concrete properties were simulated by oil emulsions with different dielectric permittivity, where corroded bars were immersed in the emulsions. However, in such an experimental setup, all results are based on the theories and therefore cannot faithfully represent real structures.

3.1.1. Long-Term Corrosion Monitoring

Long-term monitoring of corrosion may ensure a better understanding of its effect on GPR signal attributes. Several studies [17–20,56–58] have been conducted to distinguish and correlate significant attributes of corrosion development and GPR signal. The conclusions from these studies are divided into: (1) initiation phase, (2) formation of cracks and (3) spalling of concrete cover.

Initiation Phase

The application of electrical current in the accelerated corrosion process induces the faster motion of chloride ions due to the electrical potential gradient, and this mechanism is called migration [32]. As this process thrives, a decrease in GPR amplitude is reported by Lai et al. [17]. According to the authors' assertation, the accumulation of chloride ions around the anode absorbs the energy of the electromagnetic wave, which also causes the delay of the wave.

Formation of Cracks

After the initiation phase, the researchers had noticed a steady trend of change in the signal's attributes until the wide crack is visible on the concrete surface. This phase is characterized by the formation of corrosion products that migrate into the surrounding concrete. The increased amplitude of the reflected wave was reported in Reference [57]. The rebars were subjected to external power supply until a longitudinal crack was visible on the concrete surface. The authors claimed that the migration of corrosion products into the shallower concrete cover zone enlarges the intersection points of the signal with different interfaces—concrete, microcracks, corrosion products—and leads to the increased amplitude. This was also confirmed in References [17,56,58]. In Reference [18], the experiment was set up to exclude the effects of moisture and chlorides on the GPR signal. The specimens were stored for two months to achieve stable moisture and chloride content before accelerated corrosion. Here, the increased amplitude of the GPR signal was then attributed to the effect of corrosion only. This was also outlined in Reference [20].

Spalling

In addition to the effect of corrosion development on the GPR amplitude, the effect of crack propagation and the occurrence of wide cracks on the amplitude of the GPR signal was also noted by Lai et al. [56]. A decrease in amplitude was observed after the occurrence of a wide longitudinal crack. This was explained by the scattering of signal energy caused by additional irregularities when a wide crack propagates through the concrete cover. The

extension of the experimental setup was presented in Reference [20] to obtain a better representation of the crack influence on the signal amplitude.

3.1.2. Conclusions from Laboratory Simulated Corrosion Inspection

The corrosion process can be divided into the initiation and propagation phases, with each phase having specific effects on concrete microstructures. From the long-term corrosion monitoring experiments, the influence of corrosion promotion on GPR attributes was summarized, as in Figure 3.
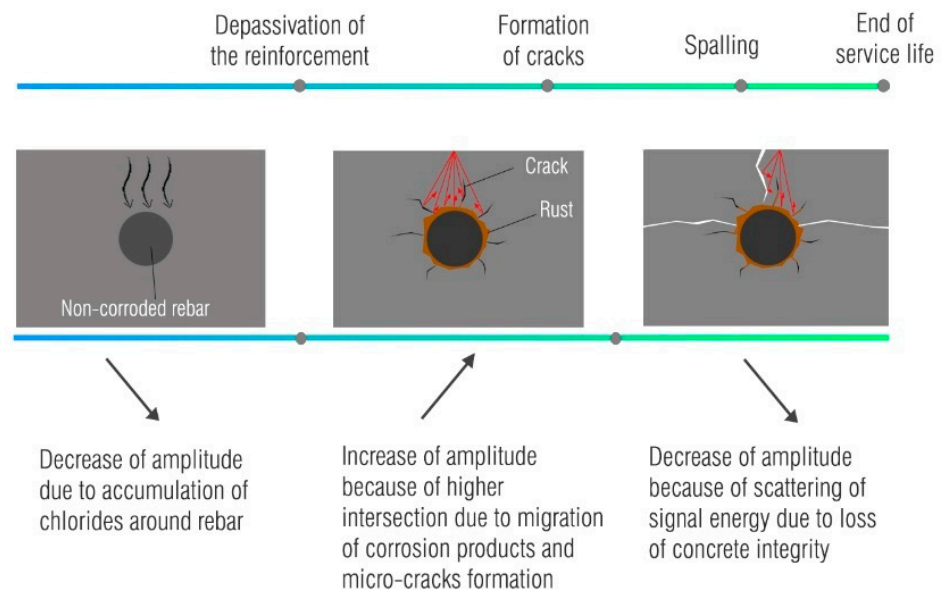

Figure 3. Changes in the GPR signal during corrosion process.

The effects shown in Figure 3 are determined by the accelerated corrosion processes, in particular the formation of corrosion products on the surface of the reinforcing bar, their diffusion into the concrete cover and thus, crack propagation. These effects modify the amplitude in terms of different reflection coefficient and different dielectric properties of the concrete cover. The ability of corrosion products to migrate depends on the moisture content in the concrete cover since their movement is favored in the presence of moisture [59]. Similarly, the ability of their migration depends on the duration of the acceleration process. When accelerated corrosion with high current density is established in a short timeframe, it leads to increased crack width due to the sudden accumulation of corrosion products and increased pressure around the reinforcement [50,60]. Therefore, an appropriate current density should be selected to ensure the best possible simulation of natural conditions still within a reasonable timeframe [50,61].

The results of these studies also indicate that laboratory simulated corrosion studies mentioned above do not provide relevant results unless the level of corrosion is properly described. In these studies, results were recorded before and after corrosion acceleration and conflicting results were reported. Some authors reported higher amplitudes at the end of the experiments, while others reported lower amplitudes. Since these studies differ in terms of experiments setup, corrosion level and induced damage, it is possible that the observed changes in the GPR signal were recorded during different stages of the corrosion processes.

3.2. On-Site Corrosion Inspection

Most of the published research focuses on the application of GPR to the assessment of bridge decks, while other structures are represented to a lesser extent (tunnels, buildings, wharves, etc.). In terms of geographic location, most studies using GPR are conducted in

the United States of America. The authors are sure that this is also a consequence of the existence of relevant standards [62].

The use of ground-penetrating radar data for condition assessment of concrete bridges dates back to the early 1980s [63]. The amplitude of the ground-penetrating radar signal during an inspection is affected by the presence of structural elements, variations in cover depth, moisture, chlorides [22,64,65] and other variables. Therefore, a simple approach to evaluating changes in the GPR signal is not practical. Coexisting influences with other phenomena, such as variations in moisture and chlorides, are unavoidable and prevent the development of methods for direct location of corroded rebar. Therefore, indirect methods are used in which the localization of corroded areas is correlated with the areas of high signal attenuation. Attenuation has been found to be strongly related to the increased conductivity around the rebar [22] caused by the accumulated chloride ions and corrosion products [25].

The inspection of concrete piers and wharves is very similar to the inspection of bridge decks where moisture and chlorides are the main causes of deterioration. The use of ground-penetrating radar has also been reported in the inspection of tunnels. It was noted that the complicated design and compound deterioration mechanisms of these structures made a simple corrosion assessment impossible. Instead, the data was used to assess the overall condition.

Quantification of attenuation can be determined by numerical analysis of the signal or by visual analysis of B-scans. These are discussed in more detail in the following sections.

3.2.1. Numerical Analysis of GPR Attributes

The ASTM standard [62] for the evaluation of concrete bridge decks using ground-penetrating radar proposes two procedures for numerical analysis using GPR data. The first procedure is based on considering the reflection amplitude from the bridge deck bottom and the bridge deck surface. The second procedure considers the reflection amplitudes from the top reinforcement layer. In most cases, the reflection amplitudes from the top reinforcement are considered for corrosion evaluation. The amplitude is derived from the A-scan.

Numerical analysis is usually performed by normalizing the amplitude, which represents the deterioration rate, and is calculated as follows [66]:

$$\text{Normalized amplitude[dB]} = -20\log\frac{\text{signal amplitude}}{\text{reference signal amplitude}} \tag{1}$$

The signal amplitudes are compared to the reference signal amplitude which is usually the amplitude with the lowest degree of attenuation and represents sound concrete [66]. The GSSI [67] suggests 32,767 for 16-bit data and 2,147,483,648 for 32-bit data as the reference signal amplitude. This approach may be inconvenient when a concrete structure is in an advanced stage of deterioration and high attenuation is primarily detected. The differences between amplitudes are then smaller and the deterioration could be underestimated [68,69]. On the other hand, if the structure is in a relatively good condition, the attenuation may be misinterpreted. In this case, the attenuation could come from a different source, namely the variation of the concrete cover thickness. In such cases, it is recommended to consider the whole amplitude and not only the attenuation zones [70]. Other approaches have also been used, with Dinh et al. [25] using the average direct coupling wave as the reference amplitude. According to Pashoutani et al. [71], the use of a constant value of a reference amplitude does not take into account the contribution of concrete surface quality to the signal amplitude, even to the normalized amplitude. Therefore, a normalization procedure was proposed in which each signal amplitude is normalized to its own direct coupling amplitude. In order to eliminate the influence of the cover depth variation on the signal amplitude, Barnes et al. [21] demonstrated an amplitude correction method. It was shown that subtracting the depth-dependent amplitude loss gives a better correlation of ground-penetrating radar amplitude maps with ground truth results than maps without correction.

The method is based on determining the linear-dependent function of signal loss from the two-way travel time (TWTT) for the 90th percentile value of normalized amplitude. The 90th percentile value of the normalized amplitude is supposed to represent the sound concrete where the attenuation is mainly caused by the propagation of the signal through the dielectric material, i.e., the dielectric loss [25]. After correction of the amplitude, the attenuation should represent the signal loss due to chloride and moisture, i.e., the conductive loss. The method was improved after it was found that the conductive loss was also depth-dependent, so that an additional correction was necessary [25]. Two automated methods for depth correction have also been proposed [72]. In these studies, the correction was performed at the two-way travel time level. A more accurate correction could be performed if the linear function is determined using the real reinforcement depth instead of the two-way travel time [71]. This procedure requires the determination of the real velocities of the signal.

Obviously, it is of interest to establish a threshold for attenuation that is suitable for identifying the area of deterioration. However, a universally applicable threshold has not been established. It is usually based on the experience of the analyst and is related to a specific case [21]. There have been several attempts to relate the attenuation, mostly in comparison with thresholds of other methods. In References [73–76], ground-penetrating radar data were correlated with half-cell potential data, with the aim of determining the threshold value of attenuation. In Reference [75], the ROC (Receiver Operating Characteristic) curve was used, and in Reference [76], the author used statistical parameters to obtain the threshold value. In the second paper, the relationship between the percentage of corroded area, based on the results obtained with the half-cell potential at several bridges, and the product of the mean and skewness of the amplitude of the ground-penetrating radar, was established. The relationship can be used to predict the corroded area based on the analysis of the statistical parameters of the amplitudes. In some studies [77,78], the k-means clustering method was used to determine thresholds values.

Numerical analysis is generally used to obtain the deterioration map, which in most cases is the spatial distribution of normalized amplitudes. The main steps of the numerical approach in the condition assessment of concrete bridge decks are shown in Figure 4. The ability of the numerical approach to provide autonomous assessment of concrete structures using GPR is one of the reasons for its predominant use, while the algorithms for automatic reinforcement selection can be found in References [79,80].
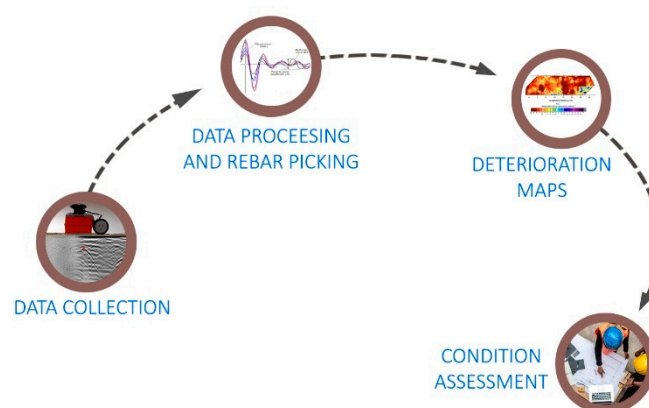

Figure 4. Numerical approach in condition assessment of concrete bridge decks.

The results obtained by periodical inspections can be collected in databases, so that the correlation of successive data allows continuous monitoring of the progress of deterioration. Dinh et al. [65] also proposed a method based on comparing the complete waveform (amplitudes and shapes of the electromagnetic wave) at a point with baseline data. The advantage of this method is that it excludes non-corrosion attenuation causes. However, baseline data is required for proper detection of deterioration, which is often not available.

The method was improved in Reference [81] and the waveform was compared with the simulated waveform. The simulated waveform has the original direct wave, but it has no reflected wave, so it simulates full attenuation. The higher similarity with the simulated wave correlates with a higher degree of deterioration. Hong et al. [82] proposed a method to monitor the corrosion process by comparing different GPR data using the image registration technique.

Despite the deterioration maps, the statistical distribution of amplitudes had shown the relationship with the condition of the structure. In Reference [83], where several bridges with different environmental conditions were observed, it was found that after correcting the amplitude depth, the distribution of the amplitude of the sound deck was symmetrical with high kurtosis. In contrast, severely damaged concrete exhibited higher dispersion of amplitude distribution with lower value of kurtosis. This statistical dependence has been previously confirmed [74]. An automated crack tracking method based on the analysis of the processed amplitude of the ground-penetrating radar was presented in Reference [84]. The model considers the amplitude compared with the threshold value. The final result of the model is a three-dimensional (3D) visualization of the cracks, which provides the possibility to evaluate their geometry. However, the reliability of the model depends on the threshold value, which is difficult to determine accurately.

3.2.2. Visual-Based or Combined Analysis of GPR Attributes

In addition to the numerical approach, a visual or combined visual and numerical approach has been supported by a number of authors [22,77,85]. The visual approach implies the visual analysis of B-scans. This method is highly dependent on the expertise of the analyst, especially in the case of severely damaged structures [86], so the final conclusion is prone to error. As noted by some authors [22], numerical analysis of amplitudes misinterprets most anomalies that alter the signal and are not causes of deterioration (surface anomalies, reinforcement spacing, reinforcement depth, structural variations). Due to of these drawbacks, a method is proposed in which an analyst reviews the ground-penetrating radar profiles (B-scans), considers the reflections of the reinforcement and concrete surfaces and marks the boundaries of deteriorated areas. The profiles are processed, and the final output is the corrosion map. The detailed procedure is described in Reference [87]. This method was improved to overcome the subjective opinion of analysts in visual-based interpretation [85]. A set of if/then rules was created to locate anomalies that alter the signal but do not indicate deterioration. Dinh et al. [77] used visual analysis of ground-penetrating radar profiles as a tool to determine the number of condition categories as input to the k-means clustering method. It is a combined method: after determining the number of condition categories, the amplitudes of the signal are grouped and thresholds between the groups are determined. The corrosion map obtained in this way was used for the deterioration modelling of concrete bridge decks presented in Reference [88]. Dawood et al. [89] presented an improved visual-based analysis of ground-penetrating radar data for the detection of air and water voids in tunnels. Moreover, an evaluation flowchart based on inspection of pier structure considering B-scans and GPR signal energy was proposed in Reference [90].

3.2.3. Condition Assessment by Combination of Multiple NDT

Ground-penetrating radar has a number of advantages over other non-destructive techniques (NDT), and it is not surprising that it has shown much interest in replacing other techniques. It is completely non-destructive, and it is rational to give it precedence over other techniques that make surveying slow and less efficient. In the next sections, a brief overview is shown on current research results obtained by comparing GPR data with other test methods, such as electrical resistivity (ER), half-cell potential (HCP), chain drag (CD), hammer sounding (HS), infrared thermography (IRT), acoustic emission (AE) and impact-echo (IE). These studies are summarized in Table 2.

Electrical resistivity and half-cell potential are fundamental tools for determining the probability of corrosion in the condition assessment of concrete structures. A good correlation has been found in the analysis of electrical resistivity and GPR data [81,91–93]. However, such behavior is to be expected as both techniques are affected by the conductivity of the concrete [91].

The comparison between HCP and GPR data can be found in References [21,24,69,73,74,81,92,93]. All observations were obtained by superimposing the signal attenuation and potential maps. In most studies, a good correlation was found since the attenuation is indicative of a corrosive environment and coincides with the areas of extremely negative half-cell potentials [92]. However, when the degree of deterioration is low, the ground-penetrating radar could overestimate corroded areas [69].

Other techniques can also serve for condition assessment and correctly predict potential deterioration due to corrosion propagation. These techniques include chain drag (CD), hammer sounding (HS), infrared thermography (IRT), acoustic emission (AE) and impact-echo (IE). Compared to the chain-drag method, the ground-penetrating radar is effective while the deterioration level ranged between 10% and 50% [69]. However, the divergence between the result of the ground-penetrating radar and the acoustic scanning system was observed in Reference [94], where the authors investigated the suitability of these techniques for delamination detection. The area of high attenuation was larger than the delaminated area detected by the acoustic system because the ground-penetrating radar generally detects the deterioration earlier than the acoustic system. The GPR can detect deterioration before delamination occurs. Also, the comparative feasibility study on delamination detection using ground-penetrating radar (GPR) and infrared thermography (IRT) based on ROC (Receiver Operating Characteristic) analysis showed that IRT is more reliable than GPR in detecting delamination [95]. However, the contribution of IRT is limited to a shallow cover depth, while GPR can provide a deeper insight. Also, the usefulness of GPR in predicting repair quantities was presented in Reference [96], where the results of ground-penetrating radar matched the depth of removal measured by LiDAR (Light Detection and Ranging) method after hydro-demolition.

Table 2. Review of studies that combined GPR with other techniques.

Study	Year	Other Techniques	GPR (GHz)		Main Findings
			Air-Coupled	Ground-Coupled	
Comparison with other NDT					
Barnes et al. [24]	2000	HCP, CD	1	-	Agreement on spatial distribution of deteriorated areas; 65.1% and 66.2% correctly predicted deteriorated areas compared to HCP and CD, respectively.
Scott et al. [97]	2003	IE, CD	2.4	1.5	GPR systems could not detect whole delaminated areas.
Barnes et al. [69]	2004	HCP, CD	1	-	GPR was effective in predicting damaged areas when the degree of deterioration is between 10% and 50%.
Rhazi et al. [73]	2007	HCP	-	1.5	The values for the degree of attenuation were proposed based on the correlation with HCP.

Table 2. *Cont.*

Study	Year	Other Techniques	GPR (GHz)		Main Findings
			Air-Coupled	Ground-Coupled	
Barnes et al. [21]	2008	HCP, CD	-	1.5	The correlation between GPR and HCP and CD was improved after the depth correction.
Maser et al. [74]	2012	HCP, IE, HS	1 and 2	1.5 and 2.6	The agreement between GPR and HCP was 90.2%, and between GPR and IE was 79.3%.
Simi et al. [98]	2012	IE, CD	-	2	Moisture and corrosion maps produced with commercial software showed good spatial agreement with IE and CD.
Gucunski et al. [91]	2013	ER	-	1.5	The good agreement between GPR and ER; 95% of the locations where ER $\leq$ 40 kΩcm agreed with the location where GPR amplitude was <15 dB.
Pailes et al. [93]	2015	ER, HCP, IE, CD, HS	-	1.5	The best spatial agreement compared to different NDT was between GPR and ER, and GPR and sounding techniques (CD and HS).
Dinh et al. [81]	2017	ER, HCP, IE	-	1.5	Correlation between GPR and other NDT was determined by a traditional numerical analysis and a method based on comparison with a simulated waveform; better agreement was found using ER and HCP than IE.
Sun et al. [94]	2018	AE, CD	-	1.5	GPR showed a larger deteriorated area than AE. GPR detected deteriorated areas near joints, while AE did not.
Sultan et al. [95]	2018	HS, IRT	-	1.6	Compared to the IRT, GPR was less accurate in detecting delamination.
Dinh et al. [92]	2019	ER, HCP	-	1.5	GPR maps produced by the method based on SAFT showed good correlation with HCP and ER. In one case, the correlation with ER was better than with HCP.
Combination with other NDT					
Maser [99]	2009	GPR, IRT	-	-	The combination of GPR and IRT was effective in condition assessment. The GPR assisted the IRT in detecting deeper delamination.

Table 2. *Cont.*

Study	Year	Other Techniques	GPR (GHz)		Main Findings
			Air-Coupled	Ground-Coupled	
Gucunski et al. [23]	2010	GPR, ER, HCP, IE, USW	-	1.5	This combination of NDT can characterize different levels of deterioration. GPR brought effectiveness in the speed of inspection as the fastest technology from these five.
Gucunski et al. [100]	2013	GPR, ER, IE, USW	-	2	GPR deterioration maps were effectively implemented in a robotic system for bridge deck evaluation.
Alani et al. [101]	2014	GPR, deflection and vibration system	-	2	GPR results were combined with the deflection and vibration system to create a FEM model; GPR was used to locate rebar and detect cracks and potential moisture areas.
Kim et al. [102]	2016	GPR, ER, IE	-	2	GPR results were combined with ER and IE to calculate the condition index for estimation of service life.
Abu Dabous [103]	2017	GPR, IRT	-	1.6	Maps obtained with GPR and IRT were overlapped to form areas of possible delamination; the detected area was used to determine the condition rating.
Omar et al. [104]	2018	GPR, IRT	1	1.6	A method based on the integrated results obtained with GPR and IRT was proposed.
Ahmed et al. [105]	2018	GPR, ER, HCP, IE	-	-	Data fusion model from GPR, ER, HCP and IE maps was developed; fusion was on pixel and feature level.
Solla et al. [106]	2019	GPR, IRT	-	2.3	The paper proposes a procedure for anomaly detection based on joint observation of GPR signal and IRT temperature.
Kilic et al. [107]	2020	GPR, IRT, laser distance sensor, camera	-	2	The effectiveness of the integrated techniques was demonstrated on a bridge; GPR was used to detect water leakage, large cracks and corrosion.
Rashidi et al. [108]	2020	GPR, ER, HCP, IE, USW	-	1.5	The results from NDT were used to determine condition indices calculated using divergence from the ideal distribution using the Jensen–Shannon method.

In a very detailed study, Omar et al. [109] presented the weaknesses and advantages of the most commonly used methods for condition assessment of concrete bridges. The conclusion was that none of the commonly used techniques are able to detect active corrosion, delamination and vertical cracking simultaneously, so that the most reliable condition assessment lies in a combination of multiple techniques. Such an approach ensures accurate condition assessment as deterioration can be detected from its onset to an advanced stage [23].

The simultaneously used non-destructive techniques usually consider methods such as ground-penetrating radar, electrical resistivity, half-cell potential, ultrasonic surface waves, impact-echo, etc. In References [14,100,110], an example of integration of different non-destructive testing methods in robotic systems, RABIT (Robotics Assisted Bridge Inspection Tool), was presented, which ensures real-time visualization of the concrete deck condition. Here, the evaluation is supported by a Jensen–Shannon probability method that focuses on the determination of the condition index [108]. Additional support in the interpretation of GPR data for delamination detection can be provided by infrared thermography (IRT) [99,103,104,107]. Solla et al. [106] demonstrated the technique to inspect a military base in an advanced stage of corrosion with visible signs of damage such as cracking and spalling. The results obtained with GPR were combined with the IRT technique. The corrosion assessment was based on the observation of GPR signal attenuation, changes in signal velocity and amplitude polarity. Overall, high signal attenuation was declared to indicate the presence of mineral salts and moisture, while reverse reflection polarity could be a sign of voids. The same parameters have been used in the assessment of wastewater plants [111], although the corrosion process is different in this case.

Deterioration modelling was part of the study in Reference [102], in which deterioration curves were developed based on the condition assessment of 10 bridges. Similar assessments were carried out by Alani et al. [101], where finite element models were constructed based on inputs from ground-penetrating radar and the deflection and vibration sensor system. In Reference [105], a data fusion model for bridge deck evaluation was developed based on the combination of the results from the ground-penetrating radar, half-cell potential method, electrical resistivity method and impact-echo method. In Reference [112], the ground-penetrating radar data combined with the capacitive technique and the impact-echo method were correlated with durability indicators for the overall assessment of the wharf.

3.2.4. Conclusions from the On-Site Corrosion Inspection

The previous section has shown that corrosion assessment in on-site corrosion testing is mostly based on the assessment of the attenuated areas identified by signal amplitude analysis. Most of the studies are carried out on the bridge decks. In terms of comparison with other NDT, GPR has been compared with various techniques used for the service life condition assessment of the structures, Figure 5.

The high correlation between the electrical resistivity and the attenuation maps obtained with ground-penetrating radar is to be expected, as the signal depends on the material properties, so the conductive medium generated by moisture and chlorides changes its properties. In general, the GPR has shown good agreement with the HCP. However, there are certain situations where the GPR does not agree very well with the HCP. In cases where moisture and chlorides provide a favorable environment for corrosion, but their concentration is not sufficient to start corrosion, the GPR and HCP maps may differ. The applicability of ground-penetrating radar in detecting delamination is also uncertain [113]. In many cases, it does not detect delamination directly, and the assessment is based on the localization of deteriorated areas [114]. Moreover, the visual signs of delamination are not always visible on B-scans [87]. If the delamination is too thin to be detected by the antenna, it will not show any detectable change on the scan.

In summary, additional information, such as the age of the structure or the environmental conditions, may be helpful in analyzing GPR results. Moreover, this additional

information can be obtained with other NDT, so a suitable combination of NDT can be a very powerful tool for the condition assessment of concrete structures.
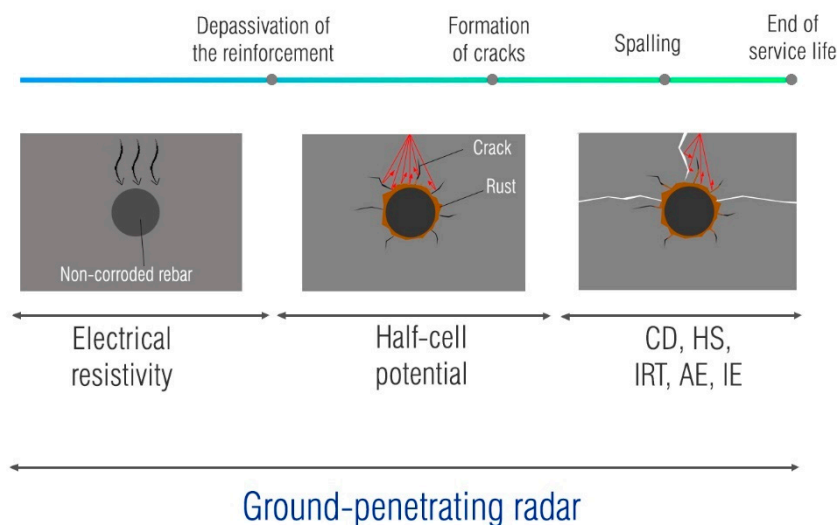

Figure 5. Multiple NDT used for the condition assessment.

4. Conclusions

This paper investigated the evaluation of corrosion probability in concrete using ground-penetrating radar. The study analyzed laboratory and on-site investigations and the results were related to the evolution of the corrosion process. Advantages and recommendations for future research are presented below.

GPR is a completely non-destructive method, which gives it an advantage over other techniques for corrosion assessment of reinforced concrete. Its ability to examine large areas in a short time, together with providing information on the depth and spacing of reinforcement, makes it a multifunctional NDT. The literature review identified certain challenges in the use of GPR for corrosion assessment, one of the main being the understanding of the influence of concrete conditions on GPR parameters. In fact, in most laboratory studies, moisture and chloride content were controlled after depassivation of the reinforcement. On-site in real conditions, variations of moisture and chloride content are inevitable, which makes the detection of corroded areas based only on the observation of amplitude potentially ambiguous. Since opposing data have been reported in the literature, further laboratory studies are needed to show the influence of the change in dielectric properties of the concrete cover on the GPR amplitude and the change in reflection coefficient due to the formation of corrosion products and their migration. Since an absolute comparison of studies is difficult due to the variance in experimental design and the degree of damage induced by the accelerated corrosion process, further studies should correlate the degree of damage with the change in GPR amplitude. Obtaining concluding results from the proposed research topics could enable the use of GPR as a stand-alone tool for detecting corroded areas, moving from its use for the detection of corrosive environment towards detection of corrosion itself.

In conclusion, as the knowledge of the effect of corrosion on the GPR signal increases, GPR will be a very valuable tool for condition assessment of reinforced concrete structures. This method will certainly be improved, leading to an upgrade of the construction management system and making the assessment more reliable with reduced maintenance costs.

Institutional Review Board Statement: Not applicable.

Informed Consent Statement: Not applicable.

Data Availability Statement: Not applicable.

Conflicts of Interest: Authors declare no conflict of interest. The funders had no role in the design of the study; in the collection, analyses, or interpretation of data; in the writing of the manuscript, or in the decision to publish the results.

References

1. Croatian, P. *Building Act, NN 153/2013*; Official Gazette: Zagreb, Croatia, 2017.
2. Mehta, B.P.K.; Burrows, R.W. Building Durable Structures in the 21st Century. *Concr. Int.* **2001**, *23*, 57–63.
3. Bossio, A.; Monetta, T.; Bellucci, F.; Lignola, G.P.; Prota, A. Modeling of concrete cracking due to corrosion process of reinforcement bars. *Cem. Concr. Res.* **2015**, *71*, 78–92. [CrossRef]
4. Yan, L.; Chouw, N. Behavior and analytical modeling of natural flax fibre-reinforced polymer tube confined plain concrete and coir fibre-reinforced concrete. *J. Compos. Mater.* **2013**, *47*, 2133–2148. [CrossRef]
5. Vecchio, F.J.; Bucci, F. Analysis of Repaired Reinforced Concrete Structures. *J. Struct. Eng.* **1999**, *125*, 644–652. [CrossRef]
6. Navarro, I.J.; Yepes, V.; Martí, J.V.; González-Vidosa, F. Life cycle impact assessment of corrosion preventive designs applied to prestressed concrete bridge decks. *J. Clean. Prod.* **2018**, *196*, 698–713. [CrossRef]
7. Cao, Y.; Dong, S.; Zheng, D.; Wang, J.; Zhang, X.; Du, R.; Song, G.; Lin, C. Multifunctional inhibition based on layered double hydroxides to comprehensively control corrosion of carbon steel in concrete. *Corros. Sci.* **2017**, *126*, 166–179. [CrossRef]
8. Luo, H.; Su, H.; Dong, C.; Li, X. Passivation and electrochemical behavior of 316L stainless steel in chlorinated simulated concrete pore solution. *Appl. Surf. Sci.* **2017**, *400*, 38–48. [CrossRef]
9. Pan, X.; Shi, Z.; Shi, C.; Ling, T.C.; Li, N. A review on concrete surface treatment Part I: Types and mechanisms. *Constr. Build. Mater.* **2017**, *132*, 578–590. [CrossRef]
10. Ohtsu, M. Introduction. In *Innovative AE and NDT Techniques for On-Site Measurement of Concrete and Masonry Structures*; Ohtsu, M., Ed.; Springer: Dordrecht, Germany, 2016; pp. 1–4.
11. Núñez-Nieto, X.; Solla, M.; Lorenzo, H. Applications of GPR for Humanitarian Assistance and Security. In *Civil Engineering Applications of Ground Penetrating Radar*; Pajewski, L., Benedetto, A., Eds.; Springer: New Delhi, India, 2015; pp. 301–326.
12. Annan, A.P. Electromagnetic Principles of Ground Penetrating Radar. In *Ground Penetrating Radar: Theory and Applications*; Jol, M.H., Ed.; Elsevier B.V.: Amsterdam, The Netherlands, 2009; pp. 1–40.
13. Daniels, D.J. Introduction. In *Ground Penetrating Radar*, 2nd ed.; The Institution of Electrical Engineers: London, UK, 2004; pp. 1–11.
14. Gucunski, N.; Basily, B.; Kim, J.; Duong, T.; Maher, A.; Dinh, K.; Azari, H.; Ghasemi, H. Assessing Condition of Concrete Bridge Decks by Robotic Platform RABIT for Development of Deterioration and Predictive Models. In Proceedings of the 8th International Conference on Bridge Maintenance, Safety and Management (IABMAS), Foz do Iguacu, Brazil, 26–30 June 2016.
15. Reichling, K.; Raupach, M.; Wiggenhauser, H.; Stoppel, M.; Dobmann, G.; Kurz, J. BETOSCAN—Robot controlled non-destructive diagnosis of reinforced concrete decks. In Proceedings of the NDTCE'09, Non Destructive Testing in Civil Engineering, Nantes, France, 30 June–3 July 2009.
16. Hubbard, S.S.; Zhang, J.; Monteiro, P.J.M.; Peterson, J.E.; Rubin, Y. Experimental Detection of Reinforcing Bar Corrosion Using Nondestructive Geophysical Techniques. *ACI Mater. J.* **2003**, *100*, 501–510. [CrossRef]
17. Lai, W.W.L.; Kind, T.; Stoppel, M.; Wiggenhauser, H. Measurement of Accelerated Steel Corrosion in Concrete Using Ground-Penetrating Radar and a Modified Half-Cell Potential Method. *J. Infrastruct. Syst.* **2013**, *19*, 205–220. [CrossRef]
18. Hong, S.; Lai, W.W.L.; Wilsch, G.; Helmerich, R.; Helmerich, R.; Günther, T.; Wiggenhauser, H. Periodic mapping of reinforcement corrosion in intrusive chloride contaminated concrete with GPR. *Constr. Build. Mater.* **2014**, *66*, 671–684. [CrossRef]
19. Hong, S.; Lai, W.W.L.; Helmerich, R. Experimental monitoring of chloride-induced reinforcement corrosion and chloride contamination in concrete with ground-penetrating radar. *Struct. Infrastruct. Eng.* **2015**, *11*, 15–26. [CrossRef]
20. Wong, P.T.W.; Lai, W.W.L.; Sham, J.F.C.; Poon, C. Hybrid non-destructive evaluation methods for characterizing chloride-induced corrosion in concrete. *NDT E Int.* **2019**, *107*. [CrossRef]
21. Barnes, C.L.; Trottier, J.F.; Forgeron, D. Improved concrete bridge deck evaluation using GPR by accounting for signal depth-amplitude effects. *NDT E Int.* **2008**, *41*, 427–433. [CrossRef]
22. Tarussov, A.; Vandry, M.; De La Haza, A. Condition assessment of concrete structures using a new analysis method: Ground-penetrating radar computer-assisted visual interpretation. *Constr. Build. Mater.* **2013**, *38*, 1246–1254. [CrossRef]
23. Gucunski, N.; Romero, F.; Kruschwitz, S.; Feldmann, R.; Abu-Hawash, A.; Dunn, M. Multiple complementary nondestructive evaluation technologies for condition assessment of concrete bridge decks. *Transp. Res. Rec.* **2010**, 34–44. [CrossRef]

24. Barnes, C.L.; Trottier, J.F. Ground-Penetrating Radar for Network-Level Concrete Deck Repair Management. *J. Transp. Eng.* **2000**, *126*, 257–262. [CrossRef]

25. Dinh, K.; Gucunski, N.; Kim, J.; Duong, T.H. Understanding depth-amplitude effects in assessment of GPR data from concrete bridge decks. *NDT E Int.* **2016**, *83*, 48–58. [CrossRef]

26. Lai, W.W.L.; Dérobert, X.; Annan, A.P. A review of Ground Penetrating Radar application in civil engineering: A 30-year journey from Locating and Testing to Imaging and Diagnosis. *NDT E Int.* **2018**, *96*, 58–78. [CrossRef]

27. Tosti, F.; Ferrante, C. Using Ground Penetrating Radar Methods to Investigate Reinforced Concrete Structures. *Surv. Geophys.* **2020**, *41*, 485–530. [CrossRef]

28. Abu Dabous, S.; Feroz, S. Condition monitoring of bridges with non-contact testing technologies. *Autom. Constr.* **2020**, *116*. [CrossRef]

29. Clarivate Analytics Web of Science. Available online: www.webofknowledge.com (accessed on 30 October 2020).

30. Science Direct Scopus. Available online: https://www.scopus.com (accessed on 30 October 2020).

31. Beushausen, H.; Torrent, R.; Alexander, M.G. Performance-based approaches for concrete durability: State of the art and future research needs. *Cem. Concr. Res.* **2019**, *119*, 11–20. [CrossRef]

32. Bertolini, L.; Elsener, B.; Pedeferri, P.; Redaelli, E.; Polder, R. *Corrosion of Steel in Concrete: Prevention, Diagnosis, Repair*, 2nd ed.; Wiley-VCH Verlag GmbH & Co.: Weinheim, Germany, 2013.

33. Broomfield, J.P. *Corrosion of Steel in Concrete: Understanding, Investigation and Repair*, 2nd ed.; Taylor and Francis: London, UK, 2003.

34. Tuutti, K. *Corrosion of Steel in Concrete*; Swedish Cement and Concrete Research Institute: Stockholm, Sweden, 1982.

35. Alexander, M.; Beushausen, H. Durability, service life prediction, and modelling for reinforced concrete structures—Review and critique. *Cem. Concr. Res.* **2019**, *122*, 17–29. [CrossRef]

36. Andrade, C.; Alonso, C.; Gulikers, J.; Polder, R.; Cigna, R.; Vennesland, O.; Salta, M.; Raharinaivo, A.; Elsener, B. Test methods for on-site corrosion rate measurement of steel reinforcement in concrete by means of the polarization resistance method. *Mater. Struct.* **2004**, *37*, 623–643. [CrossRef]

37. Elsener, B.; Andrade, C.; Gulikers, J.; Polder, R.; Raupach, M. Half-cell potential measurements—Potential mapping on reinforced concrete structures. *Mater. Struct.* **2003**, *36*, 461–471. [CrossRef]

38. ASTM C876-91. *Standard Test Method for Half-Cell Potentials of Uncoated Reinforcing Steel in Concrete*; ASTM International: West Conshohocken, PA, USA, 1999.

39. Hornbostel, K.; Larsen, C.K.; Geiker, M.R. Relationship between concrete resistivity and corrosion rate—A literature review. *Cem. Concr. Compos.* **2013**, *39*, 60–72. [CrossRef]

40. Song, H.W.; Saraswathy, V. Corrosion monitoring of reinforced concrete structures—A review. *Int. J. Electrochem. Sci.* **2007**, *2*, 1–28. [CrossRef]

41. Polder, R.; Andrade, C.; Elsener, B.; Vennesland, O.; Gulikers, J.; Weidert, R.; Raupach, M. Test methods for on site measurement of resistivity of concrete. *Mater. Struct.* **2000**, *33*, 603–611. [CrossRef]

42. Cassidy, N.J. Electrical and Magnetic Properties of Rocks, Soils and Fluids. In *Ground Penetrating Radar: Theory and Applications*; Jol, H.M., Ed.; Elsevier B.V.: Amsterdam, The Netherlands, 2009; pp. 41–72.

43. Laurens, S.; Balayssac, J.P.; Rhazi, J.; Arliguie, G. Influence of concrete relative humidity on the amplitude of ground-penetrating radar (GPR) signal. *Mater. Struct.* **2002**, *35*, 198–203. [CrossRef]

44. Sbartaï, Z.M.; Laurens, S.; Balayssac, J.; Arliguie, G.; Ballivy, G. Ability of the direct wave of radar ground-coupled antenna for NDT of concrete structures. *NDT E Int.* **2006**, *39*, 400–407. [CrossRef]

45. Hugenschmidt, J.; Loser, R. Detection of chlorides and moisture in concrete structures with ground penetrating radar. *Mater. Struct.* **2008**, *41*, 785–792. [CrossRef]

46. Senin, S.F.; Hamid, R. Ground penetrating radar wave attenuation models for estimation of moisture and chloride content in concrete slab. *Constr. Build. Mater.* **2016**, *106*, 659–669. [CrossRef]

47. Dérobert, X.; Villain, G.; Balayssac, J.P. Influence of concrete carbonation on electromagnetic permittivity measured by GPR and capacitive techniques. *J. Environ. Eng. Geophys.* **2018**, *23*, 443–456. [CrossRef]

48. Ahmad, S. Techniques for inducing accelerated corrosion of steel in concrete. *Arab. J. Sci. Eng.* **2009**, *34*, 95–104.

49. Malumbela, G.; Moyo, P.; Alexander, M. A step towards standardising accelerated corrosion tests on laboratory reinforced concrete specimens. *J. South African Inst. Civ. Eng.* **2012**, *54*, 78–85.

50. El Maaddawy, T.A.; Soudki, K.A. Effectiveness of Impressed Current Technique to Simulate Corrosion of Steel Reinforcement in Concrete. *J. Mater. Civ. Eng.* **2003**, *15*, 41–47. [CrossRef]

51. Yuan, Y.; Ji, Y.; Shah, S.P. Comparison of Two Accelerated Corrosion Techniques for Concrete Structures. *ACI Struct. J.* **2007**, *104*, 344–347.

52. Sossa, V.; Pérez-Gracia, V.; González-Drigo, R.; Rasol, M.A. Lab non destructive test to analyze the effect of corrosion on ground penetrating radar scans. *Remote Sens.* **2019**, *11*, 2814. [CrossRef]

53. Raju, R.K.; Hasan, M.I.; Yazdani, N. Quantitative relationship involving reinforcing bar corrosion and ground-penetrating radar amplitude. *ACI Mater. J.* **2018**, *115*, 449–457. [CrossRef]

54. Zaki, A.; Johari, M.A.; Hussin, W.M.A.W.; Jusman, Y. Experimental Assessment of Rebar Corrosion in Concrete Slab Using Ground Penetrating Radar (GPR). *Int. J. Corros.* **2018**, *2018*. [CrossRef]

55. Hasan, M.I.; Yazdani, N. An experimental study for quantitative estimation of rebar corrosion in concrete using ground penetrating radar. *J. Eng.* **2016**, *2016*. [CrossRef]

56. Lai, W.W.L.; Kind, T.; Wiggenhauser, H. Detection of accelerated reinforcement corrosion in concrete by ground penetrating radar. In Proceedings of the XIII Internartional Conference on Ground Penetrating Radar, Lecce, Italy, 21–25 June 2010.

57. Zhan, B.J.; Lai, W.W.L.; Kou, S.C.; Poon, C.S.; Tsang, W.F. Correlation between accelerated steel corrosion in concrete and ground penetrating radar parameters. In Proceedings of the International RILEM Conference on Advances in Construction Materials Through Science and Engineering, Hong Kong, China, 5–7 September 2011.

58. Lai, W.W.L.; Kind, T.; Wiggenhauser, H. Using ground penetrating radar and time-frequency analysis to characterize construction materials. *NDT E Int.* **2011**, *44*, 111–120. [CrossRef]

59. Hong, S. GPR-Based Periodic Monitoring of Reinforcement Corrosion in Chloride- Contaminated Concrete. Ph.D. Thesis, TU Berlin, Berlin, Germany, 2015.

60. Said, M.E.; Hussein, A.A. Induced Corrosion Techniques for Two-Way Slabs. *J. Perform. Constr. Facil.* **2019**, *33*. [CrossRef]

61. Altoubat, S.; Maalej, M.; Shaikh, F.U.A. Laboratory Simulation of Corrosion Damage in Reinforced Concrete. *Int. J. Concr. Struct. Mater.* **2016**, *10*, 383–391. [CrossRef]

62. ASTM D6087-08. *Standard Test Method for Evaluating Asphalt-Covered Concrete Bridge Decks Using Ground Penetrating Radar*; ASTM International: West Conshohocken, PA, USA, 2008.

63. Saarenketo, T. NDT Transportation. In *Ground Penetrating Radar: Theory and Applications*; Jol, H.M., Ed.; Elsevier B.V.: Amsterdam, The Netherlands, 2009; pp. 395–444.

64. Belli, K.M.; Birken, R.A.; Vilbig, R.A.; Wadia-Fascetti, S.J. Simulated GPR investigation of deterioration in reinforced concrete bridge decks. In Proceedings of the Symposium on the Application of Geophysics to Engineering and Environmental Problems 2013, Denver, CO, USA, 17–21 March 2013.

65. Dinh, K.; Zayed, T.; Romero, F.; Tarussov, A. Method for analyzing time-series GPR data of concrete bridge decks. *J. Bridg. Eng.* **2015**, *20*. [CrossRef]

66. Diamanti, N.; Annan, A.P.; Redman, J.D. Concrete Bridge Deck Deterioration Assessment Using Ground Penetrating Radar (GPR). *J. Environ. Eng. Geophys.* **2017**, *22*. [CrossRef]

67. GSSI. *RADAN 7 Manual*; Geophysical Survey Systems, Inc.: Nashua, NH, USA, 2015.

68. Barnes, C.L.; Trottier, J.F. Phenomena and conditions in bridge decks that confound ground-penetrating radar data analysis. *Transp. Res. Rec.* **2002**, 57–61. [CrossRef]

69. Barnes, C.L.; Trottier, J.F. Effectiveness of Ground Penetrating Radar in Predicting Deck Repair Quantities. *J. Infrastruct. Syst.* **2004**, *10*, 69–76. [CrossRef]

70. Parrillo, B.; Roberts, R. Bridge deck condition assessment using ground penetrating radar. In Proceedings of the 9th European Conference on NDT (ECNDT), Berlin, Germany, 25–29 September 2006.

71. Pashoutani, S.; Zhu, J. Ground Penetrating Radar Data Processing for Concrete Bridge Deck Evaluation. *J. Bridg. Eng.* **2020**, *25*. [CrossRef]

72. Romero, F.A.; Barnes, C.L.; Azari, H.; Nazarian, S.; Rascoe, C.D. Validation of Benefits of Automated Depth Correction Method Improving Accuracy of Ground-Penetrating Radar Deck Deterioration Maps. *Transp. Res. Rec.* **2015**, 100–109. [CrossRef]

73. Rhazi, J.; Dous, O.; Laurens, S. A New Application of the GPR Technique To Reinforced Concrete. In Proceedings of the 4th Middle NDT Conference and Exhibition, Manama, Bahrain, 2–5 December 2007.

74. Maser, K.; Martino, N.; Doughty, J.; Birken, R. Understanding and detecting bridge deck deterioration with ground-penetrating radar. *Transp. Res. Rec.* **2012**, 116–123. [CrossRef]

75. Martino, N.; Maser, K.; Birken, R.; Wang, M. Determining ground penetrating radar amplitude thresholds for the corrosion state of reinforced concrete bridge decks. *J. Environ. Eng. Geophys.* **2014**, *19*, 175–181. [CrossRef]

76. Martino, N.; Maser, K.; Birken, R.; Wang, M. Quantifying Bridge Deck Corrosion Using Ground Penetrating Radar. *Res. Nondestruct. Eval.* **2016**, *27*, 112–124. [CrossRef]

77. Dinh, K.; Zayed, T.; Moufti, S.; Shami, A.; Jabri, A.; Abouhamad, M.; Dawood, T. Clustering-Based Threshold Model for Condition Assessment of Concrete Bridge Decks with Ground-Penetrating Radar. *Transp. Res. Rec.* **2015**, 81–89. [CrossRef]

78. Alsharqawi, M.; Zayed, T.; Shami, A. Ground penetrating radar-based deterioration assessment of RC bridge decks. *Constr. Innov.* **2020**, *20*, 1–17. [CrossRef]

79. Dinh, K.; Gucunski, N.; Duong, T.H. An algorithm for automatic localization and detection of rebars from GPR data of concrete bridge decks. *Autom. Constr.* **2018**, *89*, 292–298. [CrossRef]

80. Ma, X.; Liu, H.; Wang, M.L.; Birken, R. Automatic detection of steel rebar in bridge decks from ground penetrating radar data. *J. Appl. Geophys.* **2018**, *158*, 93–102. [CrossRef]

81. Dinh, K.; Gucunski, N.; Kim, J.; Duong, T.H. Method for attenuation assessment of GPR data from concrete bridge decks. *NDT E Int.* **2017**, *92*, 50–58. [CrossRef]

82. Hong, S.; Wiggenhauser, H.; Helmerich, R.; Dong, B.; Dong, P.; Xing, F. Long-term monitoring of reinforcement corrosion in concrete using ground penetrating radar. *Corros. Sci.* **2017**, *114*, 123–132. [CrossRef]

83. Rhee, J.Y.; Shim, J.; Kee, S.H.; Lee, S.Y. Different Characteristics of Radar Signal Attenuation Depending on Concrete Condition of Bare Bridge Deck. *KSCE J. Civ. Eng.* **2020**, *24*, 2049–2062. [CrossRef]

84. Benedetto, A. A three dimensional approach for tracking cracks in bridges using GPR. *J. Appl. Geophys.* **2013**, *97*, 37–44. [CrossRef]

85. Abouhamad, M.; Dawood, T.; Jabri, A.; Alsharqawi, M.; Zayed, T. Corrosiveness mapping of bridge decks using image-based analysis of GPR data. *Autom. Constr.* **2017**, *80*, 104–117. [CrossRef]

86. Martino, N.; Maser, K. Comparison of air-coupled GPR data analysis results determined by multiple analysts. In Proceedings of the SPIE Conference on Health Monitoring of Structural and Biological Systems, Las Vegas, NV, USA, 21–24 March 2016.

87. Dinh, K.; Zayed, T.; Tarussov, A. GPR image analysis for corrosion mapping in concrete slabs. In Proceedings of the Canadian Society of Civil Engineering 2013 Conference, Montreal, QC, Canada, 29 May–1 June 2013.

88. Alsharqawi, M.; Zayed, T.; Abu Dabous, S. Integrated condition rating and forecasting method for bridge decks using Visual Inspection and Ground Penetrating Radar. *Autom. Constr.* **2018**, *89*, 135–145. [CrossRef]

89. Dawood, T.; Zhu, Z.; Zayed, T. Deterioration mapping in subway infrastructure using sensory data of GPR. *Tunneling Undergr. Sp. Technol.* **2020**, *103*. [CrossRef]

90. Sham, J.F.C.; Wallace, W.L.L. Diagnosis of reinforced concrete structures by Ground Penetrating Radar survey-case study. In Proceedings of the 9th International Workshop on Advanced Ground Penetrating Radar (IWAGPR), Edinburgh, UK, 28–30 June 2017.

91. Gucunski, N.; Parvardeh, H.; Romero, F.; Pailes, B.M. Deterioration progression monitoring in concrete bridge decks using periodical NDE surveys. In Proceedings of the Second Conference on Smart Monitoring, Assessment and Rehabilitation of Civil Structures (SMAR 2013), Istanbul, Turkey, 9–11 September 2013.

92. Dinh, K.; Gucunski, N.; Zayed, T. Automated visualization of concrete bridge deck condition from GPR data. *NDT E Int.* **2019**, *102*, 120–128. [CrossRef]

93. Pailes, B.M.; Gucunski, N. Understanding Multi-modal Non-destructive Testing Data Through the Evaluation of Twelve Deteriorating Reinforced Concrete Bridge Decks. *J. Nondestruct. Eval.* **2015**, *34*, 1–14. [CrossRef]

94. Sun, H.; Pashoutani, S.; Zhu, J. Nondestructive evaluation of concrete bridge decks with automated acoustic scanning system and ground penetrating radar. *Sensors* **2018**, *18*, 1955. [CrossRef] [PubMed]

95. Sultan, A.A.; Washer, G.A. Comparison of Two Nondestructive Evaluation Technologies for the Condition Assessment of Bridge Decks. *Transp. Res. Rec.* **2018**, *2672*, 113–122. [CrossRef]

96. Varnavina, A.V.; Sneed, L.H.; Khamzin, A.K.; Torgashov, E.V.; Anderson, N.L. An attempt to describe a relationship between concrete deterioration quantities and bridge deck condition assessment techniques. *J. Appl. Geophys.* **2017**, *142*, 38–48. [CrossRef]

97. Scott, M.; Rezaizadeh, A.; Delahaza, A.; Santos, C.G.; Moore, M.; Graybeal, B.; Washer, G. A comparison of nondestructive evaluation methods for bridge deck assessment. *NDT E Int.* **2003**, *36*, 245–255. [CrossRef]

98. Simi, A.; Manacorda, G.; Benedetto, A. Bridge deck survey with high resolution Ground Penetrating Radar. In Proceedings of the 14th International Conference on Ground Penetrating Radar (GPR), Shanghai, China, 4–8 June 2012.

99. Maser, K.R. Integration of ground penetrating radar and infrared thermography for bridge deck condition testing. In Proceedings of the NDTCE'09, Non Destructive Testing in Civil Engineering, Nantes, France, 30 June–3 July 2009.

100. Gucunski, N.; Maher, A.; Ghasemi, H. Condition assessment of concrete bridge decks using a fully autonomous robotic NDE platform. *Bridg. Struct.* **2013**, *9*, 123–130. [CrossRef]

101. Alani, A.M.; Aboutalebi, M.; Kilic, G. Integrated health assessment strategy using NDT for reinforced concrete bridges. *NDT E Int.* **2014**, *61*, 80–94. [CrossRef]

102. Kim, J.; Gucunski, N.; Dinh, K. Similarities and differences in bare concrete deck deterioration curves from multi NDE technology surveys. In Proceedings of the SPIE Conference on Health Monitoring of Structural and Biological Systems, Las Vegas, NV, USA, 21–24 March 2016.

103. Abu Dabous, S.; Yaghi, S.; Alkass, S.; Moselhi, O. Concrete bridge deck condition assessment using IR Thermography and Ground Penetrating Radar technologies. *Autom. Constr.* **2017**, *81*, 340–354. [CrossRef]

104. Omar, T.; Nehdi, M.L.; Zayed, T. Rational Condition Assessment of RC Bridge Decks Subjected to Corrosion-Induced Delamination. *J. Mater. Civ. Eng.* **2018**, *30*. [CrossRef]

105. Ahmed, M.; Moselhi, O.; Bhowmick, A. Two-tier data fusion method for bridge condition assessment. *Can. J. Civ. Eng.* **2018**, *45*, 197–214. [CrossRef]

106. Solla, M.; Lagüela, S.; Fernández, N.; Garrido, I. Assessing rebar corrosion through the combination of nondestructive GPR and IRT methodologies. *Remote Sens.* **2019**, *11*, 1705. [CrossRef]

107. Kilic, G.; Caner, A. Augmented reality for bridge condition assessment using advanced non-destructive techniques. *Struct. Infrastruct. Eng.* **2020**. [CrossRef]

108. Rashidi, M.; Azari, H.; Nehme, J. Assessment of the overall condition of bridge decks using the Jensen-Shannon divergence of NDE data. *NDT E Int.* **2020**, *110*. [CrossRef]

109. Omar, T.; Nehdi, M.L.; Zayed, T. Performance of NDT Techniques in Appraising Condition of Reinforced Concrete Bridge Decks. *J. Perform. Constr. Facil.* **2017**, *31*. [CrossRef]

110. Gucunski, N.; Basily, B.; Kim, J.; Yi, J.; Duong, T.; Dinh, K.; Kee, S.H.; Maher, A. RABIT: Implementation, performance validation and integration with other robotic platforms for improved management of bridge decks. *Int. J. Intell. Robot. Appl.* **2017**, *1*, 271–286. [CrossRef]

111. Manhães, P.M.B.; Araruna Júnior, J.T.; Chen, G.; Anderson, N.L.; dos Santos, A.B. Ground penetrating radar for assessment of reinforced concrete wastewater treatment plant. *J. Civ. Struct. Heal. Monit.* **2020**. [CrossRef]

112. Villain, G.; Sbartaï, Z.M.; Derobert, X.; Garnier, V.; Balayssac, J.P. Durability diagnosis of a concrete structure in a tidal zone by combining NDT methods: Laboratory tests and case study. *Constr. Build. Mater.* **2012**, *37*, 893–903. [CrossRef]
113. Hoegh, K.; Khazanovich, L.; Worel, B.J.; Yu, H.T. Detection of subsurface joint deterioration. *Transp. Res. Rec.* **2013**, 3–12. [CrossRef]
114. Gucunski, N.; Romero, F.; Shokouhi, P.; Makresias, J. Complementary Impact Echo and Ground Penetrating Radar Evaluation of Bridge Decks on I-84 Interchange in Connecticut. In Proceedings of the Geo-Frontiers Congress 2005, Austin, TX, USA, 24–26 January 2005.

Paper II
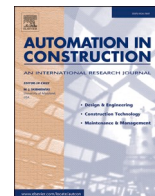
Characterization of ground penetrating radar signal during simulated corrosion of concrete reinforcement

Ksenija Tesic [a], Ana Baricevic [a,*], Marijana Serdar [a], Nenad Gucunski [b]

[a] *University of Zagreb, Faculty of Civil Engineering, Department of Materials, Fra Andrije Kacica-Miosica 26, 10000 Zagreb, Croatia*
[b] *Department of Civil and Environmental Engineering, Rutgers, The State University of New Jersey, 96 Frelinghuysen Road, Piscataway, NJ 08854, USA*

A R T I C L E I N F O

A B S T R A C T

In this paper, the adequacy of the experimental design in the accelerated corrosion process with the impressed current technique (IC) for ground penetrating radar (GPR) inspection was investigated. The aim of the study is to observe how the GPR signal amplitude behaves under different distributions of corrosion products generated by different exposure conditions in the IC technique. To investigate this, two different experimental setups were prepared. The results are summarized, discussed, and supported by visual evidence, other non-destructive techniques, and electromagnetic theory. The main finding is that the position of the sodium chloride solution required to ensure accelerated corrosion of the reinforcement determines the behaviour of the GPR signal, as it affects the position of the corrosion product layer and its distribution in the concrete cover.

1. Introduction

The designed and expected service life of reinforced concrete (RC) structures could be seriously compromised if adequate maintenance is not performed during their service. One of the main problems leading to disturbed service life of RC structures is corrosion of reinforcement [1–4]. Corrosion involves symbiotic processes in the concrete and on the surface of the reinforcement. In the case of chloride-induced corrosion, it starts with the penetration of chlorides into the concrete, which triggers the depassivation of the reinforcement once the chloride concentration reaches a critical level [5]. The inability to sustain the passive layer leads to a series of chemical reactions at the reinforcement, resulting in the formation of corrosion products, which in turn can cause cracking or even spalling of the concrete cover [6–8]. The optimal maintenance strategy should include the detection of corrosion during the initiation period to minimize the repair effort and the overall maintenance cost. However, complexity, duration of inspection, and ultimately costs, are often the main drivers for choosing a maintenance strategy. Infrastructure owners are often guided by cost alone and choose visual inspection as the only means of decision making, omitting that it is impossible to detect corrosion in the initial stages by visual inspection alone. Therefore, the use of appropriate non-destructive techniques (NDT) is a viable solution.

The attractiveness of non-destructive testing stems primarily from the type of inspection and secondarily from the time required to perform it [9–11]. Nevertheless, in addition to the great accessibility, there should be a research community that ensures the reliability of the results and the continuous improvement of the techniques. One of the techniques that is constantly growing in the field of structural assessment is ground penetrating radar (GPR) [12–15]. The main role of GPR in civil engineering is to locate reinforcement and tendon ducts and to estimate the thickness of concrete cover. It is based on radiation of electromagnetic (EM) waves into the concrete and the detection of the echoes from an object or defect [16]. However, special efforts are made for corrosion characterization of reinforcement in RC structures using GPR [13,17–24]. The technique, which can simultaneously collect data on the location of reinforcement and corrosion condition, undoubtedly contribute to an effective maintenance strategy.

The principle of corrosion assessment with GPR is to observe the perturbation of reflected energy strength when comparing sound and corroded reinforcing bars. The reflected energy changes due to changes:

 i) at the interface between concrete and steel,
ii) in the material.

The changes at the concrete-steel interface due to the corrosion of the rebars contribute to the changes in the reflection coefficient [25], so that the total reflection of the signal is different compared to sound rebars. In

---

addition, the changes in the condition of the surrounding concrete due to the causes and consequences of the corrosion process (e.g., water and chloride penetration, migration of corrosion products into the concrete cover, cracks, etc.) lead to changes in the registered amplitude of the echo. In particular, this leads to changes in the permittivity and conductivity of the concrete, which cause a change in the attenuation coefficient [26], further changing the strength of the echoes. The influence of water and chlorides in concrete on the strength of reflected energy has been proven by laboratory tests [27–32]. Furthermore, special efforts have been made to observe the effects of the formation of corrosion products around the rebars and their propagation in the concrete cover and to observe how they affect the change in the GPR signal [19,20,33–36]. Numerous studies have reported conflicting results on the effect of corrosion products on GPR signal amplitude, Table 1, and this has been discussed in detail in [18]. The corrosion process was usually accelerated in the laboratory using the impressed current technique (IC), Table 1, where the corrosion trigger is the applied potential difference between the observed rebar and another metal. Two main methods for acquiring the GPR attributes found in the literature are: a) monitoring during corrosion acceleration and b) data collection before and after corrosion acceleration. The experimental setup during corrosion acceleration also varied. In some of these studies, the rebars were exposed to current under dry conditions [20,34], while in most of these studies, the specimens were partially immersed in a sodium chloride solution below the rebar during the corrosion acceleration [19,20,36–38]. In the same studies, the GPR investigation was performed from the surface that was on the opposite side of the reinforcement from the solution level. It is in the nature of the impressed current technique that the experimental setup, e.g., the position of the electrodes and the solution level, affect the pattern of distribution of the corrosion products [39,40]. In the study [40] it was shown that the rust accumulation was more intense on the side facing the solution level. This means that the solution level below the reinforcement level produces a corrosion pattern that is different from natural corrosion [2]. Considering the principle of GPR, this could lead to misleading conclusions during GPR inspection if the current density and/or exposure time are not sufficient, especially when monitoring the corrosion process.

2. Research objective

Motivated by the above discussion, the main objective is formulated, Fig. 1. The main objective of this work is to investigate how different corrosion patterns due to different solution positions affect the GPR signal during an accelerated corrosion process with impressed current technique.

In the present study, two experimental setups were designed. The difference between the experimental setups was the position of the sodium chloride solution during the corrosion process. In the 1st experimental setup, the solution was below the reinforcement level as in most studies reported in the literature [19,20,36–38], while in the 2nd experimental setup it was above the reinforcement, considering the effect of solution on distribution of corrosion products [40]. In both experimental setups, parameters of the concrete that affect the GPR signal, such as the chloride content, moisture content, and crack width, were monitored while the corrosion parameters and the GPR signal were observed simultaneously.

3. Experimental program

3.1. Production of specimens

The specimens were prepared using cement CEM I 42.5 R, river aggregate (0/4 mm, 4/8 mm and 8/16 mm), potable water and chemical admixtures (superplasticizer and air-entraining admixture). The mix design and properties of fresh and hardened concrete are summarized in Table 2. Slump was determined after mixing, and compressive strength

Table 1

Review of laboratory studies on the influence of corrosion of reinforcement on GPR attributes, taken and adapted from [18].

Study	Technique for accelerated corrosion test	Method of acquiring the GPR attributes	Change in the GPR attributes	
			Trend of amplitude change	Main findings
Hubbard et al. [41]	Impressed current technique	Before and after corrosion acceleration	↓	Decrease in amplitude and increase in reflection travel time; the authors pointed out a possible influence of the wetting of the concrete cover during the experiment on the results.
Raju et al. [37]			↑	Increase in amplitude with a higher degree of corrosion and larger diameter of rebars. Established relationship between GPR amplitude and mass loss.
Zaki et al. [38]			↑↓	Different influence of corrosion process on GPR amplitude in rebars with different degrees of corrosion; the authors reported that the results could be influenced by the different moisture and chloride content in concrete.
Lai et al. [19]		Monitoring during corrosion acceleration	↑	Increase in amplitude and decrease in reflection travel time due to higher number of reflection points between concrete, steel, corrosion products, and cracks.
Zhan et al. [42]			↑	Increase in amplitude and decrease in reflection travel time. Established relationship between GPR amplitude and mass loss.
Hong et al. [20]			↑	Increase in amplitude and no change in peak frequency of the signal when corrosion products are formed.
Hong et al. [33]			↑	Increase in amplitude; more pronounced effect with increasing diameter of reinforcement. No effect of corrosion

Table 1 (*continued*)

Study	Technique for accelerated corrosion test	Method of acquiring the GPR attributes	Change in the GPR attributes	
			Trend of amplitude change	Main findings
Wong et al. [34]			↑↓	product formation on peak frequency. Increase in amplitude and then decrease as the crack widened.
Liu et al. [36]			↑	Increase in amplitude; the H-Alpha scattering classification was used to characterize the changes in signal with corrosion process.
Sossa et al. [35]	Corroded rebars cast in concrete	Before and after corrosion acceleration	↓	Decrease in amplitude and blurred hyperbola in the B-scan as a result of changes at the interface between concrete and steel.
	Curing chamber		↓	Decrease in amplitude and blurred hyperbola in the B-scan as a result of changes at the interface between concrete and steel and changes in the concrete due to rust, cracks and delamination.

after 28 days on 150 mm cube samples according to European standards [43,44].

The design of the specimens is shown in Fig. 2. The specimens were 700 mm × 300 mm × 250 mm, with two reinforcing bars (Φ/l = 20 / 400 mm) and a concrete cover of 50 mm. The sides of the specimens were coated with epoxy, as was the part of the rebar that was outside the specimens, Fig. 3a. The rebars had wires for electrical connection for the accelerated corrosion test, which were prepared before casting. The connection between the rebar and the wire was protected with an impermeable mastic, Fig. 3b.

3.2. Experimental setup for corrosion acceleration

The main objective of the experimental study was to characterize the changes in the GPR signal during accelerated corrosion of reinforcement in concrete using two different experimental designs. The main difference between the two experimental designs was the position of the aggressive sodium chloride solution during the accelerated corrosion process. The first experimental setup was selected as representative of the tests performed chosen to date replicate previously published research results [19,20,36–38], while the second experimental setup aimed to ensure distribution of the corrosion products in the concrete cover [40].

3.2.1. 1st experimental setup – chloride solution below corroding rebar

In the 1st experimental setup, specimens were first immersed in a container filled with 3.5% sodium chloride solution for 11 days. The immersion was intended to force the accumulation of chlorides on the surface, thus forcing the initiation of the corrosion process from above as soon as the rebar was exposed to the external current. After immersion,

the level of the solution was lowered below the level of the rebars. The specimens were left for 19 days to stabilize the moisture content throughout the concrete cover of the specimen. Then they were connected to an external power supply to accelerate the corrosion of the reinforcement. The total applied current was 0.038 A, which corresponds to a current density of 200 μA/cm^2. Three specimens were subjected to the accelerated corrosion process, which differed in the duration of the process. The duration was determined as a function of the targeted mass loss according to Faraday's law [45]. The targeted mass losses were 5%, 7.5% and 10%, corresponding to durations of the accelerated corrosion process of 39, 59 and 78 days, respectively.

3.2.2. 2nd experimental setup – chloride solution above corroding rebar

In the 2nd experimental setup, the 3.5% sodium chloride solution was placed in a container made of polystyrene sheets that occupied the entire top surface of the specimens. Initially, the solution was stored without a power supply for 5 days to stabilize the potential corresponding to the required current. By day 10, a total current of 0.114 A was applied, corresponding to a current density of 600 μA/cm^2. The higher current density, than in the 1st experimental setup, was intended to ensure a greater amount of corrosion products in the concrete cover. On the 10th day, the hairline crack appeared on the surface of the specimens. It was concluded that maintaining the higher current density (600 μA/cm^2) would probably lead to a sudden accumulation of corrosion products around the rebar without gradual migration into the concrete cover, which is not the case in reality. For this reason, the current was reduced to a value of 0.038 A, which corresponds to a current density of 200 μA/cm^2. In this experimental setup, three specimens were also subjected to the corrosion process for 39, 59, and 78 days. The arrangement of the 1st and 2nd experimental setups is shown in Table 3.

3.3. Assessment methods

The moisture and chloride content in the concrete cover were monitored along with the crack width during the corrosion acceleration process, as they have a great influence on all the corrosion attributes presented in this paper.

In the 1st experimental setup, relative humidity was monitored using the PosiTector CMM IS concrete moisture meter, with probes embedded at a depth of 50 mm. In the 2nd experimental setup, moisture content was determined by taking samples from the exposed surface. The samples were cylinders with a diameter of 18 mm and a height of 50 mm. The cylinders were cut to a height of 10 mm and then the mass of each piece was calculated (m_1), to obtain a gradual distribution of moisture in the concrete cover. The final moisture content w, where m_2 is the mass of each piece after drying to a constant weight, was determined as follows:

$$w = \frac{m_1 - m_2}{m_2} \cdot 100\% \tag{1}$$

Two different physical properties were measured in the two experimental setups. The sensors used to measure relative humidity in the 1st experimental setup were not applicable in the 2nd setup due to the submerged surface of the specimens. However, the relationship between these two properties is established [46,47].

The total chloride content was determined by potentiometric titration. First, the concrete powder was taken every 10 mm to a depth of 50 mm. A known amount of the concrete powder was placed in a beaker and mixed with 100 ml of deionized water and 10 ml of a 5 mol/l nitric acid (HNO$_3$) solution. The solution was then heated to boiling with constant stirring and stirred for another 3 min. The solution was then titrated with 0.1 M silver nitrate (AgNO$_3$).

Each moisture and chloride monitoring measurement was performed on one specimen from a series, assuming that the other specimens were exposed to the same conditions. During the corrosion process, the cylinders for moisture characterization were taken from the top of the
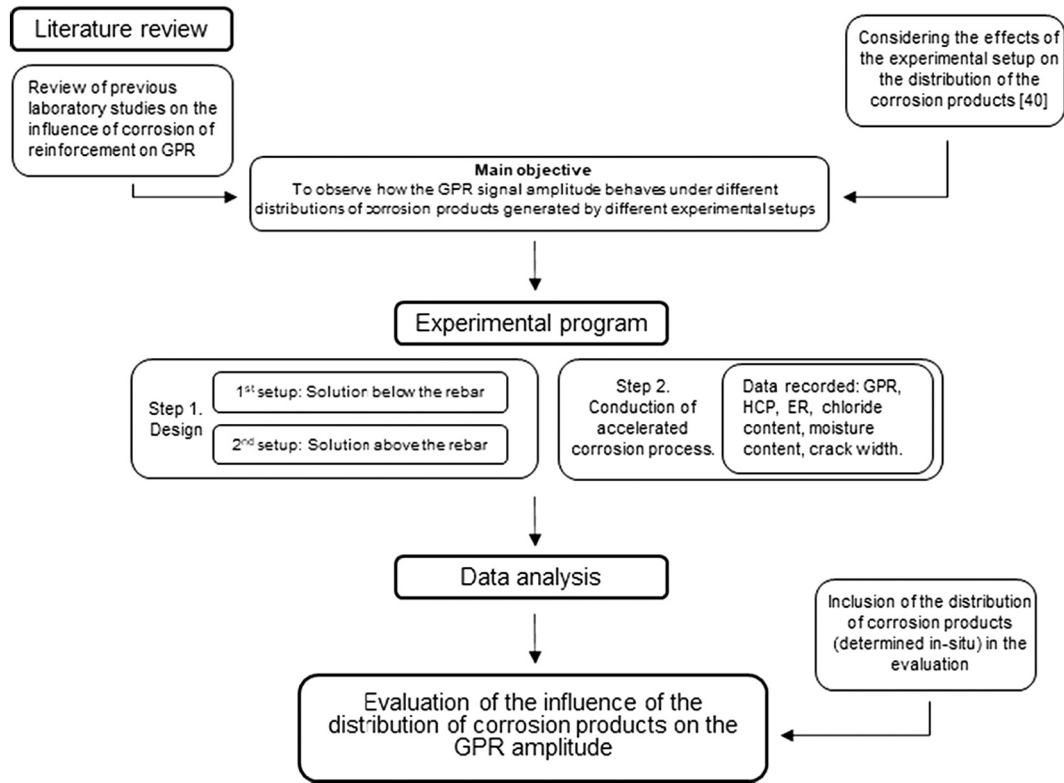
Fig. 1. Research methodology.

Table 2
Concrete mix design and properties of fresh and hardened concrete.

Concrete mix design						
Cement [kg/m³]	Potable water [kg/m³]	River aggregate [kg/m³]			Chemical admixtures [kg/m³]	
		0/4 mm	4/8 mm	8/16 mm	superplasticizer	air-entraining admixture
401	121	843	501	579	2	1.6
Properties of fresh and hardened concrete						
Slump [mm]		Air-content [%]			Compressive strength with standard deviation [MPa]	
180		5			51.5 ± 3.4	

concrete near the edges of the specimen on the cathode rebar side. The concrete powder was taken near the anode. The sampling locations were chosen to be far enough to avoid the influence of the resulting holes on the GPR measurements.

Relative humidity and moisture content were determined on days 7, 10, 14, 28, 42, 56, and 70 of the corrosion process. Chloride content was determined on days 14, 28, 42, 56, and 70. In addition, chloride content was determined before the start of the accelerated corrosion process (day 0) for the 1st experimental setup and on days 7 and 10 for the 2nd experimental setup. Chlorides were also determined at the end of the corrosion process (days 39, 59, 78) for each specimen above the anode for both experimental setups.

Crack width was measured every 7 days, on day 10, and at the end of the testing period for each specimen using a crack width ruler at 5 points along the crack. The final value was determined as the average of 5 data points.

During the experiments, the current density and thus the applied current was kept constant, while the applied voltage varied according to the changes in the resistance of the specimens. For this reason, the change in voltage was also monitored. The data acquisition system was

set to record the voltage value every hour throughout the experiments.

3.3.1. Monitoring of corrosion attributes

GPR examination was performed every 7 days. In addition, it was performed on day 10 and at the end of the test period for each specimen. The GPR used in this study was Geophysical Survey Systems Inc. (GSSI) 2.7 GHz device. The scan interval of the instrument was 8 scans/cm, with the scan sampled in 512 data points. The scan range was 5 ns. The scans were processed using RADAN 7 software. The raw GPR data was processed with a bandpass filter and background removal. A constant one-point gain was also used.

In both experiments, data were collected from above. In the 2nd experimental setup, the solution was removed each time data were collected. The surface was cleaned with a cloth so that no excess water was visible on the surface. The GPR profiles were recorded perpendicular to the rebars. A total of 10 profiles were recorded each time, of which 5 were type A and 5 were type B (Fig. 4). Monitoring of reflected signal strength was based on observation of peak amplitudes derived from the scan over the anode rebar. The amplitudes were extracted and the final amplitude was determined as the average of 10 profiles. The amplitude is reported as normalized amplitude A in dB, expressed as

$$A = 20log_{10}\frac{A_t}{A_0} \quad [dB]$$

A_t — amplitude at time,

A_0 — amplitude before corrosion. (2)

Monitoring of half-cell potential (HCP) as well as electrical resistivity (ER) was performed on the same days as GPR, except for the 2nd experimental setup before corrosion, where HCP and ER could not be measured due to extremely dry conditions. The half-cell potential is a semi-destructive technique for evaluating corrosion probability [48]. It is based on measuring of the potential difference between the reference electrode and the rebar. In this study, the Proceq Profometer Corrosion was used, and the reference electrode was the CSE (copper/copper
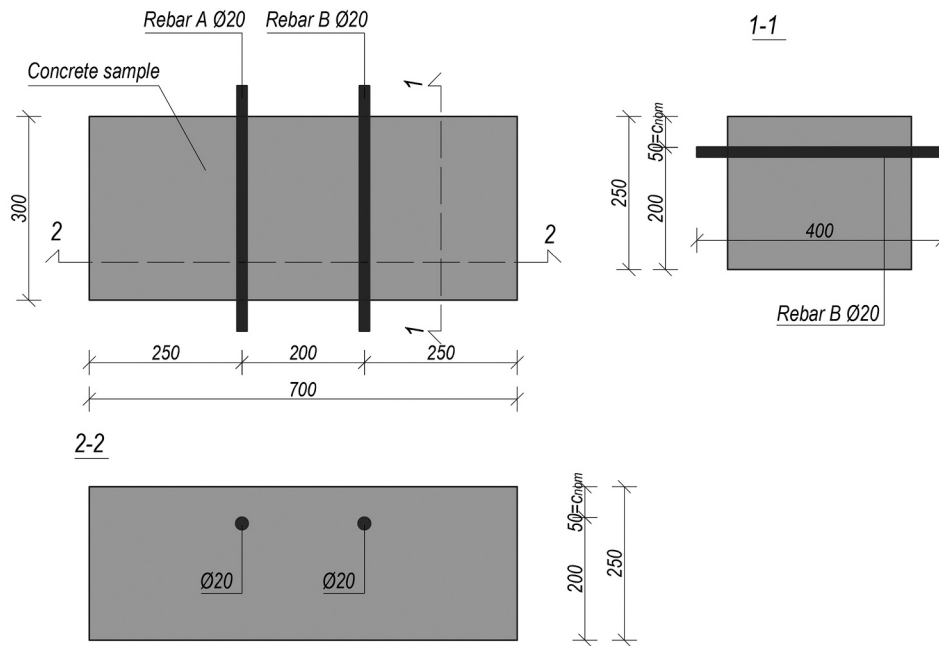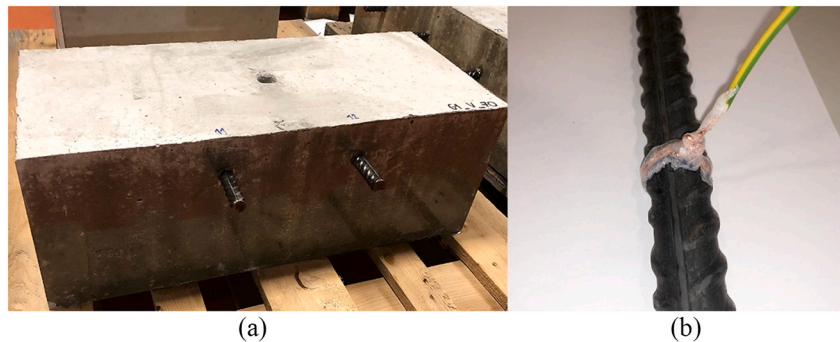
Fig. 2. Design of the specimen.

Fig. 3. a) Epoxy coated sides of the specimen, b) connection between rebar and wire.

sulphate electrode). During the measurement, the reference electrode was placed over the anode rebar. The potential values above -200 mV CSE indicate that the corrosion probability is $<$10%, while it is $>$90% for values below -350 mV CSE [48].

Measuring the electrical resistivity of concrete is another method for assessing the corrosion risk [49]. Proceq Canin + Corrosion Analyzing Instrument with Wenner probe was used to measure the electrical resistivity of concrete. The resistivity was measured beyond the anode region with the probe oriented at a 45° to the direction of the rebar. If resistivity is 50–100 kΩcm the corrosion risk is low, 10–50 kΩcm - corrosion risk is moderate, and $<$ 10 kΩcm - corrosion risk is high [49].

In the 1st experimental setup, the surface was moistened 20 min before the measurements of HCP and ER. Both measurements were taken after GPR data collection was completed. During the GPR, HCP, and ER measurements, the anode and cathode were temporarily disconnected from the power supply.
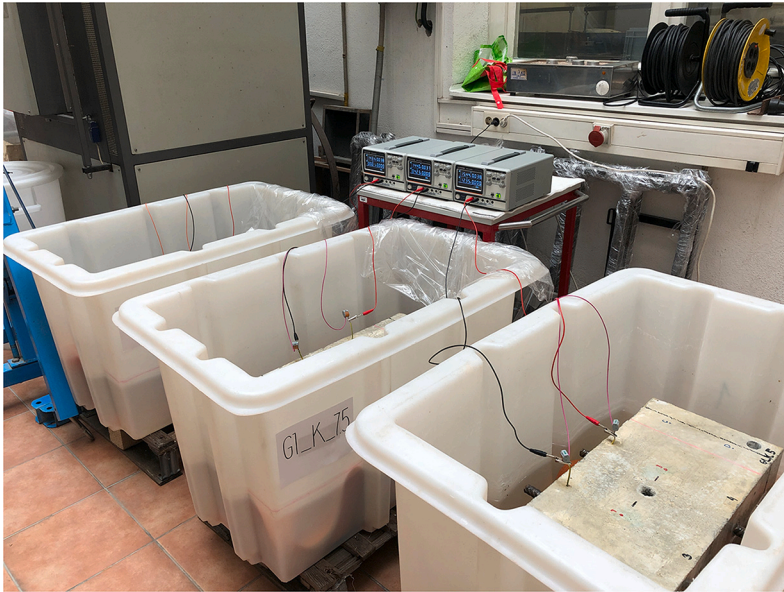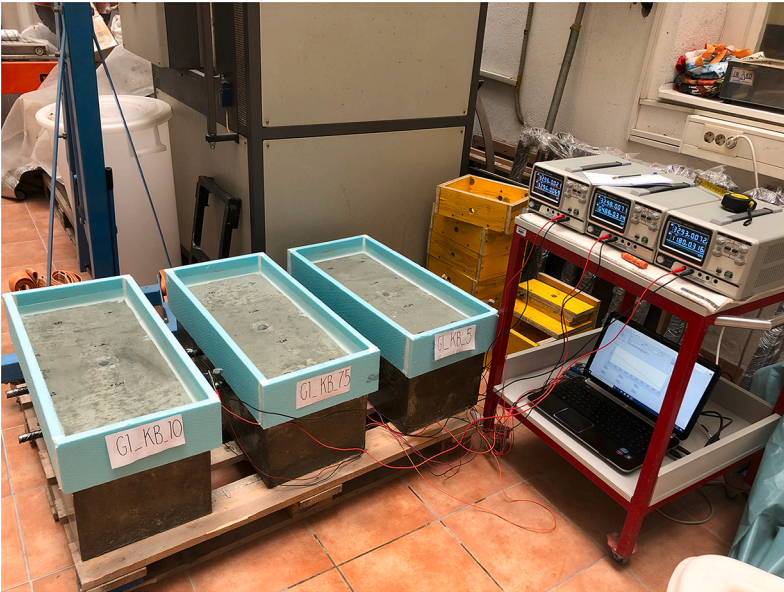
4. Results

Relative humidity for 1st and moisture content for 2nd experimental setup during testing period are shown in Table 4.

In the 1st experimental setup, a high relative humidity of the concrete was maintained at the depth of the reinforcement, although the level of the sodium chloride solution was below the level of the

reinforcement. In the 2nd experimental setup, a stable moisture content in the concrete pores was observed only after seven days of the accelerated process and remained stable throughout the process. This is evident from the low value of the standard deviation around the average value of 4.8% for all depths. The distribution of moisture was such that there was no moisture gradient, but the moisture was evenly distributed over the concrete cover.

Fig. 5 shows the change in normalized amplitude (a), chloride content (b), crack width (c), resulting applied voltage (d), half-cell potential (e) and electrical resistivity (f) during the corrosion process for both setups. In general, the normalized GPR amplitude in the case of the 1st experimental setup did not show a significant change in value nor a clear trend of change during the evolution of the corrosion process. The changes were very subtle and ranged from -1.2 dB to 1.6 dB. From the chloride profiles, it can be concluded that the chloride content in the concrete cover showed the greatest change between days 0 and 14. While the specimens were immersed in the solution before the potential was applied, the chlorides accumulated in a shallow zone on the concrete surface. Once the potential was applied, it affected the migration of the chloride ions [2] so that the chloride content was uniformly distributed over all depths during the corrosion process. In addition, the chlorides from the solution that was under the rebars were able to migrate around the rebars. The formation of corrosion products, which have a larger volume than steel [50], leads to higher stresses around the

Table 3

Specimens subjected to the accelerated corrosion process in 1st and 2nd experimental setup.

	1st experimental setup			2nd experimental setup		
Stabilization period without a power supply	11 days immersion in 3.5% sodium chloride solution			5 days exposure to 3.5% sodium chloride solution		
Current density [μA/cm²]	200			600, then 200 after 10 days		
Duration [days]	39	59	78	39	59	78
Specimen	K1_5	K1_7.5	K1_10	K2_5	K2_7.5	K2_10
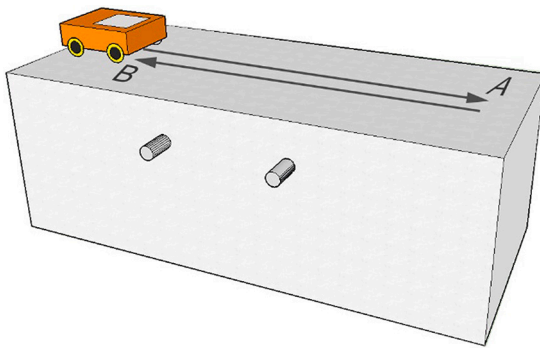
Fig. 4. GPR profiles orientation.

Table 4
Relative humidity and moisture content.

Day of accelerated corrosion process [days]	1st experimental setup	2nd experimental setup				
	Relative humidity RH [%]	Moisture content w [%]				
		0–10	10–20	20–30	30–40	40–50
7	95.1	5.7	5.8	5.1	3.8	4.8
10	94.3	5.8	5.2	3.8	4.4	4.9
14	92	6.0	4.8	3.3	4.3	4.3
28	79.4	5.2	4.7	5.0	4.0	5.2
42	86.6	5.8	4.0	4.5	5.3	4.3
56	79.4	4.9	4.9	4.2	4.7	3.2
70	77.9	5.7	3.8	4.3	6.0	5.0
	RH mean value with standard deviation					
	86.4 ± 7.5	w mean value with standard deviation				
		4.8 ± 0.7				
	Corresponding w calculated from RH, according to [47]					
	5.1	Corresponding RH calculated from w, according to [47]				
		82.7				

rebars, which in turn leads to cracks in the concrete cover. The specimens were designed so that the crack was initiated from the top surface. Two out of three specimens from the 1st experimental setup showed longitudinal cracks above the anode bars. In addition, the specimens with cracks exhibited different behaviour, with the crack on K1_5 occurring 14 days before K1_7.5. Looking at the distribution of corrosion products shown in Table 5, it is clear that there was an initial disturbance in specimen K1_5. It appears that there was an initial defect at the interface between the reinforcement and the concrete that caused an accelerated accumulation of corrosion products on the left side of the specimen where the connection to the power supply was located. This caused the appearance of a wider crack on the top surface and was also noted by the faster decrease in the applied voltage for specimen K1_5 compared to specimen K1_7.5, while the current density remained constant (Fig. 5d). The applied voltage curves for the specimens with cracks were lower than the curve for the specimen without cracks, and this is more pronounced for the specimens where the crack occurred earlier. However, none of the effects described above had a significant effect on the GPR amplitude.

In contrast, different results were reported for the 2nd experimental setup. The GPR amplitudes for all three specimens followed a decreasing trend during the accelerated corrosion process. The largest decrease in amplitude was observed by day 10, where the curve showed a steep slope (see Fig. 5a). This is consistent with the higher current density applied by day 10 (Table 3). The decrease in amplitude continued after day 10, but at a slower rate. The specimen exposed to the accelerated corrosion process for the longest time exhibited the greatest signal loss, which was −11.5 dB on day 78 (corresponding to an amplitude loss of

73%). During the process, the chloride content in the concrete cover also changed, Fig. 5b. The chloride profiles taken near the anode showed a gradient in chloride content, while the profiles taken above the anode (at the end of each testing period; at 39, 59 & 78 day) at the end of the process showed a more uniform distribution. In addition, the chloride content values were higher above the anode. This is to be expected since there were cracks above the anode that allowed greater chloride penetration. In addition, the closer proximity of the anode affected the higher attraction of chloride ions. As for the development of cracks, the specimens of the 2nd experimental setup showed almost the same behaviour during the process. The cracks appeared on the 10th day and expanded at the same rate for all specimens. The resulting applied voltage (Fig. 5d) initially showed higher values corresponding to the higher current density (Table 3). The voltage corresponding to the specimen K2 _5 was slightly lower than that of the other two specimens, Fig. 5d.

The value of the half-cell potential is an indicator of the ease of electron release [51], with more negative values indicating that the release is facilitated, suggesting a corrosion process. Considering the ASTM recommendation [48], the measured potential in both experiments was almost always below the of −350 mV value (Fig. 5e), indicating a corrosion process. The values for concrete resistivity show a similar behaviour (Fig. 5f). However, in this case, the different design of the experimental setups was reflected in slight differences in the resistivity values. The shift to a lower value for the 2nd experimental setup was most likely due to a higher chloride content [49], Fig. 5b, caused by the presence of sodium chloride solution at the top of the specimen. Nevertheless, the resistivity values were rather constant during the accelerated corrosion process and were around the value of 10 kΩcm.

5. Discussion

In this study, two different experimental setups were designed in which an accelerated corrosion process was carried out to monitor the effects of the process on the changes in GPR signal amplitude. In addition, several other methods were performed in parallel with GPR monitoring to substantiate the results. The results are discussed further with respect to two experimental setups.

For the 1st experimental setup, the GPR signal amplitude did not change significantly during the corrosion acceleration, while half-cell potential, electrical resistivity, and cracks occurrence result indicated an active corrosion process. At the end of the testing period, all specimens were opened at the location of the anode rebar to confirm corrosion activity. The specimen sections and the corrosion pattern through the anode are shown in Table 5. The corrosion pattern was considered for 2/3 of the bar in the centre of the specimen. On each side of the specimen, 5 cm is disregarded because the corrosion products present there are mainly the result of the pronounced corrosion at the contact between the rebar and the wires for electrical connection, as well as the leakage of the rebar on the outside of the contact with the concrete.

From the table above, it can be seen that the steel consumption due to corrosion, the formation of corrosion products and their migration in the 1st experimental setup occurred mainly below the rebar (84.5% for K1_5 and 94.3% for K1_7.5). Especially, when the orientation and position of GPR profiles is taken into account, Fig. 4. The position of the electrolyte in the 1st experimental arrangement forced the movement of chlorides from the electrolyte to the underside of the rebar and resulted in the reactions occurring mainly in this area. Furthermore, the location of corrosion reaction had an influence on the results obtained with the GPR. In fact, the propagation of the corrosion products from the bottom of the rebar affected the changes on the surface of the rebar and the surrounding concrete, which had a minor effect on the reflected GPR signal. This is because the metal, in this case the rebar, is considered a perfect reflector [52]. This means that when the electromagnetic waves encounter the reinforcement, they are completely reflected back to the receiving antenna. Thus, throughout the accelerated process, the scan above the anode represents the wave that has propagated only through
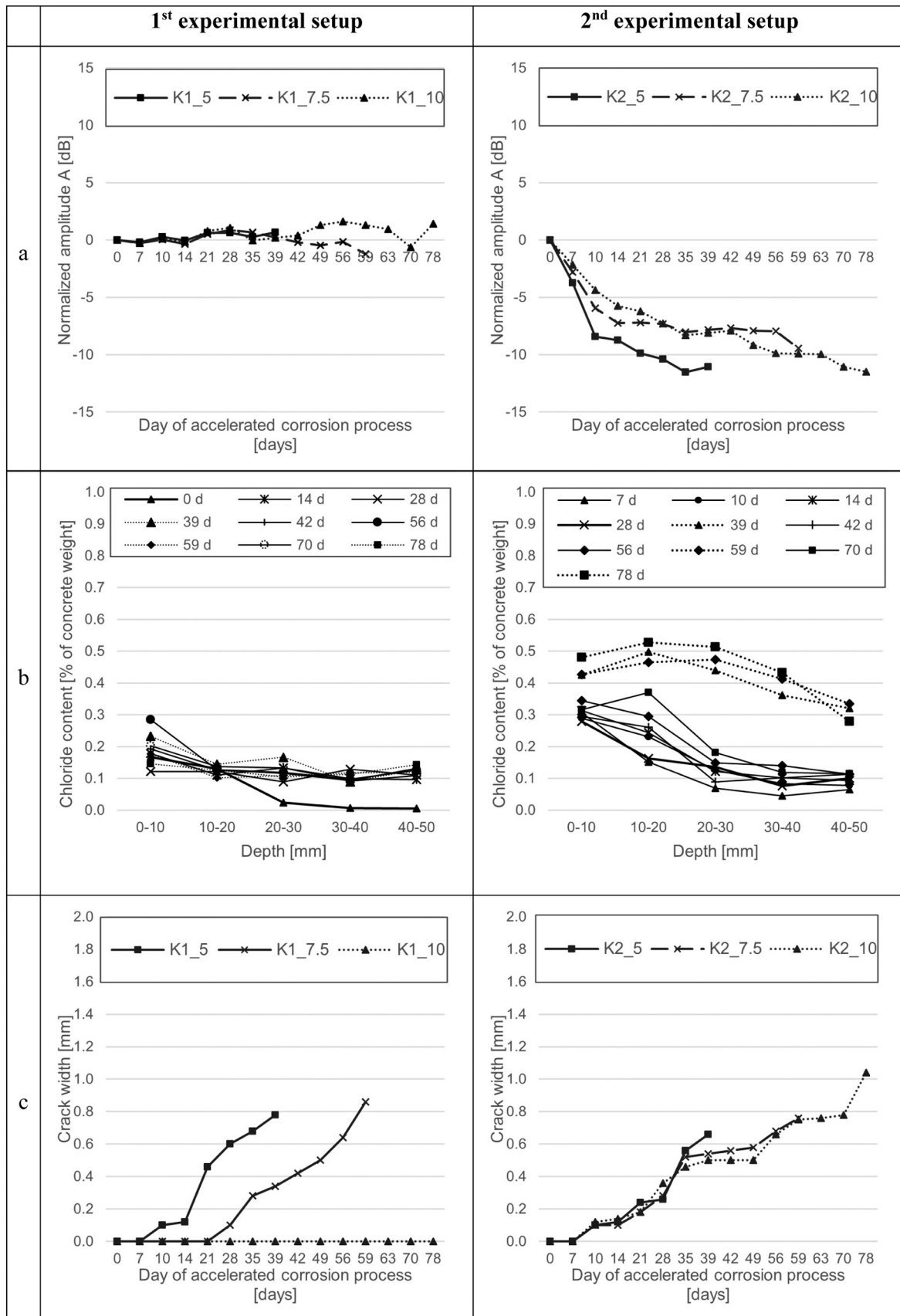
Fig. 5. a) Normalized GPR amplitude, b) chloride profiles, c) crack width, d) resulting applied voltage, e) half-cell potential and f) electrical resistivity during the corrosion process for samples designed according to the 1st experimental setup (diagrams on the left) and the 2nd experimental setup (diagrams on the right).
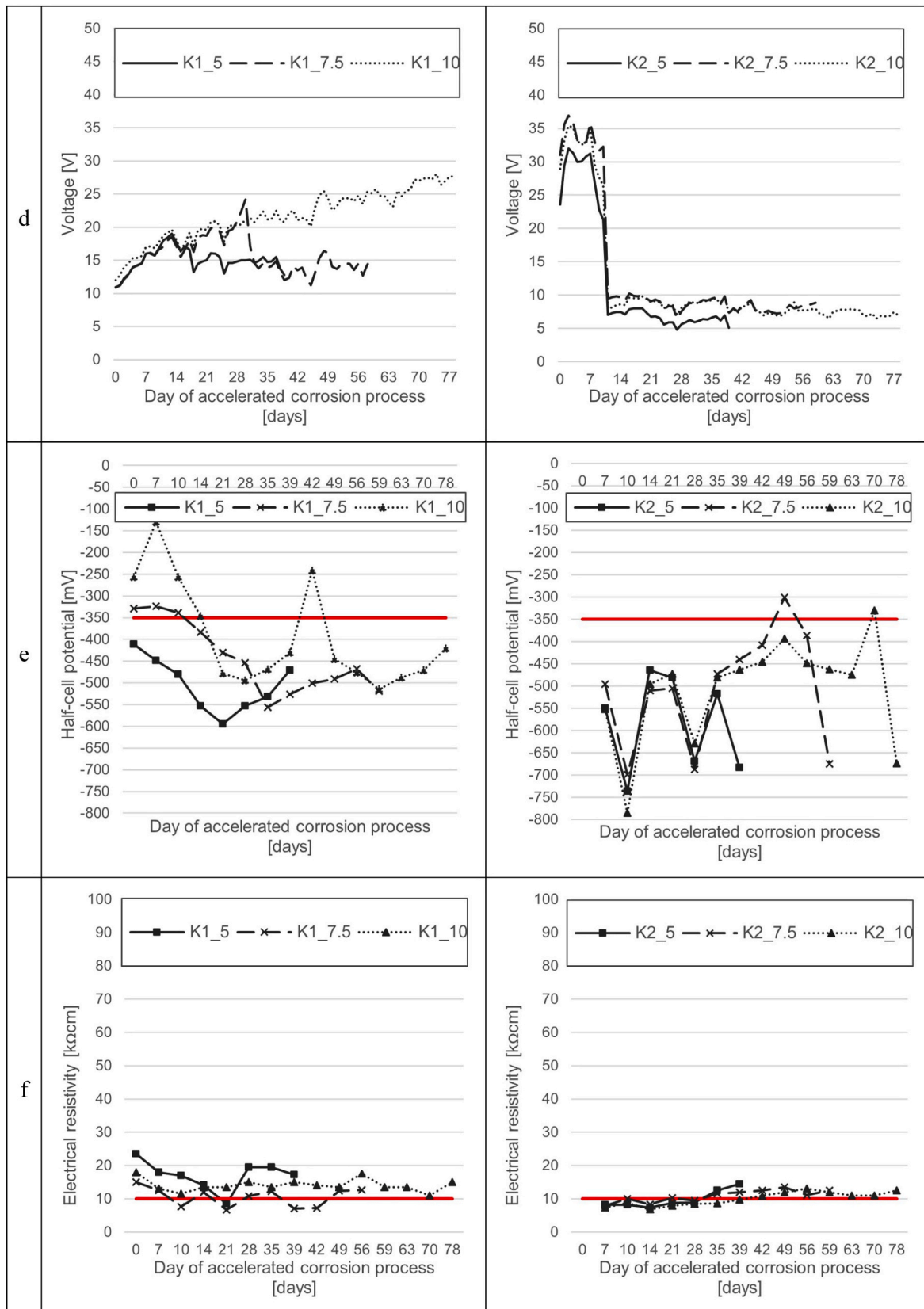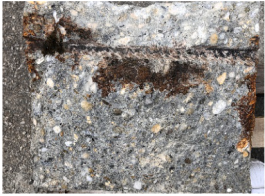
Fig. 5. (*continued*).

the concrete cover. In the case of the 1st experimental setup, the condition of the concrete cover was stable throughout the testing period, therefore the amplitude was also stable. First, the moisture content in

the concrete cover had stabilized after the drying period, which had no further effect on the change of amplitude. Second, and more importantly, the propagation of corrosion products from the bottom of the

Table 5

Characterization of corrosion activity based on the sections through the anode bar.

Specimen	Section through the anode bar		Area under corrosion products	
	Figure of the cross section	Corrosion pattern in observed area	above the rebar	below the rebar
1st experimental setup				
K1_5			15.5%	84.5%
K1_7.5			5.7%	94.3%
K1_10		no corrosion detected		
2nd experimental setup				
K2_5			67.2%	32.8%
K2_7.5			73.8%	26.2%
K2_10			60%	40%

rebar could not affect the GPR signal since the signal did not reach this layer, because of the experimental arrangement with a perfect reflector, reinforcement, placed between the GPR and the corrosion layer.

In specimen K1_10, there was no significant corrosion of the reinforcement for reasons unknown to the authors, as shown in Table 5. The absence of cracks on the concrete surface proves this fact. This is an explanation for the slight amplitude divergence on day 35 between specimens K1_7.5 and K1_10. Comparing these two specimens, it is suspected that the widening of the cracks in specimen K1_7.5 after day 35 (Fig. 5c) began to affect the dispersion of the waves [34], resulting in a slight decrease in amplitude in this specimen. However, this deviation

is no longer observed in specimen K1_5 after the day 14, when a crack occurred. In summary, the results show that cracks up to 0.9 mm do not lead to a significant change in GPR response.

Considering the results and the discussion about this experimental setup, it can be concluded that this experimental arrangement cannot accurately represent corrosion-induced changes that would be relevant for monitoring with ground penetrating radar. Moreover, this corrosion case does not correspond to the actual corrosion state of reinforced concrete structures, where corrosion mainly occurs on the side of the rebar facing the concrete cover [2].

The results obtained with the GPR in the 2nd experimental

arrangement differed from those of the 1st experimental arrangement. Although the values of half-cell potential and concrete resistivity indicated that the corrosion process developed at the same rate as in the case of the 1st experimental setup, the gradual changes in the GPR signal were observed here. At the end of the testing period, all specimens were opened at the location of the anode rebar to confirm corrosion activity. The sections through the anode rebars are shown in Table 5.

The first and the most important thing noted after opening the specimens was the distribution of the corrosion products. In this setup, the distribution of the corrosion products resembled more the natural corrosion of the reinforcement than the distribution in the first experiment, as the area under the corrosion products over the reinforcement was 67.2%, 73.8% and 60% for K2_5, K2_7.5 and K2_10, respectively. The products formed mainly at the top of the rebar and migrated through the concrete cover to the top of the specimen. The corrosion products had accumulated mostly in the narrow area around the rebar and gradually filled the pores of the concrete cover. The layer of corrosion products was most pronounced on the specimen with the highest degree of corrosion (K2_10).

The significant decrease in GPR amplitude strength that occurred in the 2nd experimental setup (Fig. 5a) was caused by several factors – water, chlorides dissolved in water, and corrosion products. This phenomenon can be explained by the reduction in amplitude due to: i) the change in the reflection coefficient of the steel and, ii) signal attenuation caused by changes in the properties of the surrounding concrete. The former is related to the change at the interface between concrete and steel, which is associated with the formation of corrosion products on the side of the reinforcement facing the concrete cover. Indeed, the amount of reflected energy at this surface is approximately equal to the contrast of the dielectric constants of these two materials [25]. The iron oxides have a lower dielectric constant than steel [52,53], so the energy reflected from the corrosion products in the narrow region of accumulation around the rebars is less than that of the noncorroding steel. As the signal propagates through the thin layer of accumulated corrosion products, it suffers additional signal loss as a result of additional propagation through the material [26]. Since the thickness of the corrosion product layer around the rebar is small, these reflections most likely overlap and result in an overall decrease in reflected energy.

The second cause of the significant reduction in amplitude is the combined action of water, chlorides dissolved in water, and corrosion products that have penetrated the concrete cover. These three affect the properties of the concrete in which the electromagnetic waves propagate. The electromagnetic properties of concrete, which is a mixture of different constituents, could be represented by the combined properties of solid particles, air, and water in the concrete pores [54]. After the specimen was treated with a sodium chloride solution from above, the ingress of the solution increased the amount of water in the concrete pores compared to the concrete before corrosion. It is known that this leads to a decrease in signal amplitude [30]. This effect is most pronounced in the first seven days and is associated with the amplitude decrease in Fig. 5a. The moisture content stabilized after the seventh day (Table 4), so it can be assumed that changes in moisture content do not further affect the amplitude change. However, under the influence of the current applied to the rebars, the chlorides migrated from the solution into the concrete pores (Fig. 5b) and further increased the salinity of the water in the pores, resulting in additional attenuation due to the increased conductivity [26]. The migration of corrosion products into the pores of the concrete caused the air component in the mix being partially replaced by the corrosion product component, which further changed the dielectric properties of the mix. Comparing the dielectric properties of air and iron oxides, the iron oxides exhibit higher permittivity and conductivity [26,53,55], resulting in additional signal loss. Even though concrete is considered a non-magnetic material in most cases, the presence of iron oxides in materials such as magnetite can cause non-negligible attenuation [26]. These changes are most pronounced in the first 10 days and are related to the higher corrosion rate of the reinforcement caused by the higher applied current density.

The last influencing factor is a crack, which appeared after the 10th day in all specimens above the anode. However, from the 1st experimental setup, it was concluded that a crack of up to 0.9 mm has a negligible effect on the dissipation of EM energy, so it is considered that it did not contribute significantly to the attenuation of the signal. The observed effect is in agreement with the numerical simulations on the influence of corrosion induced cracks on the GPR signal reported in [56]. There it was found that cracks up to 1 mm have a small effect on the GPR amplitude.

Based on the results obtained and the above discussion, it can be concluded that the solution facing the surface where the GPR inspection is performed is more suitable for observing the corrosion induced by the impressed current in the laboratory. The limitation of this study is the inevitable change in the salinity of the water in the concrete pores, which prevented the isolated effect of the spread of corrosion products on the GPR amplitude from being observed. Further studies will focus on isolating these two effects.

The ability of non-destructive methods to detect the corrosion process is highly dependent on the technique used. Half-cell potential and electrical resistivity detect corrosion regardless of the location of the corrosion layer with respect to the rebar and the concrete surface, while ground penetrating radar requires a change on the side of the rebar facing the concrete surface being tested. Therefore, in the second experimental setup, all non-destructive methods were able to detect the corrosion, while the GPR had sufficient resolution and stability in testing to detect the progression of the process over time, enabling quantitative analysis of the kinetics of the corrosion process over time.

Considering the real structures, the second experimental setup is closer to the natural evolution of the corrosion process, so the present study confirms that the GPR can be used to evaluate the corrosion of reinforcement in RC structures. However, certain limitations must be emphasised. It will be difficult to use the GPR as a stand-alone test method when evaluating structures for which historical data are not available and which are to be evaluated only once. In this case, the electrochemical methods, especially HCP, are more appropriate, even though they are destructive. If the testing of the structures extends over a longer period of time and is planned as a continuous monitoring of the structure, the GPR might be a better solution, as it provides a unique opportunity for non-destructive characterization of the corrosion kinetics. In addition, the GPR method could allow automation of the assessment of reinforced concrete structures. Currently, the limitations of GPR applications are the time-consuming data analysis and the insufficiently developed techniques for quantifying the reinforcement diameter.

6. Conclusion

In the present experimental study, the aim was to determine the influence of the different distributions of corrosion products caused by different experimental setups on the GPR signal amplitude in laboratory simulations. Due to the contradictory results on the influence of corrosion on the GPR signal reported in the literature, two experimental setups were designed: the first one replicates the setup of previous reported studies, and the second produces distribution closer to the natural corrosion process.

The results presented clearly show that the position of the sodium chloride solution during the accelerated corrosion process determines the location of corrosion products layer and their distribution in the concrete cover, which in turn determines the behaviour of the GPR signal. If the solution is below the rebar level, the formation of corrosion products occurs mainly from the bottom of the rebars. The migration of corrosion products also occurs mainly in the direction of the solution and deeper into the concrete. In that case, although all corrosion parameters clearly indicated corrosion propagation, the GPR amplitude did not change significantly. This can be attributed to the stable

condition of the concrete cover during the experiment and the inability of the signal to surpass fully reflective reinforcement to reach corrosion product layer. On the other hand, when the solution was at the top of the specimens, the formation of corrosion products and their migration is directed towards the upper surface of the concrete. In that case, the GPR amplitude had a decreasing trend throughout the corrosion propagation. The changes in GPR signal were influenced by the combined effect of changes at the interface between concrete and steel and changes in the material. Therefore, the second case better represents the corrosion of the reinforcement in real structures, as well as the changes that would be relevant for monitoring with ground penetrating radar. This experimental setup is more suitable for inspection with GPR in cases where corrosion is induced by impressed current technique. When comparing GPR with other electrochemical methods (HCP and ER), GPR was able to detect the progression of the corrosion process, while HCP and ER showed only minor changes in the progress of corrosion.

Further research is needed to isolate the effects of each material parameter (e.g. the moisture content, chlorides) independently to determine their contribution to the overall change in the GPR signal, and to observe the effects of the combined parameters to create different environmental conditions.

Funding

Declaration of Competing Interest

The authors declare that they have no known competing financial interests or personal relationships that could have appeared to influence the work reported in this paper.

## Data availability

Data will be made available on request.

References

[1] M. Alexander, H. Beushausen, Durability, service life prediction, and modelling for reinforced concrete structures – review and critique, Cem. Concr. Res. 122 (2019) 17–29, https://doi.org/10.1016/j.cemconres.2019.04.018.

[2] L. Bertolini, B. Elsener, P. Pedeferri, R.B. Polder, Corrosion of Steel in Concrete: Prevention, Diagnosis, Repair, Wiley, Weinheim, 2003. ISBN: 9783527308002.

[3] X. Shi, N. Xie, K. Fortune, J. Gong, Durability of steel reinforced concrete in chloride environments: an overview, Constr. Build. Mater. 30 (2012) 125–138, https://doi.org/10.1016/j.conbuildmat.2011.12.038.

[4] D. Banic, D. Bjegovic, G. Balabanic, Study of corrosion rate in reinforced-concrete, Gradevinar J. Croat. Assoc. Civ. Eng. 60 (2008) 123–132.

[5] U. Angst, B. Elsener, C.K. Larsen, Ø. Vennesland, Critical chloride content in reinforced concrete - a review, Cem. Concr. Res. 39 (2009) 1122–1138, https://doi.org/10.1016/j.cemconres.2009.08.006.

[6] S. Ahmad, Reinforcement corrosion in concrete structures, its monitoring and service life prediction - a review, Cem. Concr. Compos. 25 (2003) 459–471, https://doi.org/10.1016/S0958-9465(02)00086-0.

[7] M. Otieno, H. Beushausen, M. Alexander, Chloride-induced corrosion of steel in cracked concrete – part I: experimental studies under accelerated and natural marine environments, Cem. Concr. Res. 79 (2016) 373–385, https://doi.org/10.1016/j.cemconres.2015.08.009.

[8] D. Bjegovic, M. Serdar, A. Baricevic, M.J. Rukavina, Assessing condition of concrete pier after three decades of exposure to sea water, Gradevinar J. Croat. Assoc. Civ. Eng. 67 (2015) 1155–1164, https://doi.org/10.14256/JCE.1188.2014.

[9] M. Solla, B. Riveiro, P. Arias, H. Lorenzo, Introduction, in: B. Riveiro, M. Solla (Eds.), Non-Destructive Techniques for the Evaluation of Structures and Infrastructure, first ed., CRC Press, London, 2016, pp. 3–6, https://doi.org/10.1201/b19024.

[10] D.M. McCann, M.C. Forde, Review of NDT methods in the assessment of concrete and masonry structures, NDT & E Int. 34 (2001) 71–84, https://doi.org/10.1016/S0963-8695(00)00032-3.

[11] S. Abu Dabous, S. Feroz, Condition monitoring of bridges with non-contact testing technologies, Autom. Constr. 116 (2020), 103224, https://doi.org/10.1016/j.autcon.2020.103224.

[12] T. Omar, M.L. Nehdi, T. Zayed, Performance of NDT techniques in appraising condition of reinforced concrete bridge decks, J. Perform. Constr. Facil. 31 (2017) 04017104, https://doi.org/10.1061/(asce)cf.1943-5509.0001098.

[13] A. Tarussov, M. Vandry, A. De La Haza, Condition assessment of concrete structures using a new analysis method: ground-penetrating radar computer-assisted visual interpretation, Constr. Build. Mater. 38 (2013) 1246–1254, https://doi.org/10.1016/j.conbuildmat.2012.05.026.

[14] K. Dinh, N. Gucunski, T.H. Duong, An algorithm for automatic localization and detection of rebars from GPR data of concrete bridge decks, Autom. Constr. 89 (2018) 292–298, https://doi.org/10.1016/j.autcon.2018.02.017.

[15] W.W.-L. Lai, X. Dérobert, P. Annan, A review of ground penetrating radar application in civil engineering: a 30-year journey from locating and testing to imaging and diagnosis, NDT & E Int. 96 (2018) 58–78, https://doi.org/10.1016/j.ndteint.2017.04.002.

[16] D.J. Daniels, Ground Penetrating Radar, second ed., The Institution of Electrical Engineers, London, 2004. ISBN: 9780863413605.

[17] K. Dinh, N. Gucunski, J. Kim, T.H. Duong, Understanding depth-amplitude effects in assessment of GPR data from concrete bridge decks, NDT & E Int. 83 (2016) 48–58, https://doi.org/10.1016/j.ndteint.2016.06.004.

[18] K. Tesic, A. Baricevic, M. Serdar, Non-destructive corrosion inspection of reinforced concrete using ground-penetrating radar: a review, Materials (Basel). 14 (2021) 975, https://doi.org/10.3390/ma14040975.

[19] W.-L. Lai, T. Kind, M. Stoppel, H. Wiggenhauser, Measurement of accelerated steel corrosion in concrete using ground-penetrating radar and a modified half-cell potential method, J. Infrastruct. Syst. 19 (2013) 205–220, https://doi.org/10.1061/(ASCE)IS.1943-555X.0000083.

[20] S. Hong, W.W.-L. Lai, G. Wilsch, R. Helmerich, R. Helmerich, T. Günther, H. Wiggenhauser, Periodic mapping of reinforcement corrosion in intrusive chloride contaminated concrete with GPR, Constr. Build. Mater. 66 (2014) 671–684, https://doi.org/10.1016/j.conbuildmat.2014.06.019.

[21] C.L. Barnes, J.F. Trottier, D. Forgeron, Improved concrete bridge deck evaluation using GPR by accounting for signal depth-amplitude effects, NDT & E Int. 41 (2008) 427–433, https://doi.org/10.1016/j.ndteint.2008.03.005.

[22] N. Gucunski, F. Romero, S. Kruschwitz, R. Feldmann, A. Abu-Hawash, M. Dunn, Multiple complementary nondestructive evaluation Technologies for Condition Assessment of concrete bridge decks, Transp. Res. Rec. (2010) 34–44, https://doi.org/10.3141/2201-05.

[23] K. Dinh, N. Gucunski, J. Kim, T.H. Duong, Method for attenuation assessment of GPR data from concrete bridge decks, NDT & E Int. 92 (2017) 50–58, https://doi.org/10.1016/j.ndteint.2017.07.016.

[24] K. Dinh, N. Gucunski, Factors affecting the detectability of concrete delamination in GPR images, Constr. Build. Mater. 274 (2021), 121837, https://doi.org/10.1016/j.conbuildmat.2020.121837.

[25] ACI Committee 228, Nondestructive Test Methods for Evaluation of Concrete in Structures, American Concrete Institute, Farmington Hills, MI, 1998. https://www.concrete.org/publications/internationalconcreteabstractsportal/m/details/id/5119. (Accessed 10 July 2021).

[26] N.J. Cassidy, Electrical and magnetic properties of rocks, soils and fluids, in: H. M. Jol (Ed.), Ground Penetrating Radar Theory and Applications, Elsevier, Amsterdam, 2009, pp. 41–72, https://doi.org/10.1016/B978-0-444-53348-7.00002-8.

[27] S. Laurens, J.P. Balayssac, J. Rhazi, G. Klysz, G. Arliguie, Non-destructive evaluation of concrete moisture by GPR: experimental study and direct modeling, Mater. Struct. 38 (2005) 827–832, https://doi.org/10.1007/BF02481655.

[28] G. Klysz, J.P. Balayssac, Determination of volumetric water content of concrete using ground-penetrating radar, Cem. Concr. Res. 37 (2007) 1164–1171, https://doi.org/10.1016/j.cemconres.2007.04.010.

[29] X. Dérobert, J. Iaquinta, G. Klysz, J.P. Balayssac, Use of capacitive and GPR techniques for the non-destructive evaluation of cover concrete, NDT & E Int. 41 (2008) 44–52, https://doi.org/10.1016/j.ndteint.2007.06.004.

[30] S.F. Senin, R. Hamid, Ground penetrating radar wave attenuation models for estimation of moisture and chloride content in concrete slab, Constr. Build. Mater. 106 (2016) 659–669, https://doi.org/10.1016/j.conbuildmat.2015.12.156.

[31] J. Hugenschmidt, R. Loser, Detection of chlorides and moisture in concrete structures with ground penetrating radar, Mater. Struct. 41 (2008) 785–792, https://doi.org/10.1617/s11527-007-9282-5.

[32] S. Laurens, J.P. Balayssac, J. Rhazi, G. Arliguie, Influence of concrete relative humidity on the amplitude of ground-penetrating radar (GPR) signal, Mater. Struct. 35 (2002) 198–203, https://doi.org/10.1007/BF02533080.

[33] S. Hong, W.-L. Lai, R. Helmerich, Experimental monitoring of chloride-induced reinforcement corrosion and chloride contamination in concrete with ground-penetrating radar, Struct. Infrastruct. Eng. 11 (2015) 15–26, https://doi.org/10.1080/15732479.2013.879321.

[34] P.T.W. Wong, W.W.L. Lai, J.F.C. Sham, C. Poon, Hybrid non-destructive evaluation methods for characterizing chloride-induced corrosion in concrete, NDT & E Int. 107 (2019), 102123, https://doi.org/10.1016/j.ndteint.2019.05.008.

[35] V. Sossa, V. Pérez-Gracia, R. González-Drigo, M.A. Rasol, Lab non destructive test to analyze the effect of corrosion on ground penetrating radar scans, Remote Sens. 11 (2019) 2814, https://doi.org/10.3390/rs11232814.

[36] H. Liu, J. Zhong, F. Ding, X. Meng, C. Liu, J. Cui, Detection of early-stage rebar corrosion using a polarimetric ground penetrating radar system, Constr. Build. Mater. 317 (2022), 125768, https://doi.org/10.1016/j.conbuildmat.2021.125768.

[37] R.K. Raju, M.I. Hasan, N. Yazdani, Quantitative relationship involving reinforcing bar corrosion and ground-penetrating radar amplitude, ACI Mater. J. 115 (2018) 449–457, https://doi.org/10.14359/51702187.

[38] A. Zaki, M.A.M. Johari, W.M.A.W. Hussin, Y. Jusman, Experimental assessment of rebar corrosion in concrete slab using ground penetrating radar (GPR), Int. J. Corros. 2018 (2018) 5389829, https://doi.org/10.1155/2018/5389829.

[39] C. Fu, N. Jin, H. Ye, J. Liu, X. Jin, Non-uniform corrosion of steel in mortar induced by impressed current method: an experimental and numerical investigation, Constr. Build. Mater. 183 (2018) 429–438, https://doi.org/10.1016/j.conbuildmat.2018.06.183.

[40] J. Chen, C. Fu, H. Ye, X. Jin, Corrosion of steel embedded in mortar and concrete under different electrolytic accelerated corrosion methods, Constr. Build. Mater. 241 (2020), 117971, https://doi.org/10.1016/j.conbuildmat.2019.117971.

[41] S.S. Hubbard, J. Zhang, P.J.M. Monteiro, J.E. Peterson, Y. Rubin, Experimental detection of reinforcing Bar corrosion using nondestructive geophysical techniques, ACI Mater. J. 100 (2003) 501–510, https://doi.org/10.14359/12957.

[42] B.J. Zhan, W.W.L. Lai, S.C. Kou, C.S. Poon, W.F. Tsang, Correlation between accelerated steel corrosion in concrete and ground penetrating radar parameters, in: C. Leung, K.T. Wan (Eds.), International RILEM Conference on Advances in Construction Materials through Science and Engineering, RILEM Publications SARL, Hong Kong, China, 2011.

[43] HZN Standards Publications, HRN EN 12350–2:2019, Testing fresh concrete – Part 2: Slump-test, Croatian Standards Institute, Zagreb, 2019. https://repozitorij.hzn.hr/norm/HRN+EN+12350-2%3A2019 (accessed October 8, 2021).

[44] HZN Standards Publications, HRN EN 12390–3:2019, Testing Hardened Concrete - Part 3: Compressive Strength of Test Specimens, Croatian Standards Institute, Zagreb, 2019. https://repozitorij.hzn.hr/norm/HRN+EN+12390-3%3A2019 (accessed October 8, 2021).

[45] T.A. El Maaddawy, K.A. Soudki, Effectiveness of impressed current technique to simulate corrosion of steel reinforcement in concrete, J. Mater. Civ. Eng. 15 (2003) 41–47, https://doi.org/10.1061/(ASCE)0899-1561(2003)15:1(41).

[46] C. Andrade, J. Sarría, C. Alonso, Relative humidity in the interior of concrete exposed to natural and artificial weathering, Cem. Concr. Res. 29 (1999) 1249–1259, https://doi.org/10.1016/S0008-8846(99)00123-4.

[47] M. Cunningham, When is a concrete slab dry enough?, in: Build, April/May, 2008, pp. 25–26, B105–25-DrySlab.pdf, buildmagazine.org.nz. (Accessed 8 October 2021).

[48] ASTM, C876–91: Standard Test Method for Half-Cell Potentials of Uncoated Reinforcing Steel in Concrete. https://www.astm.org/c0876-91r99.html, 1999. (Accessed 8 October 2021).

[49] R. Polder, C. Andrade, B. Elsener, Ø. Vennesland, J. Gulikers, R. Weidert, M. Raupach, Test methods for on site measurement of resistivity of concrete, Mater. Struct. 33 (2000) 603–611, https://doi.org/10.1007/BF02480599.

[50] A. Poursaee, Corrosion of steel in concrete structures, in: A. Poursaee (Ed.), Corrosion of Steel in Concrete Structures, Elsevier, London, 2016, pp. 19–33, https://doi.org/10.1016/B978-1-78242-381-2.00002-X.

[51] A. Poursaee, C.M. Hansson, Potential pitfalls in assessing chloride-induced corrosion of steel in concrete, Cem. Concr. Res. 39 (2009) 391–400, https://doi.org/10.1016/j.cemconres.2009.01.015.

[52] D.J. Clem, T. Schumacher, J.P. Deshon, A consistent approach for processing and interpretation of data from concrete bridge members collected with a hand-held GPR device, Constr. Build. Mater. 86 (2015) 140–148, https://doi.org/10.1016/j.conbuildmat.2015.03.105.

[53] W.M. Haynes, CRC Handbook of Chemistry and Physics, 97th ed., CRC Press, Boca Raton, 2017. ISBN: 9781498754286.

[54] U.B. Halabe, K. Maser, E.A. Kausel, Propagation characteristics of electromagnetic waves in concrete, in: Massachusetts Institute of Technology, Civil Engineering, Report No.: ARO 2462U.3-EG-UIR, 1989.

[55] R.M. Cornell, U. Schwertmann, The Iron Oxides, Wiley, Weinheim, 2003. ISBN: 9783527302741.

[56] S. Hong, D. Chen, B. Dong, Numerical simulation and mechanism analysis of GPR-based reinforcement corrosion detection, Constr. Build. Mater. 317 (2022), 125913, https://doi.org/10.1016/j.conbuildmat.2021.125913.

Paper III
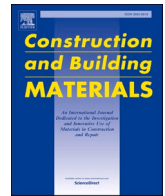
Quantifying the impact of parameters of chloride-induced reinforcement corrosion on the GPR signal

Ksenija Tesic [a], Ana Baricevic [a,*], Marijana Serdar [a], Nenad Gucunski [b]

[a] *University of Zagreb Faculty of Civil Engineering, Department of Materials, Fra Andrije Kacica-Miosica 26, Zagreb 10000, Croatia*
[b] *Department of Civil and Environmental Engineering, Rutgers, The State University of New Jersey, 500 Bartholomew Road, Piscataway, NJ 08854, USA*

ARTICLE INFO

ABSTRACT

The sensitivity of the high-frequency ground penetrating radar (GPR) signal to changes within the reinforced concrete (RC) makes it a valuable tool for corrosion assessment of RC structures. The most important parameters in chloride-induced corrosion are moisture content, chloride content, and reinforcement diameter loss. The objective of this laboratory study was to investigate and quantify the influence of these parameters on the GPR signal. Of particular interest was to determine which of the observed parameters the GPR is most sensitive to. Furthermore, particular emphasis was placed on understanding the influence of corrosion products, which has not met the consensus in the existing literature. The parameters were studied on a total of forty-two specimens where the reflector of the GPR waves was the reinforcement embedded in the concrete specimen. Based on the experimental data, values of normalized amplitude related to the evaluation of corrosion by GPR were proposed.

1. Introduction

During the initiation phase of chloride-induced corrosion, the main parameters to consider in the inspection of reinforced concrete (RC) structures are moisture and chloride content within the concrete, while in the propagation phase it is a loss of reinforcement cross-section. Unfortunately, in most cases, the parameter that triggers the need for a detailed assessment of RC structures is a visible sign of corrosion on the surface of the structure, e.g., cracks, rust stains, concrete spalling etc. The main reasons for reluctance to perform a detailed assessment in the early stages of corrosion are the duration of the inspection, its complexity and finally the cost. However, the consequences of corrosion [1–5] remind us forcefully on the need of detailed assessment of reinforced concrete structures as part of proactive, rather than reactive infrastructure asset management.

The step towards more efficient maintenance of the RC structures could be the repeated inspection using non-destructive testing (NDT) [6–9]. The main advantages of NDT are more frequent inspection of large areas and shorter inspection time while being completely non-invasive. In recent decades, ground penetrating radar (GPR) has gained importance as a valuable non-destructive testing method in the inspection of structures [10–16]. The analysis of characteristics of electromagnetic waves emitted by the GPR and reflected due to changes

in the interior structure of an element under inspection is of core interest [17,18]. In addition to the wide application of GPR in civil engineering to reconstruct the invisible interior of structural elements [12,19–21], the evaluation of reinforcement corrosion by GPR is of particular interest, but also presents a significant challenge [11,22–27]. Most parameters affecting corrosion of reinforcement in concrete have been previously studied with GPR: moisture content [28–31], chloride content [31–35] and reinforcement corrosion [23,36–40]. While it would be remarkable that one technique could detect all the important parameters affecting the corrosion process, the analysis is more complicated because more than one influential parameter is involved and usually only one outcome parameter is measured, namely the strength of the reflected signal [41–43]. Table 1 gives an overview of laboratory studies on the influence of moisture, chlorides, and corrosion on the GPR signal.

Regarding the reflector, it can be seen from Table 1 that the studies that focused on the moisture/chloride content aimed to show the relationship between the parameters of the concrete and the parameter of the GPR, independently of the corrosion of the rebar. For the corrosion initiation phase, the concrete parameters can be considered independent of the rebar corrosion, but for the corrosion propagation phase, the influence of the corrosion products must be considered. In addition, the effect of corrosion products on the amplitude change is ambiguous and no consensus has yet been reached on whether the corrosion products

---

attenuate or amplify the GPR signal [24,37,38,45,46]. Some of the possible reasons for this ambiguity could be that the laboratory experiments unintentionally created an environment in which the amplitude change was additionally altered by other factors such as moisture and chloride fluctuations [11,48], or that the amplitude change did not depend on the corrosion products because the spread of the corrosion products was not appropriate [22].

The main objective of this study is to investigate and quantify the influence of all the main parameters involved in chloride-induced corrosion of reinforcement in concrete: moisture, chlorides, and corrosion products, on the amplitude of GPR signal. The parameters were investigated on a total of forty-two reinforced concrete specimens, where the GPR signal reflector was the reinforcement. The experimental setup for laboratory-induced corrosion was carefully selected to ensure that the corrosion pattern was suitable for investigation by GPR. The comparison of the influence of the observed parameters has been summarised, and recommendations are given for the amplitude values stemming from the corrosion evaluation of RC structures by GPR.

2. Materials and methods

2.1. Materials and specimen preparation

The concrete specimens were prepared using cement CEM I 42.5 R cement, river aggregate (0/4 mm, 4/8 mm, and 8/16 mm), and potable water. The cement content was 300 kg/m^3, and the water-to-cement ratio was 0.6.

The investigations were performed on concrete specimens 300 mm × 200 mm × 90 mm with a reinforcing bar (20 mm diameter and 300 mm length) and a concrete cover of 50 mm, Fig. 1. The part of the reinforcing bar that was outside the specimen was coated with epoxy resin. The geometry of the specimens was designed to simulate the cut-
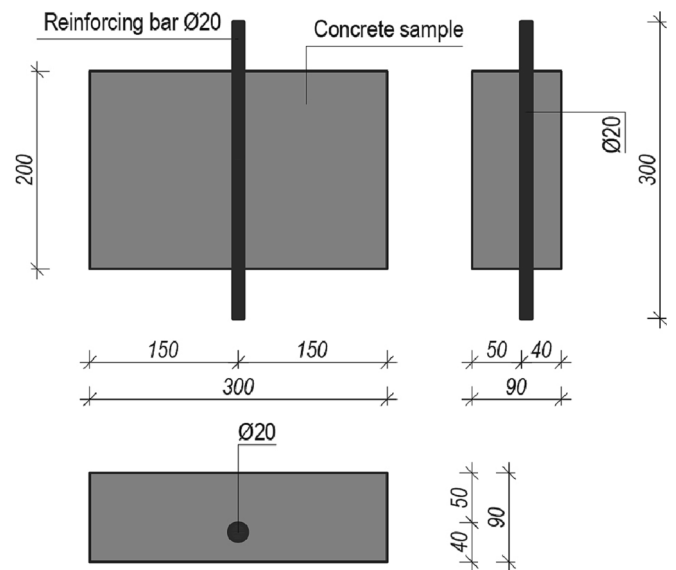

Fig. 1. Specimen design (dimensions in millimetres).

outs of the reinforced concrete elements, but at the same time to be suitable for testing with GPR. All dimensions were chosen to eliminate the overlapping of signals from two adjacent reflectors, considering the performance of the device and the principles of signal propagation.

A total of forty-two specimens were cast. They were divided into three groups of specimens: 1) group to observe the influence of moisture, 2) group to observe the influence of chlorides, and 3) group to observe the influence of corrosion products on the GPR signal.

Table 1
Review of laboratory studies on the effects of moisture content, chloride content and reinforcement corrosion on GPR signal.

Property	Trend of amplitude change	Equation	Function	Reflector	Depth [cm]	Reference
Moisture content	↓	n/a	n/a	Slab bottom	7	Laurens et al. [28]
	↓	A = A$_i$/A$_{air}$	A = –0.044 w + 0.959	Slab bottom	8	Sbartaï et al. [30]
	↓	A = A$_i$/A$_{air}$	A = –0.063 w + 0.9	Slab bottom	12	Klysz et al. [29]
	↓	n/a	n/a	Slab bottom	8	Hugenschmidt et al. [32]
	↓	A= (20/D) log (A$_i$/A$_C$)	A = –12.695 w – 11.51	Slab bottom	7	Senin et al. [31]
	↓	A = 20 log (A$_{DW}$/A$_i$)	A = 1.859 w^3 – 34.259 w^2 + 212.395 w – 405.836	Rebar	8	Kaplanvural et al. [44]
Chloride content	↓	n/a	n/a	Slab bottom	8	Sbartaï et al. [33]
	↓	n/a	n/a	Slab bottom	8	Hugenschmidt et al. [32]
	↓	A= (20/D) log (A$_i$/A$_C$)	A = –6.867 × – 123.91	Slab bottom	7	Senin et al. [31]
Reinforcement corrosion	↓	n/a	n/a	Rebar	1.9 and 3.8	Hubbard et al. [45]
	↑↓	n/a	n/a	Rebar	7	Zaki et al. [46]
	↑	n/a	n/a	Rebar	2.5 and 7.5	Lai et al. [24]
	↑	n/a	n/a	Rebar	7	Hong et al. [23]
	↑↓	n/a	n/a	Rebar	6	Wong et al [38]
	↓	n/a	n/a	Rebar	8 and 7	Sossa et al. [37]
	↑	n/a	n/a	Rebar	3	Liu et al. [47]
	↓	n/a	n/a	Rebar	5	Tesic et al. [22]

Note: A$_i$ – amplitude of reflected wave, A$_{air}$ – amplitude of wave recorded in air, A$_C$ – amplitude on control specimen, D – specimen height, A$_{DW}$ – amplitude of direct wave, w – volumetric water content (%), x – free chloride content, n/a – not available.

2.1.1. Reaching different moisture conditions

Specimens prepared for observation of the effect of moisture on the GPR signal were brought to a saturation level of 15–20%, 45–50%, or 75–80%. A total of nine specimens were prepared for this purpose, three for each saturation range. The specimens were first dried to a constant mass, then saturated to 100%, and finally dried in an oven at 50 °C to the desired degree of saturation. The desired saturation level *w* was determined according to the following equation,

$$w = (m_3 - m_1)/(m_2 - m_1) \cdot 100 \ [\%] \tag{1}$$

where m_1 is the mass after drying to constant mass, m_2 is the mass after saturation, and m_3 is the mass up to the desired saturation level.

2.1.2. Reaching different chloride-rich conditions

Chlorides were introduced into concrete specimens in two ways, first by adding sodium chloride (NaCl) into the concrete mix (referred to herein as internal chlorides), and second by subjecting the specimens to wet-dry cycles by immersion in sodium chloride solutions, (external chlorides).

A total of 1.19 kg/m^3, 1.98 kg/m^3, 2.97 kg/m^3, 4.95 kg/m^3, 9 kg/m^3, and 14.94 kg/m^3 of sodium chloride were dissolved into potable water and added to the concrete during mixing in the first procedure. The amounts of chlorides correspond to the following chloride concentrations: 0.24%, 0.4%, 0.6%, 1%, 1.8% and 3% of the cement mass, m_c. Eighteen specimens were prepared according to the procedure described above, three for each concentration. All specimens were tested at 0% (dry), 15–20%, 45–50%, 75–80%, and 100% (fully saturated) saturation levels.

The second procedure involved immersing the specimens in a 2%, 3.5%, or 5% sodium chloride solution. The procedure consisted of four cycles of wetting (five days immersion in the solution) and drying (two days drying in the air). Specimens were then immersed until saturation in the same solutions and dried to a saturation level of 0% (dry), 15–20%, 45–50%, and 75–80% and tested with GPR. Three specimens were immersed in each solution, making a total of nine specimens prepared for the described procedure.

2.1.3. Reaching different stages of corrosion

The intended stages of corrosion of the reinforcement in the concrete specimens were achieved by exposing the reinforcement to external current from the laboratory power supply. The specimens had wires for electrical connection that were prepared before casting. The connection between the reinforcement and the wire was protected with an impermeable mastic. On top of the specimens was a container made of polystyrene sheets in which water was placed during the accelerated corrosion process (Fig. 2). The objective was to keep the concrete cover partially wet to force the gradual spread of the corrosion products into the concrete cover. The power supply was set to a voltage of 32 V, but

Fig. 2. The setup for the accelerated corrosion process.

with an upper current limit of 0.025 A, corresponding to a current density of 200 μA/cm^2. A total of six specimens were subjected to the accelerated corrosion process, which differed in the duration of exposure to the external current. The specimens were exposed to the accelerated process for 90, 120, 150, 180, 210, and 240 days. After the accelerated process, the specimens were left under laboratory conditions without a water container for 3 months to stabilize the concrete cover condition, and then the GPR test was performed. The saturation level under laboratory conditions was in the range of 60–65%. This was done to exclude the influence of water content variations in the concrete cover and to ensure that the signal change was only due to the influence of corrosion products.

2.2. GPR measurements

The GPR used in this study was Geophysical Survey Systems Inc. (GSSI) 2.7 GHz device. The scan interval of the instrument was 8 scans/cm, with the scan sampled in 512 data points. The scan range was 5 ns. The scans were processed using RADAN 7 software. The raw GPR data was processed with a bandpass filter and background removal. A constant one-point gain was also used.

GPR profiles were taken from the top of the specimens as shown in Fig. 3. One GPR profile corresponded to the three specimens in a series that came from the same mixture and had the same condition. Two control samples were placed on the sides of the specimens. In addition, a metal plate was placed at the bottom of the series of specimens. The exception was the specimens made for the observation of the influence of the corrosion process, where the profile contained three specimens with different degrees of corrosion between two control specimens. The GPR profiles were taken perpendicular to the reinforcing bars. A total of ten profiles were taken, five forward and five reverse profiles, Fig. 3.

The analysis of the influence of the observed effects on the GPR signal was based on the observation of the peak amplitudes of the signal reflected from the rebar, derived from the scan over the rebar. The amplitudes were extracted, and the final amplitude was determined as the average of ten profiles. The amplitude reported herein is the normalized amplitude *A* in dB, expressed as:

1) Moisture assessment

$$A = 20 \log_{10}(A_m/A_0) \ [dB] \tag{2}$$

where A_m is amplitude at a given saturation level and A_0 is amplitude of the same specimen in dry condition,

2) Chloride assessment

$$A_1 = 20 \log_{10}(A_{Cl}/A_0) \ [dB] \tag{3}$$

where A_{Cl} is amplitude at a given chloride concentration and A_0 is amplitude of the specimen without chlorides at the same degree of saturation.

In addition, the influence of chlorides on the GPR signal is expressed by the amplitude A,

$$A = 20 \log_{10}(A_{Cl}/A_0) \ [dB] \tag{4}$$

where A_{Cl} is amplitude at a given chloride concentration and A_0 is amplitude of the same specimen in dry condition*.[1]

3) Corrosion assessment

$$A = 20 \log_{10}(A_C/A_0) \ [dB] \tag{5}$$

---

[1] For the specimens immersed in the solution, the dry condition was reached before the wet-dry cycles.
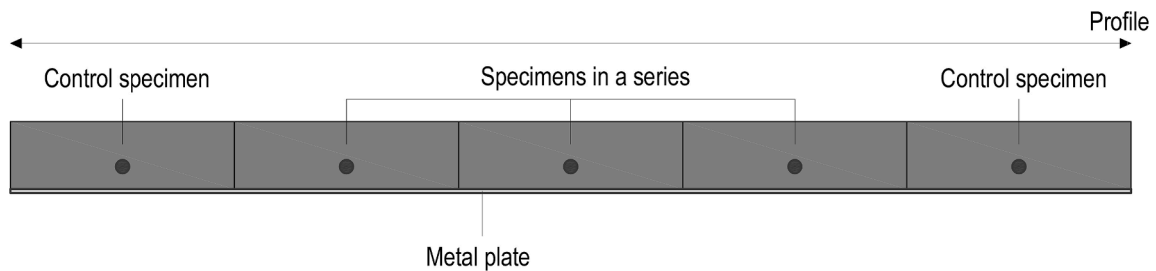
Fig. 3. GPR profiles.

where A_C is amplitude at a given stage of corrosion and A_0 is amplitude of the same specimen before corrosion.

It should be mentioned that the values of the amplitudes A_m, A_{Cl}, A_C, and A_0 depend on the particular GPR device and its construction. Also, the values of the amplitudes recorded after propagation through the material depend on the centre frequency of the device. The higher the centre frequency, the greater the attenuation of the signal as it propagates through the same material compared to a device with a lower centre frequency [17]. However, given the normalization procedures (Eqs. (2)–(5)) and the fact that commercially available GPR devices for concrete inspection operate in a similar frequency range, it can be assumed that the results obtained in this work should also apply to investigations other than this particular GPR.

2.3. Chloride profiles

For the specimens prepared for the observation of the influence of chlorides on the GPR signal, the total chloride content was determined by potentiometric titration. The concrete powder was taken every 10 mm to a depth of 50 mm, i.e., to the depth of reinforcement. A known amount of the concrete powder was placed in a beaker and mixed with 100 ml of deionized water and 10 ml of a 5 mol/l nitric acid (HNO_3) solution. The solution was then heated to boiling with constant stirring and stirred for an additional 3 min, according to [49]. The solution was then titrated with 0.1 M silver nitrate ($AgNO_3$). The amount of chlorides is expressed as percentage of the mass of the cement, m_c.

2.4. Reinforcement mass loss

Reinforcement mass loss was measured in the specimens where the effect of corrosion products was observed. All bars were weighed and labelled before mixing the concrete. After the GPR measurements, all specimens were opened at the section where the reinforcement had been placed. After pulling out the reinforcement, the corrosion products were removed mechanically. An angle grinder with a cup brush was used for this purpose. The reinforcement was not additionally cleaned, as it was brought to a metallic gloss by mechanical cleaning. After the corrosion products were removed, the mass of the cleaned rebar was measured. The final mass loss Δm was determined as follows,

$$\Delta m = (m_1 - m_2)/m_1 \cdot 100 \ [\%] \tag{6}$$

where m_1 is the mass of the rebar before concrete mixing and m_2 is the mass of the cleaned rebar after the corrosion process.

3. Results

3.1. Effect of moisture

The normalized amplitude A according to Eq. (2), obtained on a group of specimens where the effect of moisture on the GPR signal was observed is shown in Fig. 4.

The amplitude loss increases with the degree of saturation – the maximum amplitude loss occurs for fully saturated specimens, and according to the normalization to the dry specimen, amplitude A reaches -13.62 dB at a propagation depth of 50 mm. Accordingly, 2.72 dB is lost on each centimetre of concrete when the concrete pores are filled with water. When the pores are half-filled, the loss is one half. This means that the relationship between the normalized amplitude and the degree of saturation can be well expressed in linear terms. However, it was found that larger changes occur at the ends of the saturation range, i.e., below 20% and above 80%. The amplitude loss is related to the mechanisms resulting from the presence of water molecules in the pores of the concrete, i.e., the pore water [50]. When the concrete specimens are exposed to an electromagnetic field, the dipolar molecules tend to
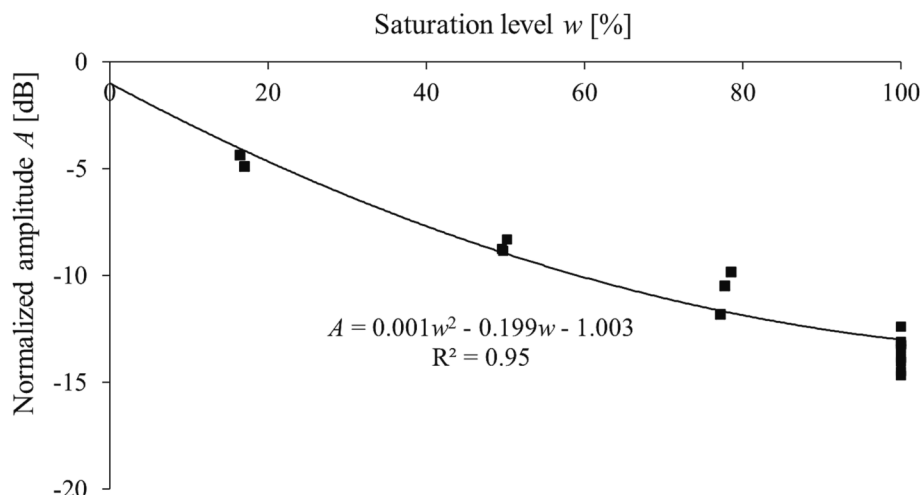

Fig. 4. The normalized amplitude A as a function of the saturation level.

realign according to the applied current and form dipole moments. This effect is called dipolar polarization. As a result of the realignment and the interaction of the particles, some of the energy is converted into heat, leading to an overall decrease in amplitude. The rate of molecular polarization depends on the frequency of the incident pulse [51,52], which means that both the dielectric properties and the amplitude loss are frequency dependent. The behaviour of free water in the presence of an electromagnetic field is described by the Debye model [53]. The Debye diagram shows that there is a relaxation frequency at which the amplitude loss is highest, and this frequency is around 19 GHz for free water molecules. At this frequency, the energy is not transferred for the formation of the organized orientation moments but is consumed in the disordered motion of the molecules. If the water in the material is not completely free to move, as in concrete pores [54,55], the relaxation frequency may fall within the operating range of the GPR, resulting in additional amplitude loss.

3.2. Effect of chlorides

The chloride content, expressed as a percentage of the cement mass, calculated as explained in Section 2.3, is shown in Table 2. Each value in a row in Table 2 is the average chloride content of three specimens.

If the chlorides were added to the concrete during mixing, the chloride profiles in the concrete cover (Table 2) are quite homogeneously distributed for the specimens mentioned. Exceptions are specimens with higher chloride concentration, where the total chloride content is higher near the surface than in the depth of the reinforcement. The reason for this could be the higher water-cement ratio in the first centimetre of the specimens, which is mainly characterised by a higher porosity, thus attracting the higher chloride content [56]. In contrast to the chloride profiles for internal chlorides, the profiles for external profiles tend to show the gradient of the chlorides at the concrete cover. The first centimetre facing the surface that was directly exposed to the sodium chloride solution has the highest concentration, and the concentration decreases with depth.

Fig. 5 shows the normalized amplitude functions according to Eq. (3) as a function of chloride concentration c (mean value in concrete cover). The internal chlorides are marked in black, and the external ones are in magenta. If the amplitude of the reflected wave at a given saturation level for a mixture containing chlorides is normalized to the amplitude of a specimen with the same saturation level but without chlorides (Eq. (3)), the loss can be attributed only to the effect of the chlorides. The positive numbers of A_1 are not included in Fig. 5. The reason for the positive numbers could be slight geometry differences between the two specimens used for normalization, or the position of the rebar in the specimen could influence the described occurrence. This is most pronounced in the examinations at the 15–20% saturation level. This means

that the influence of chlorides is lowest at low saturation levels.

The effect of the chlorides is apparent; it causes amplitude loss. This is mainly the consequence of the increased conductivity of the heterogeneous material [13,50], where the charged ions dissolved in the pore water consume energy in random collisions due to the presence of an electromagnetic field. According to this normalization procedure, the loss for the mixtures with an average chloride content of 0.7% of m_c is –1.6 dB, 1.2% of m_c is –5 dB and 3.1% of m_c is –13.7 dB, all at full saturation. At half saturation, the loss for the mixture with chlorides 3.1% of m_c is –3 dB, while for the mixtures with 0.7% and 1.2% the normalized amplitude has a positive sign according to Eq. (3).

The normalization procedure according to Eq. (4) is intended to show the effect of the amplitude change due to the joint effect of water saturation and chlorides. Fig. 6. shows the behaviour of the amplitude of the GPR signal in accordance with Eq. (4). As for the internal chlorides, the loss is greatest for the mixture with the highest chloride content (3.1 % wt. of cement) and the highest saturation level (100%). The slope of the curves increases with increasing chloride content. At higher saturation levels, the combined effect of water and chlorides is greater because the conduction effects are enhanced by the presence of water due to the facilitated movement of charges in the liquid. In the low saturation range (below 20%), the losses are fairly independent of chloride content. This is probably because the movement of charged ions is restricted in the absence of water. For the mix with an average chloride content of 0.7% of the m_c (internal chlorides group), the signal loss is −14.8 dB for fully saturated specimens. For the concrete with an average chloride content of 1.2% of m_c, the loss is −18.3 dB and for the severe chloride environment with a chloride content of 3.1% of m_c, this loss is −25.6 dB, both at full saturation. For the same mixes, the losses at half-filled pores are −5.6 dB, −7.3 dB and −9.4 dB, respectively. For the specimens with external chlorides, the losses are as follows: −18.2 dB for chloride content of 1.1% of m_c, −22.3 dB for chloride content of 1.6% of m_c and −25.1 dB for chloride content of 2% of m_c, at full saturation, and −11.5 dB, −14.3 dB and −18.3 dB at half saturation.

For the comparison, the specimens to which 1% of chlorides to the m_c was added during mixing (mean chloride content is 1.2% of m_c) and the specimens exposed to a 2% sodium chloride solution (mean chloride content is 1.1% of m_c) have similar average chloride content in the concrete cover. According to Eq. (4), the loss for the first and second groups of specimens is −18.3 dB and −18.2 dB at full saturation and −7.3 dB and −11.5 dB at half saturation. The specimens to which 1.8% of chlorides to the m_c was added and the specimens exposed to a 5% sodium chloride solution have an average chloride content of 1.8% and 2% of m_c, respectively. The losses are as follows: −20.3 dB and −25.1 dB at full saturation and −10.8 dB and −18.3 dB at half saturation. The loss was found to be lower for the internal chlorides than for the external chlorides. This could be explained by the higher ratio of free to total

Table 2
The chloride content in the concrete cover.

Internal chlorides	Chlorides added in mixture [% of m_c]	Chloride concentration [% of m_c]						
		Depth [mm]					Mean value	Standard deviation
		0–10	10–20	20–30	30–40	40–50		
	0.24	0.5	0.4	0.4	0.3	0.4	0.4	0.1
	0.4	0.9	0.7	0.4	0.7	0.5	0.7	0.2
	0.6	0.7	0.6	0.8	0.8	0.6	0.7*	0.1
	1	1.9	1.1	1.1	1.1	0.8	1.2	0.4
	1.8	2.9	1.8	1.4	1.5	1.5	1.8	0.6
	3	5.2	3.1	2.5	2.3	2.6	3.1	1.2
External chlorides	Concentration of solution [%]	Chloride concentration [% of m_c]						
		Depth [mm]					Mean value	Standard deviation
		0–10	10–20	20–30	30–40	40–50		
	2	2.8	1.0	0.6	0.6	0.6	1.1	1.0
	3.5	4.2	1.4	0.9	0.8	0.6	1.6	1.5
	5	4.7	1.7	1.2	1.2	1.1	2.0	1.5

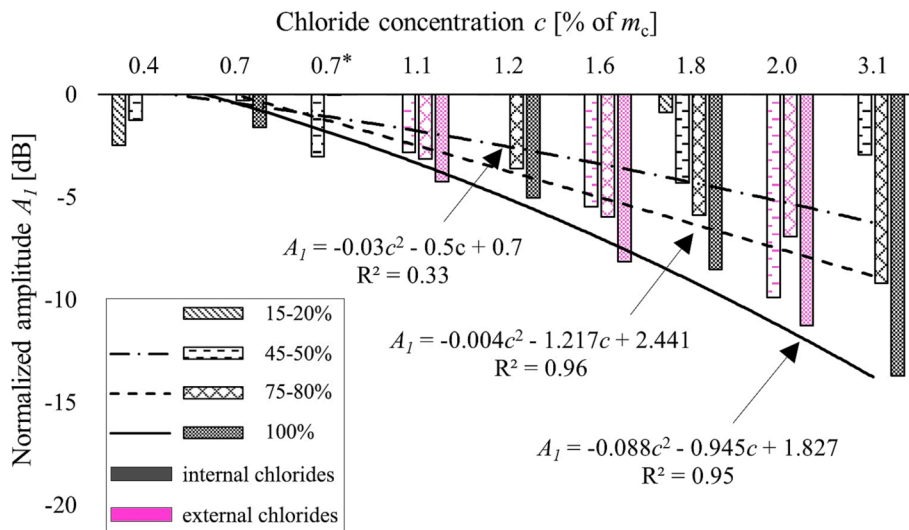 * The value that is marked with "*" in Figs. 5 and 6.

Fig. 5. The normalized amplitude A_1 as a function of chloride content.
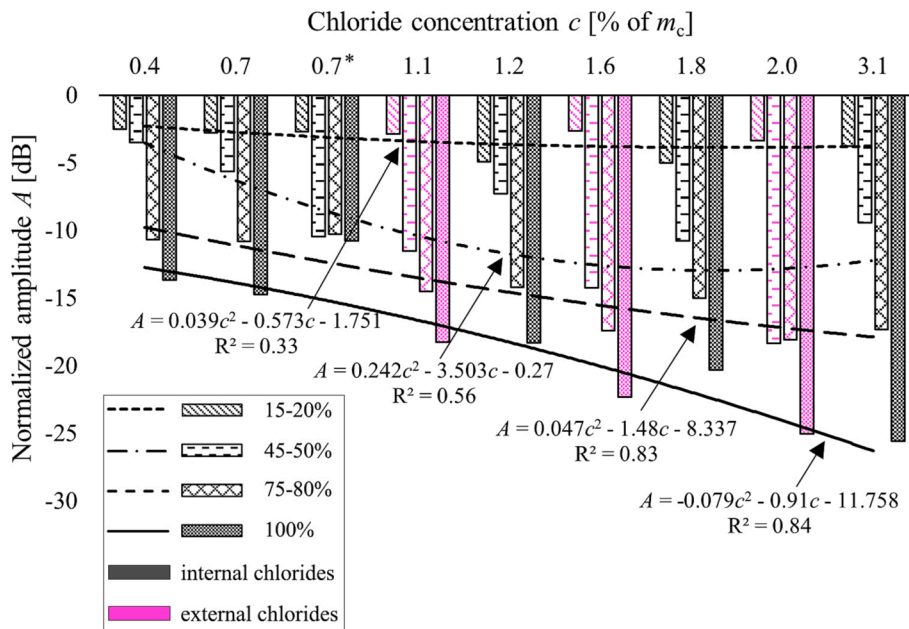

Fig. 6. The normalized amplitude A depending on the average chloride content.

chlorides in the case of the external chlorides [57], which have less restricted motions in the cement matrix compared to the bound chlorides, resulting in higher energy dissipation during particle collision.

3.3. Effect of corrosion products

The signal change due to the corrosion of the reinforcement in the concrete specimen as a function of the mass loss Δm is shown in Fig. 7. The mass loss of the specimens subjected to accelerated corrosion ranges from 0.17% to 2.1%. The main finding of this study is that the increase in corrosion degree affects the amplitude loss. The normalized amplitude according to Eq. (5) ranged from –0.4 dB to –10.8 dB.

For the majority of specimens, the degree of corrosion corresponded to a mass loss between 0.1% and 0.8%. The cross-sections through the corroded reinforcing bars of the specimens opened after completion of the accelerated corrosion process are shown in Fig. 8. It was explained in Section 2.1.3. that the container of water was present during the corrosion process to maintain the concrete cover in a partially wet

condition. In this setup, the ongoing corrosion process and the propagation of the corrosion products develop from the top of the rebar facing the side where the investigation with GPR is performed. This phenomenon was discussed in detail in reference [22]. From Fig. 8, it can be seen that the metal consumption was as explained in the previous sentence. Starting with the lowest corrosion level, the specimens that corroded for 90 days had the smallest corroded area at the top of the rebar. The specimens that corroded for 120, 150, and 180 days had the same but more pronounced corrosion pattern. Finally, the specimens with 210 and 240 days of corrosion, which exhibited the highest degree of corrosion, also had corrosion products on the bottom side of the rebar.

The lowest mass loss is 0.17% and corresponds to an amplitude loss of –0.39 dB. The rebar that corroded for 120 days had a mass loss of 0.46%. The normalized amplitude according to Eq. (5) had a minor value, but with a positive sign. The cross-section of this specimen, shown in Fig. 8, indicates that most of the corrosion products accumulate near the ends of the rebar. On the other hand, most of the radiated GPR energy is reflected from the central part of the rebar, since the profiles
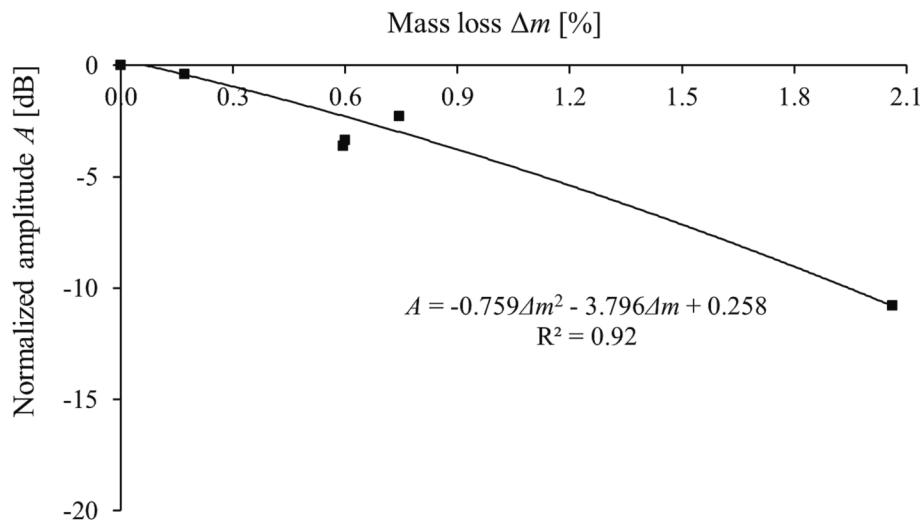
Fig. 7. The normalized amplitude A as a function of corrosion degree.

$$A = -0.759\Delta m^2 - 3.796\Delta m + 0.258$$
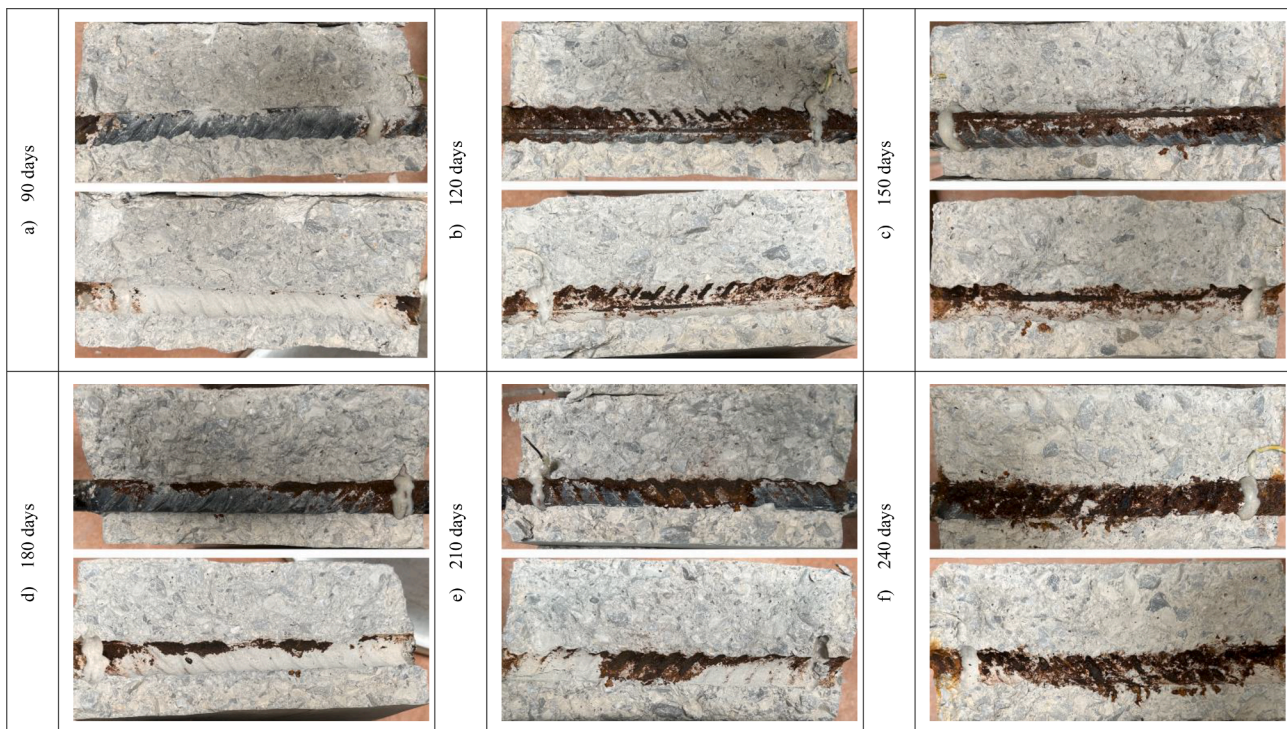$$R^2 = 0.92$$

Fig. 8. The cross-section of the corroded specimens after a) 90 days, b) 120 days, c) 150 days), d) 180 days, e) 210 days and f) 240 days of accelerated corrosion.

shown in Fig. 3 correspond to the centreline connecting the specimens. Simplifying the radiated energy as a cone with an ellipse base, as proposed in [58], the central part affected by the electromagnetic waves is the middle 1.5 cm long region of the rebar. The explanation for the lack of amplitude change in this specimen is therefore that the corrosion change did not occur in the central part of the rebar, but on the outer sides of the rebar. The two following specimens, subjected to a corrosion process for 150 and 180 days, had the same degree of corrosion corresponding to a mass loss of 0.6%, so the normalized amplitude had very similar values, –3.6 dB and –3.4 dB, respectively. The specimen with the highest degree of corrosion, i.e., 2.1 % mass loss, had an amplitude loss of –10.8 dB. This specimen had a crack at the end of the corrosion process. However, this crack was less than 1 mm thick, which did not contribute to the overall amplitude change [22,59].

The previously described amplitude loss is probably the result of two mechanisms occurring simultaneously during the propagation of the electromagnetic wave, as described in [22]. The first is the change in the concrete medium in which the wave propagates because the concrete pores are now filled with corrosion products, the iron oxides. Iron oxides have magnetic properties that can affect the amplitude loss [60]. However, this mechanism is not crucial in this study because visible migration of corrosion products toward the concrete cover is not observed (Fig. 8). Instead, the change in amplitude is the result of the change in the reflector surface. The corrosion layer over the rebar changes the reflection coefficient and thus the amplitude of the reflected wave. In addition, the wave is attenuated by the thin corrosion layer during propagation, so the total energy reflected from the steel is lower compared to the uncorroded rebar.

4. Discussion

In Section 3, the loss of GPR signal amplitude was expressed in dB and observed during the propagation of the signal in five centimetres of concrete. In the following discussion, these values are normalised to one centimetre of concrete so that the amplitude is expressed in dB/cm. Table 3 provides an overview of the influence of the corrosion-related effects on the GPR signal. The values of the normalized amplitudes shown in Figs. 4, 5 and 7 are further normalized to the following increase in the observed values: a 5% increase in the saturation level, a 0.4% (of m_c) increase in the total chloride content in concrete cover (mean value for internal and external chlorides) at saturation levels of 45–50%, 75–80%, and 100%, and a 0.1% increase in mass loss due to reinforcement corrosion. It should be mentioned that some of the specimens where the influence of chlorides was observed showed signs of corrosion on the surface of the reinforcing bars (which were detected after opening the specimens), and these were excluded from the analysis of the amplitude in Table 3.

As explained earlier, the changes in signal amplitude due to chlorides are not significant at low saturation ranges, so they are not listed.

It is not easy to select the increment of effects listed in Table 3 to compare their contribution to the overall change in the GPR signal because it is difficult to determine the possible range of effects under real conditions. Even though moisture has a significant effect on the GPR signal, the analysis can be facilitated if the measurement is chosen to avoid variations in the moisture condition. In this case, during the corrosion initiation, chloride contamination has the greatest effect on the signal change for chloride-induced corrosion. Once corrosion progresses, the chlorides and rust simultaneously contribute to the change in signal.

In this work, a dried specimen, or a specimen without chlorides with the same saturation level was used as a reference point for normalization, Eqs. (2) to (4). The normalization provided was used to express the full possible range of amplitude change as a function of specimen moisture conditions, from complete dryness to complete saturation. However, this scenario of extreme conditions is not realistic for most existing reinforced concrete structures. In the maintenance of reinforced concrete structures, the first measurement could be performed on "sound" concrete without deterioration, made after the construction of the structure, as a reference point to which the change in the GPR signal is measured, which indicates changes related to concrete corrosion. If measurements are made under similar environmental conditions, for example, if there has been no rain for several days and average temperatures are similar, extreme variations in the degree of saturation can be avoided.

To determine the value of the amplitude corresponding to the end of the corrosion initiation period, the specimens with a "critical" chloride content of 0.6% of m_c are used [61]. It can be seen from Table 2 that the specimens subjected to wet-dry cycles in 2% and 3.5% sodium chloride solutions have these chloride contents at the reinforcement level. The mean values of the amplitudes are further normalized to the amplitude of a specimen with a moisture content of 3.85% (saturation level 65%), expressed in terms of the mass of the dried specimen. According to [62], this corresponds to an ambient relative humidity of 60%. Finally, the proposed normalized amplitude value that correspond to the critical chloride content of 0.6% of m_c is shown in Table 4.

5. Conclusions

In this experimental study, the influence of moisture, chlorides, and corrosion products on the change of the GPR signal was investigated. The conclusions of this study are:

- Moisture, expressed in this work as saturation level, has strong influence on the GPR signal. However, if the inspection of the structure RC is performed under similar environmental conditions in terms of relative humidity and temperature, this parameter could be excluded from the analysis.
- The corrosion products on the surface of the reinforcement affect the amplitude loss when the signal is reflected. The mass loss of 0.1% affected the amplitude loss of –0.07 dB/cm.
- The normalized amplitude value of –0.7 dB/cm was measured for the specimens where the chloride content at the depth of reinforcement was 0.6% of m_c.

By the proposed reduction of amplitudes for different influencing factors, combined with additional measurements such as chloride content, it is possible to eliminate other factors and analyse the amplitude reduction due to the corrosion process. In addition, in accordance with the procedures described in the paper, the authors would like to emphasise the importance of baseline measurements made shortly after construction. This would open the possibility of using GPR for non-destructive and effective analysis of corrosion of reinforcement in concrete structures. In future studies, the investigations should be extended to different types of concrete in terms of strength so that they can be used for the inspection of structures. In addition, complete structure elements with reinforcement meshes and different reinforcement diameters should also be studied to determine the limits of the inspection.

CRediT authorship contribution statement

Ksenija Tesic: Writing – original draft, Visualization, Methodology, Investigation, Data curation, Conceptualization. **Ana Baricevic:** Writing – review & editing, Supervision, Methodology, Conceptualization. **Marijana Serdar:** Writing – review & editing, Project administration, Funding acquisition, Conceptualization. **Nenad Gucunski:** Writing – review & editing, Supervision.

Declaration of Competing Interest

The authors declare that they have no known competing financial interests or personal relationships that could have appeared to influence the work reported in this paper.

Table 3
Quantification of the influence of corrosion-related effects on the GPR signal.

The corrosion-related effect	Trend of amplitude change		Normalized amplitude [dB/cm]
5% increase in saturation level	↓	At the saturation level 20%–80%	–0.1
		At the saturation level below 20% and above 80%	–0.2
0.4% (of m_c) increase in chloride content	↓	At the saturation level 45–50%	–0.21
		At the saturation level 75–80%	–0.26
		At the saturation level 100%	–0.37
0.1% increase in mass loss due to reinforcement corrosion	↓	At the saturation level 60–65%	–0.07

Table 4
The proposed values of normalized amplitudes for distinguishing passive from active corrosion on an ambient relative humidity of 60%.

Corrosion status	Critical chloride content (of m_c)	Normalized amplitude [dB/cm]
Passive	<0.6	< –0.7
Active	≥0.6	≥ –0.7

References

[1] M. Domaneschi, C. Pellecchia, E. De Iuliis, G.P. Cimellaro, M.A. Morgese, A.A. Khalil, F. Ansari, Collapse analysis of the Polcevera viaduct by the applied element method, Eng. Struct. 214 (2020), 110659, https://doi.org/10.1016/j.engstruct.2020.110659.

[2] M. Alexander, H. Beushausen, Durability, service life prediction, and modelling for reinforced concrete structures – review and critique, Cem. Concr. Res. 122 (2019) 17–29, https://doi.org/10.1016/j.cemconres.2019.04.018.

[3] H. Beushausen, R. Torrent, M.G. Alexander, Performance-based approaches for concrete durability: State of the art and future research needs, Cem. Concr. Res. 119 (2019) 11–20, https://doi.org/10.1016/j.cemconres.2019.01.003.

[4] P. Pfändler, K. Bodie, U. Angst, R. Siegwart, Flying corrosion inspection robot for corrosion monitoring of civil structures – First results, in: SMAR 2019 - Fifth Conference on Smart Monitoring, Assessment and Rehabilitation of Civil Structures, SMAR, Potsdam, Germany, 2019, pp. 1–8, https://doi.org/10.3929/ETHZ-B-000365572.

[5] U.M. Angst, Challenges and opportunities in corrosion of steel in concrete, Mater. Struct. Constr. 51 (2018) 4, https://doi.org/10.1617/s11527-017-1131-6.

[6] S. Abu Dabous, S. Feroz, Condition monitoring of bridges with non-contact testing technologies, Automation in Construction 116 (2020) 103224.

[7] M. Solla, B. Riveiro, P. Arias, H. Lorenzo, Introduction, in: B. Riveiro, M. Solla (Eds.), Non-Destructive Techniques for the Evaluation of Structures and Infrastructure, first ed.,, CRC Press, London, 2016, pp. 3–6, https://doi.org/10.1201/b19024.

[8] N. Gucunski, B. Basily, J. Kim, J. Yi, T. Duong, K. Dinh, S.H. Kee, A. Maher, RABIT: implementation, performance validation and integration with other robotic platforms for improved management of bridge decks, Int. J. Intell. Robot. Appl. 1 (2017) 271–286, https://doi.org/10.1007/s41315-017-0027-5.

[9] K. Dinh, T. Zayed, F. Romero, A. Tarussov, Method for analyzing time-series GPR data of concrete bridge decks, J. Bridg. Eng. 20 (2015) 04014086, https://doi.org/10.1061/(ASCE)BE.1943-5592.0000679.

[10] T. Omar, M.L. Nehdi, T. Zayed, Performance of NDT techniques in appraising condition of reinforced concrete bridge decks, J. Perform. Constr. Facil. 31 (2017) 04017104, https://doi.org/10.1061/(asce)cf.1943-5509.0001098.

[11] K. Tesic, A. Baricevic, M. Serdar, Non-Destructive corrosion inspection of reinforced concrete using ground-penetrating radar: A Review, Materials (Basel). 14 (2021) 975, https://doi.org/10.3390/ma14040975.

[12] W.-W.-L. Lai, X. Derobert, P. Annan, A review of ground penetrating radar application in civil engineering: a 30-year journey from locating and testing to imaging and diagnosis, NDT & E Int. 96 (2018) 58–78, https://doi.org/10.1016/j.ndteint.2017.04.002.

[13] K. Dinh, N. Gucunski, J. Kim, T.H. Duong, Understanding depth-amplitude effects in assessment of GPR data from concrete bridge decks, NDT & E Int. 83 (2016) 48–58, https://doi.org/10.1016/j.ndteint.2016.06.004.

[14] K. Dinh, N. Gucunski, K. Tran, A. Novo, T. Nguyen, Full-resolution 3D imaging for concrete structures with dual-polarization GPR, Autom. Constr. 125 (2021), 103652, https://doi.org/10.1016/j.autcon.2021.103652.

[15] K. Dinh, N. Gucunski, Factors affecting the detectability of concrete delamination in GPR images, Constr. Build. Mater. 274 (2021) 121837, https://doi.org/10.1016/j.conbuildmat.2020.121837.

[16] S. Abu Dabous, S. Yaghi, S. Alkass, O. Moselhi, Concrete bridge deck condition assessment using IR Thermography and Ground Penetrating Radar technologies, Autom. Constr. 81 (2017) 340–354, https://doi.org/10.1016/j.autcon.2017.04.006.

[17] D.J. Daniels, Ground penetrating radar, 2nd ed., The Institution of Electrical Engineers, London, 2004.

[18] A.P. Annan, Electromagnetic principles of ground penetrating radar, in: H.M. Jol (Ed.), Ground Penetrating Radar Theory and Applications, Elsevier, Amsterdam, 2009, pp. 3–40, https://doi.org/10.1016/B978-0-444-53348-7.00001-6.

[19] K. Tesic, A. Baricevic, M. Serdar, Comparison of cover meter and ground penetrating radar performance in structural health assessment: case studies, Gradjevinar 73 (2021) 1131–1144, https://doi.org/10.14256/JCE.3323.2021.

[20] V. Pérez-Gracia, F.G. García García, I. Rodriguez Abad, GPR evaluation of the damage found in the reinforced concrete base of a block of flats: A case study, NDT & E Int. 41 (2008) 341–353, https://doi.org/10.1016/j.ndteint.2008.01.001.

[21] V. Perez-Gracia, M. Solla. Inspection procedures for effective GPR surveying of buildings. In: Civil Engineering Applications of Ground Penetrating Radar. Springer: New York, 2015. 97–124. https://doi.org/10.1007/978-3-319-04813-0.

[22] K. Tesic, A. Baricevic, M. Serdar, N. Gucunski, Characterization of ground penetrating radar signal during simulated corrosion of concrete reinforcement, Autom. Constr. 143 (2022), 104548, https://doi.org/10.1016/j.autcon.2022.104548.

[23] S. Hong, W.-W.-L. Lai, G. Wilsch, R. Helmerich, R. Helmerich, T. Günther, H. Wiggenhauser, Periodic mapping of reinforcement corrosion in intrusive chloride contaminated concrete with GPR, Constr. Build. Mater. 66 (2014) 671–684, https://doi.org/10.1016/j.conbuildmat.2014.06.019.

[24] W.-L. Lai, T. Kind, M. Stoppel, H. Wiggenhauser, Measurement of accelerated steel corrosion in concrete using ground-penetrating radar and a modified half-cell potential Method, J. Infrastruct. Syst. 19 (2013) 205–220, https://doi.org/10.1061/(ASCE)IS.1943-555X.0000083.

[25] A. Tarussov, M. Vandry, A. De La Haza, Condition assessment of concrete structures using a new analysis method: Ground-penetrating radar computer-assisted visual interpretation, Constr. Build. Mater. 38 (2013) 1246–1254, https://doi.org/10.1016/j.conbuildmat.2012.05.026.

[26] K. Dinh, N. Gucunski, T. Zayed, Automated visualization of concrete bridge deck condition from GPR data, NDT & E Int. 102 (2019) 120–128, https://doi.org/10.1016/j.ndteint.2018.11.015.

[27] K. Dinh, N. Gucunski, J. Kim, T.H. Duong, Method for attenuation assessment of GPR data from concrete bridge decks, NDT & E Int. 92 (2017) 50–58, https://doi.org/10.1016/j.ndteint.2017.07.016.

[28] S. Laurens, J.P. Balayssac, J. Rhazi, G. Klysz, G. Arliguie, Non-destructive evaluation of concrete moisture by GPR: experimental study and direct modeling, Mater. Struct. 38 (2005) 827–832, https://doi.org/10.1007/BF02481655.

[29] G. Klysz, J.P. Balayssac, Determination of volumetric water content of concrete using ground-penetrating radar, Cem. Concr. Res. 37 (2007) 1164–1171, https://doi.org/10.1016/j.cemconres.2007.04.010.

[30] Z.M. Sbartaï, S. Laurens, J.P. Balayssac, G. Ballivy, G. Arliguie, Effect of concrete moisture on radar signal amplitude, ACI Mater. J. 103 (2006) 419–426, https://doi.org/10.14359/18219.

[31] S.F. Senin, R. Hamid, Ground penetrating radar wave attenuation models for estimation of moisture and chloride content in concrete slab, Constr. Build. Mater. 106 (2016) 659–669, https://doi.org/10.1016/j.conbuildmat.2015.12.156.

[32] J. Hugenschmidt, R. Loser, Detection of chlorides and moisture in concrete structures with ground penetrating radar, Mater. Struct. 41 (2008) 785–792, https://doi.org/10.1617/s11527-007-9282-5.

[33] Z.M. Sbartaï, S. Laurens, J. Rhazi, J.P. Balayssac, G. Arliguie, Using radar direct wave for concrete condition assessment: Correlation with electrical resistivity, J. Appl. Geophys. 62 (2007) 361–374, https://doi.org/10.1016/j.jappgeo.2007.02.003.

[34] A. Kalogeropoulos, J. Van Der Kruk, J. Hugenschmidt, J. Bikowski, E. Brühwiler, Full-waveform GPR inversion to assess chloride gradients in concrete, NDT & E Int. 57 (2013) 74–84, https://doi.org/10.1016/j.ndteint.2013.03.003.

[35] A. Kalogeropoulos, J. Van Der Kruk, J. Hugenschmidt, S. Busch, K. Merz, Chlorides and moisture assessment in concrete by GPR full waveform inversion, Near Surf. Geophys. 9 (2011) 277–285, https://doi.org/10.3997/1873-0604.2010064.

[36] S. Hong, W.-L. Lai, R. Helmerich, Experimental monitoring of chloride-induced reinforcement corrosion and chloride contamination in concrete with ground-penetrating radar, Struct. Infrastruct. Eng. 11 (2015) 15–26, https://doi.org/10.1080/15732479.2013.879321.

[37] V. Sossa, V. Pérez-Gracia, R. González-Drigo, M.A. Rasol, Lab non destructive test to analyze the effect of corrosion on ground penetrating radar scans, Remote Sens. 11 (2019) 2814, https://doi.org/10.3390/rs11232814.

[38] P.T.W. Wong, W.W.L. Lai, J.F.C. Sham, C. Poon, Hybrid non-destructive evaluation methods for characterizing chloride-induced corrosion in concrete, NDT & E Int. 107 (2019), 102123, https://doi.org/10.1016/j.ndteint.2019.05.008.

[39] B.J. Zhan, W.W.L. Lai, S.C. Kou, C.S. Poon, W.F. Tsang, Correlation between accelerated steel corrosion in concrete and ground penetrating radar parameters, in: C. Leung, K.T. Wan (Eds.), international RILEM Conference on Advances in Construction Materials Through Science and Engineering, RILEM Publications SARL, Hong Kong, China, 2011.

[40] R.K. Raju, M.I. Hasan, N. Yazdani, Quantitative relationship involving reinforcing bar corrosion and ground-penetrating radar amplitude, ACI Mater. J. 115 (2018) 449–457, https://doi.org/10.14359/51702187.

[41] ASTM D6087-08. Standard test method for evaluating asphalt-covered concrete bridge decks using ground penetrating radar. https://www.astm.org/d6087-08r15e01.html, 2008. (Accessed 6 March 2023).

[42] M. Abouhamad, T. Dawood, A. Jabri, M. Alsharqawi, T. Zayed, Corrosiveness mapping of bridge decks using image-based analysis of GPR data, Autom. Constr. 80 (2017) 104–117, https://doi.org/10.1016/j.autcon.2017.03.004.

[43] C.L. Barnes, J.-F. Trottier, Effectiveness of ground penetrating radar in predicting deck repair quantities, J. Infrastruct. Syst. 10 (2004) 69–76, https://doi.org/10.1061/(asce)1076-0342(2004)10:2(69).

[44] İ. Kaplanvural, K. Özkap, E. Pekşen, Influence of water content investigation on GPR wave attenuation for early age concrete in natural air-drying condition, Constr. Build. Mater. 297 (2021), 123783, https://doi.org/10.1016/j.conbuildmat.2021.123783.

[45] S.S. Hubbard, J. Zhang, P.J.M. Monteiro, J.E. Peterson, Y. Rubin, Experimental detection of reinforcing bar corrosion using nondestructive geophysical techniques, ACI Mater. J. 100 (2003) 501–510, https://doi.org/10.14359/12957.

[46] A. Zaki, M.A.M. Johari, W.M.A.W. Hussin, Y. Jusman, Experimental assessment of rebar corrosion in concrete slab using ground penetrating radar (GPR), Int. J. Corros. 2018 (2018) 5389829, https://doi.org/10.1155/2018/5389829.

[47] H. Liu, J. Zhong, F. Ding, X. Meng, C. Liu, J. Cui, Detection of early-stage rebar corrosion using a polarimetric ground penetrating radar system, Constr. Build. Mater. 317 (2022), 125768, https://doi.org/10.1016/j.conbuildmat.2021.125768.

[48] S. Hong, GPR-Based periodic monitoring of reinforcement corrosion in chloride-contaminated concrete, Technischen Universität Berlin, Berlin, Germany, 2015.

[49] HZN Standards Publications, HRN EN 14629: 2007, Products and systems for the protection and repair of concrete structures - Test methods - Determination of chloride content in hardened concrete, Croatian Standards Institute, Zagreb, 2007. Accessed 6 March 2023.

[50] N.J. Cassidy. Electrical and magnetic properties of rocks, soils and fluids. In: H.M. Jol (Ed.). Gr. Penetrating Radar Theory Appl., Elsevier, Amsterdam. 2009. 41–72. https://doi.org/10.1016/B978-0-444-53348-7.00002-8.

[51] W.L. Lai, T. Kind, H. Wiggenhauser, Frequency-dependent dispersion of high-frequency ground penetrating radar wave in concrete, NDT & E Int. 44 (2011) 267–273, https://doi.org/10.1016/j.ndteint.2010.12.004.

[52] T. Bourdi, J.E. Rhazi, F. Boone, G. Ballivy, Application of Jonscher model for the characterization of the dielectric permittivity of concrete, J. Phys. D. Appl. Phys. 41 (20) (2008), 205410, https://doi.org/10.1088/0022-3727/41/20/205410.

[53] W.M. Haynes, CRC handbook of chemistry and physics, 97th ed., CRC Press, Boca Raton, 2017.

[54] L. Bertolini, B. Elsener, P. Pedeferri, R.B. Polder, Corrosion of steel in concrete: prevention, diagnosis, repair, Wiley, Weinheim, 2003.

[55] K.S. Cole, R.H. Cole, Dispersion and absorption in dielectrics I. Alternating current characteristics, J. Chem. Phys. 9 (4) (1941) 341–351.

[56] C. Arya, N.R. Buenfeld, J.B. Newman, Factors influencing chloride-binding in concrete, Cem. Concr. Res. 20 (1990) 291–300, https://doi.org/10.1016/0008-8846(90)90083-A.

[57] J. Xu, L. Jiang, W. Wang, Y. Jiang, Influence of CaCl2 and NaCl from different sources on chloride threshold value for the corrosion of steel reinforcement in concrete, Constr. Build. Mater. 25 (2011) 663–669, https://doi.org/10.1016/j.conbuildmat.2010.07.023.

[58] A.P. Annan, S.W. Cosway. Simplified GPR beam model for survey design, in: SEG technical program expanded abstracts 1992. Society of Exploration Geophysicists. 1992. 356–359. https://doi.org/10.1190/1.1822088.

[59] S. Hong, D. Chen, B. Dong, Numerical simulation and mechanism analysis of GPR-based reinforcement corrosion detection, Constr. Build. Mater. 317 (2022), 125913, https://doi.org/10.1016/j.conbuildmat.2021.125913.

[60] N.J. Cassidy, Frequency-dependent attenuation and velocity characteristics of nano-to-micro scale, lossy, magnetite-rich materials, Near Surf. Geophys. 6 (2008) 341–354, https://doi.org/10.3997/1873-0604.2008023.

[61] International Federation for Structural Concrete (fib). Model code for service life design, fib Bulletin No. 34, Lausanne, Switzerland. 2006. ISBN: 2-88394-074-6.

[62] M. Cunningham. When is a concrete slab dry enough? In: Build, April/May, 2008. 25–26. B105–25-DrySlab.pdf, buildmagazine.org.nz. (Accessed 6 March 2023).

Paper IV

Electromagnetic property selection for GPR modelling in corrosive concrete environments

Ksenija Tesic [a], Ana Baricevic [a,*], Marijana Serdar [a], Nenad Gucunski [b]

[a] *University of Zagreb, Faculty of Civil Engineering, Department of Materials, Fra Andrije Kacica-Miosica 26, 10000, Zagreb, Croatia*
[b] *Department of Civil and Environmental Engineering, Rutgers, The State University of New Jersey, 500 Bartholomew Road, Piscataway, NJ, 08854, USA*

ARTICLE INFO	ABSTRACT
	Understanding the mechanisms that alter the ground penetrating radar (GPR) electromagnetic wave propagation as a result of reinforcement corrosion is pivotal for accurate assessment of the corrosion of reinforced concrete (RC) structures. Nevertheless, the behaviour of the GPR signal during the complex corrosion process is not thoroughly understood. In this study, finite-difference time-domain (FDTD) modelling was used to analyse the effects of corrosion-related parameters, i.e., moisture, chlorides, and corrosion products, on the electric field strength. This study aims to expand the database on numerical simulations of GPR signal behaviour in corrosive environments. It also addresses the knowledge gap in modelling the frequency-dependent properties of concrete and iron oxides. Modelling approach adopted in the study was validated with experimental data obtained on laboratory specimens that correspond to the numerical models in terms of geometry and condition.

1. Introduction

Corrosion of reinforcement, defined as an electrochemical reaction that leads to the formation of rust (Bertolini et al., 2013; Nürnberger et al., 2007; Ahmad, 2003; Fan et al., 2019), resulting in cracking, spalling, and debonding of steel and concrete, i.e., shortening service life of structures, is the primary durability concern of civil engineers and building owners. It is estimated that the direct cost of corrosion is 3.1% of the gross domestic product (GDP) in America (Koch et al., 1998). Failure to systematically maintain structures, in addition to the direct and indirect costs, can jeopardize the load-bearing capacity of the structures and have disastrous consequences. Persistent efforts are being made worldwide to develop corrosion control strategies: delay (Beushausen et al., 2019; Alexander and Beushausen, 2019), early detection (Abu Dabous et al., 2017; Pashoutani and Zhu, 2020), or even interruption (Pan et al., 2017; Cao et al., 2017) of the corrosion process in reinforced concrete (RC) structures.

Early detection of corrosion should allow for a proactive response to repair efforts, reducing the cost of overall repair and potentially extending the service life of the structure. Preservation of an intact structure, shorter inspection time, and the ability to detect corrosion in its early stages are the main advantages of non-destructive testing (NDT) methods (Ahmed et al., 2020; McCann and Forde, 2001; Solla et al.,

2016; Song and Saraswathy, 2007; Rehman et al., 2016). In the last two decades, ground penetrating radar (GPR) has become one of the most useful non-destructive testing methods in the inspection of RC structures, mainly because of its ability to provide multiple information about reinforcement (e.g., location, thickness of concrete cover, corrosion state), high inspection rate, and real-time results (Lai et al., 2018; Klewe et al., 2021; Tešić et al., 2021a; Krysiński et al., 2015; Omar et al., 2017). Although GPR can process the information about the geometry of the elements of RC with high accuracy (Tešić et al., 2021b; Drobiec et al., 2019), the determination of the corrosion state based on GPR signal analysis is still being developed (Tešić et al., 2021a; Hong et al., 2014; Wong et al., 2019; Sossa et al., 2019; Tesic et al., 2022). The growing interest in this method has led to an increased interest of researchers in laboratory investigations of these phenomena, which can be roughly divided into two groups: 1) investigation of the causes of corrosion, moisture (Sbartaï et al., 2006, 2007; Laurens et al., 2002; Senin and Hamid, 2016; Kaplanvural et al., 2021), chlorides (Senin and Hamid, 2016; Hugenschmidt and Loser, 2008), carbonation (Dérobert et al., 2018), and 2) investigation of the consequences of the corrosion process, rust (Hong et al., 2014; Wong et al., 2019; Lai et al., 2013; Liu et al., 2022), and delamination (Dinh and Gucunski, 2021). The inconsistent laboratory results have shown that the characterisation of corrosion with GPR is challenging.

Finite-difference time-domain (FDTD) numerical simulations are an

---

Notations

Lowercase Latin characters

c	chloride concentration
d	exponent of CRIM
$f_1{}^I$	volume fraction of solid phase in M and Cl groups
$f_1{}^{II}$	volume fraction of solid phase in C group (pores 100% filled with corrosion products)
$f_1{}^{III}$	volume fraction of solid phase in C group (pores 60% filled with corrosion products)
$f_1{}^{IV}$	volume fraction of solid phase in C group (pores 30% filled with corrosion products)
$f_2{}^I$	volume fraction of gaseous phase in M and Cl group
$f_2{}^{II}$	volume fraction of corrosion products in C group (pores 100% filled with corrosion products)
$f_2{}^{III}$	volume fraction of gaseous phase in C group (pores 60% filled with corrosion products)
$f_2{}^{IV}$	volume fraction of gaseous phase in C group (pores 30% filled with corrosion products)
$f_3{}^I$	volume fraction of liquid phase in M and Cl groups
$f_3{}^{III}$	volume fraction of corrosion products in C group (pores 60% filled with corrosion products)
$f_3{}^{IV}$	volume fraction of corrosion products in C group (pores 30% filled with corrosion products)
h	height of the concrete at which the pores are filled with corrosion products
k	number of Debye poles
m_c	mass of cement
n	number of constituents in CRIM
w	saturation level

Uppercase Latin characters

A, A_1	normalized amplitude
A_0	amplitude in dry condition
Ac	amplitude at a given corrosion stage
A_{Cl}	amplitude at a given chloride concentration
$A_{Cl,0}$	amplitude of the specimen without chlorides at given degree of saturation
A_m	amplitude at a given saturation level
C	label for the group of specimens where the influence of corrosion products was observed
Cl	label for the group of specimens where the influence of chlorides was observed
M	label for the group of specimens where the influence of moisture was observed
N_C	number of specimens in the C group
N_M	number of specimens in M group
N_{Cl}	number of specimens in Cl group

Greek characters

Δm	mass loss of reinforcement
ε_1	dielectric permittivity of the solid phase of concrete
ε_2	dielectric permittivity of the gaseous phase of concrete
$\varepsilon_3(\omega)$	dielectric permittivity of the liquid phase of concrete
$\varepsilon_{3,R}$	real dielectric permittivity of the liquid phase of concrete
$\varepsilon_4(\omega)$	complex dielectric permittivity of corrosion products
$\varepsilon_{4,R}$	real dielectric permittivity of corrosion products
ε_∞	dielectric permittivity of water at very high frequency
$\varepsilon_I(\omega)$	complex dielectric permittivity of concrete in which pores are filled with air and pore solution
$\varepsilon_i(\omega)$	dielectric permittivity of i-th constituent of CRIM
$\varepsilon_{I,R}$	real dielectric permittivity of concrete in which pores are filled with air and pore solution
$\varepsilon_{II}(\omega)$	complex dielectric permittivity of concrete in which pores are 100% filled with corrosion products
$\varepsilon_{III}(\omega)$	complex dielectric permittivity of concrete in which pores are 60% filled with corrosion products
$\varepsilon_{IV}(\omega)$	complex dielectric permittivity of concrete in which pores are 30% filled with corrosion products
ε_r	real dielectric permittivity of concrete
ε_s	dielectric permittivity of water at a very low frequency
τ_0	relaxation time
Φ	porosity of concrete
ω	angular frequency

Acronyms

CRIM	Complex Refractive Index Model
DA	Dual Annealing
DE	Differential Evolution
FDTD	Finite-Difference Time-Domain
GDP	Gross Domestic Product
GPR	Ground Penetrating Radar
GSoC	Google Summer of Code
NDT	Non-destructive Testing
PML	Perfectly Matched Layer
PEC	Perfect Electric Conductor
PSO	Particle Swarm Optimization
RC	Reinforced Concrete

effective method for analysing the propagation of electromagnetic waves in any modelled medium and are particularly suitable for GPR modelling (Liu and Guo, 2016). Simulations have been used to predict GPR responses due to moisture in asphalt concrete pavements (Cao et al., 2022), pipes (Lei et al., 2020; Jaufer et al., 2022; Zhao and Al-Qadi, 2017) or reflections from tunnel linings (Feng et al., 2018). Several studies have used numerical simulations to predict the effects of moisture in concrete on the GPR signal (Klysz et al., 2008; Núñez-Nieto et al., 2014; Wong and Lai, 2022). However, the limited number of these studies modelled concrete with its complex, frequency-dependent properties to analyse the signal amplitude strength (Wong and Lai, 2022). Moreover, negligible number of studies (Hong et al., 2022) analysed the amplitude change obtained in numerical simulations due to the corrosive environment in concrete – chlorides and the formation of corrosion products and their propagation into concrete. In the study (Hong et al., 2022), the corrosion products were modelled with the respective real part of dielectric permittivity and electrical conductivity, neglecting the magnetic properties of iron oxides. This modelling is not suitable for electromagnetic field strength analysis because the magnetic properties could affect the change of signal amplitude.

Therefore, in light of the presented knowledge gap, numerical simulations were performed in this study on the effects of moisture, chlorides, and corrosion products in the reinforced concrete specimens on the GPR signal. The simulations included modelling of the real and imaginary parts of the dielectric permittivity of concrete as well as the magnetic properties of the corrosion products. For comparison, the specimens were also modelled using only the real, frequency-independent dielectric properties. The obtained results were compared with the experimental results on the specimens corresponding to the numerical models. Present study contributes to the elucidation of the mechanisms that modify the GPR signal during the corrosion process of reinforcement in concrete. This newfound understanding will allow more accurate procedures for GPR-based corrosion assessment.

2. Modelling workflow

2.1. GprMax software

GprMax is software for modelling and evaluation of the ground penetrating radar response in an arbitrarily designed environment (Giannopoulos, 2005; Warren et al., 2016). GprMax is an open-source software written in Python and Cython languages. It is based on solving Maxwell's equations with finite difference algorithms in the time domain (finite-difference time-domain (FDTD)) and models the space with Yee cells (Yee, 1966). In the software, it is possible to create two- and three-dimensional models. In this study, only two-dimensional modelling was used. In forward modelling, the solution of Maxwell's equations gives the strength of the electric and magnetic field for the given dielectric properties of the medium.

The electromagnetic source was modelled as a Ricker wavelet with a centre frequency of 2.7 GHz, the same centre frequency as the GPR used to obtain results on laboratory specimens, which were then compared with the results of the numerical simulations.

2.2. Geometry of numerical models

The geometry of the numerical models simulated in gprMax was determined based on the postulations in laboratory examinations. To represent the space for the propagation of the direct air wave as well as the air-concrete interface, the air space was modelled with a 0.1 m height above the specimens. The concrete specimens were modelled as rectangular objects, and the reinforcing bars at 0.05 m depth as cylindrical objects. The numerical model is shown in Fig. 1.

Three A-scans were derived from the numerical model, each of which was above the reinforcement in the observed concrete specimen.

Spatial discretization was performed using elements of size 0.001 m $\times$ 0.001 m and 0.001 m in the x, y, and z directions, respectively, for the first two groups (group M used to observe the influence of moisture and group Cl to observe the influence of chlorides). Since this resolution was not sufficient to represent the corrosion product layer and crack, the mesh was decomposed into finite elements of size 0.0001 m and 0.0001 m in the xy plane for the C specimen group used to observe the influence of corrosion products on the GPR signal. A time window of 5×10^{-9} s was chosen. For the perfectly matched layer (PML), 10 cells were used by default, so the targets of interest (rebars) were not modelled in this area.

The concrete was modelled with the appropriate material properties, which will be explained in further sections, while the reinforcing bars in the concrete and the metal plate were modelled as PEC (Perfect Electric Conductor) material.

2.3. Modelling material properties

The basis of the analysis in this study is the appropriate modelling of the dielectric properties of materials – dielectric permittivity, electrical conductivity, and magnetic permeability, since these properties are the parameters of the constitutive equations that relate Maxwell's equations themselves (Cassidy and Jol, 2009). At the same time, these properties are the input data for forward modelling with gprMax. In this study, concrete with different saturation levels and chloride concentrations, concrete with corrosion products in the pores and corroded reinforcement were modelled. A detailed explanation of laboratory specimens' design and the experimental setups can be found in (Tesic et al., 2023). A total of forty-two specimens were cast, which were divided into three groups: 1) M – group to observe the influence of moisture (9 specimens, N_M), 2) Cl – group to observe the influence of chlorides (27 specimens, N_{Cl}), and 3) C – group to observe the influence of corrosion products on the GPR signal (6 specimens, N_C), Fig. 2. The properties used to characterize the models were chosen to be as close as possible to the properties of the laboratory specimens.

2.3.1. Modelling properties of the first two groups – M and Cl specimens

The dielectric permittivity ε, is defined with its real part, which represents the ability of dipoles to realign themselves according to the electromagnetic pulse and store the energy in the form of dipole moments (Cassidy and Jol, 2009), and with its imaginary part, which represents the losses caused by these movements (Cassidy, 2008). In general, both the real and imaginary parts are frequency-dependent. Concrete is a heterogeneous material containing a solid phase (cement paste and aggregates), a liquid phase (pore solution in the concrete pores), and a gaseous phase (air in the concrete pores). Therefore, the dielectric permittivity of concrete depends on these constituents and their respective dielectric permittivity. In most cases, however, the dielectric permittivity of concrete is simplified as a single real number, also referred to as the dielectric constant (Clem et al., 2015; ACI Committee 228, 1998). This is roughly suitable for estimating, for example, the velocity of electromagnetic waves (Dérobert et al., 2008), and the desired depth of objects. The hashtag material in the gprMax software implies the dielectric constant as one of the three modelled dielectric properties. However, when analysing the strength of the electric field, simplifying the dielectric permittivity to its real part is not correct (Wong and Lai, 2022; Lai et al., 2011; Majchrowska et al., 2021; Cassidy, 2007), especially when the material contains significant amounts of water, as in this study. By introducing the imaginary part of the dielectric permittivity, the relaxation mechanisms and their influence on the signal losses are considered.

Certain models describing the dielectric permittivity are known in the literature, developed for different materials, e.g., Cole-Cole (Cole and Cole, 1941), Jonscher (Bourdi et al., 2008, 2012; Chahine et al., 2010), Havriliak-Negami (Majchrowska et al., 2021), extended Debye (Ogunsola et al., 2006; Sandrolini et al., 2007), etc. However, one of the most commonly used models is the volumetric mixing model – the Complex Refractive Index Model (CRIM) (Halabe et al., 1989, 1993; Zadhoush et al., 2021; Tsui and Matthews, 1997; Lachowicz and Rucka, 2017, 2019). The CRIM was used in this study to represent the complex dielectric permittivity of concrete, $\varepsilon_I(\omega)$. It is calculated according to the following equation,
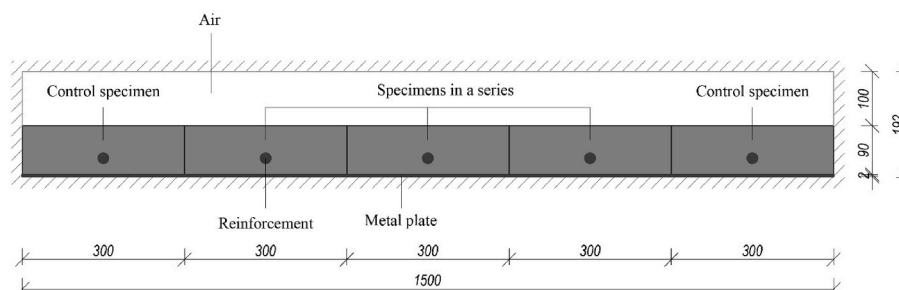

Fig. 1. The numerical model (dimensions in millimetres).

Fig. 2. The laboratory specimens: a) Group *M*, where various degrees of saturation are achieved by immersion in water, b) Group *Cl*, where various degrees of chloride concentration in the concrete cover are achieved by immersion in sodium chloride solutions, c) Group *C*, where various degrees of corrosion are achieved by exposure of the specimens to external current.

$$\varepsilon_I(\omega)^d = \sum_1^n f_i{}^I \, \varepsilon_i \, (\omega)^d \tag{1}$$

where d is the exponent of CRIM formulation, $f_i{}^I$ and $\varepsilon_i(\omega)$ are the volumetric fraction and dielectric permittivity of i_{th} constituent of total n constituents, while ω is the angular frequency. In equations (2)–(4), the volumetric fractions of three constituents, namely solid (paste and aggregate) $f_1{}^I$, gaseous (air) $f_2{}^I$, and liquid (pore solution) $f_3{}^I$ are shown,

$$f_1{}^I = (1 - \Phi) \tag{2}$$

$$f_2{}^I = (1 - w)\Phi \tag{3}$$

$$f_3{}^I = \Phi w \tag{4}$$

In the above equations, Φ represents porosity and w represents saturation level. The dielectric permittivity of the solid phase is taken to be $\varepsilon_1 = 5$ (Cassidy and Jol, 2009; Kim et al., 2016; Owusu Twumasi and Yu, 2015), and that of the air is taken to be $\varepsilon_2 = 1$ (Cassidy and Jol, 2009). The dielectric permittivity of the pore solution is expressed by the Debye equation (Balanis, 2012),

$$\varepsilon_3(\omega) = \varepsilon_\infty + \frac{\epsilon_s - \epsilon_\infty}{1 + i\omega\tau_0} \tag{5}$$

where ε_s and ε_∞ are the dielectric permittivity at very low and very high frequencies, and τ_0 is the relaxation time. The parameters of the Debye equation are well known for free water; however, in this study, the pore solution could not be described as a free liquid. In fact, most of the water in the concrete is capillary water (Bertolini et al., 2013), so the capillary tension can hold the water, which makes the relaxation mechanism different from that of free water. The mechanism of confined water begins to resemble the behaviour of ice, so that the relaxation frequency decreases compared to free water, while the relaxation time increases (Cole and Cole, 1941; Minasny, 2006). In this study, the values were $\varepsilon_s = 57.9$, $\varepsilon_\infty = 3.15$ (Minasny, 2006), and $\tau_0 = 200 \times 10^{-12}$ s (Soldatov et al., 2016). The Debye function was not additionally modelled as a function of the salinity of the water because it is assumed that the effects of salinity are accounted for by the experimentally measured conductivity of the specimen, which will be discussed later. Porosity Φ and saturation level w were determined in laboratory tests (Tesic et al., 2023) by weighing specimens in dry, saturated, and partially saturated states.

Due to the numerical solution in the time domain, the frequency-dependent, i.e., dispersive, properties could not be easily implemented in the calculation (Majchrowska et al., 2021; Giannakis and Giannopoulos, 2014; Giannakis et al., 2014). In the current version of gprMax, dispersive materials can be represented using the multi-Debye, multi-Lorentz, or multi-Drude model (Warren and Giannopoulos, 2018). Therefore, one way to implement the arbitrarily complex dielectric permittivity in gprMax is to represent the dielectric permittivity using some of the above models. For this purpose, the code developed as part of the Google Summer of Code (GSoC) 2021 programme, which is described in (Majchrowska et al., 2021) was used. With this gprMax

extension, it is possible to fit the complex dielectric permittivity to the multipole Debye expression defined as follows,

$$\varepsilon(\omega) = \varepsilon_\infty + \sum_1^k \frac{\Delta\varepsilon_i}{1 + i\omega\tau_{0,i}} \tag{6}$$

where k is the number of Debye poles. There are three optimization methods to choose from in the package: Dual Annealing (DA), Differential Evolution (DE) and Particle Swarm Optimization (PSO). In this work, the DE optimization was used. An example of concrete complex dielectric permittivity optimization defined by the CRIM and approximated by the multi-Debye expression is shown in Fig. 3. The relative approximation error between CRIM and the fitted curve was small and less than 5 % even with a sudden increase corresponding to the case where the denominator is close to zero. The region of interest, 670 MHz $< f <$ 4700 MHz, is shaded yellow.

The conductivity of a material is defined as its ability to pass free charges when the material is exposed to an electric field (Cassidy and Jol, 2009). Generally, this property is also expressed as a complex number, but it is approximated by its real value, which also represents the signal losses due to conductivity effects. For the modelling in this work, the conductivity of the specimens is determined as the reciprocal value of the resistivity, which is experimentally determined using the Wenner's probe (Polder et al., 2000). The resistivity is determined at each saturation level for each specimen.

The magnetic permeability is equal to one for the *M* and *Cl* specimen groups because the concrete was considered a nonmagnetic material.

The amplitude of the reflection of reinforcing bars was determined at the end of the modelling process. The amplitude reported in this study is the normalized amplitude *A* in dB, expressed as, for the *M* specimen group,

$$A = 20\log_{10}(A_m / A_0)[\text{dB}] \tag{7}$$

where A_m is the amplitude of reflection from the rebar at a given saturation level and A_0 is the amplitude of reflection from the rebar of the same specimen in dry condition, while is for *Cl* specimen group,

$$A_1 = 20\log_{10}(A_{Cl} / A_{Cl,0})[\text{dB}] \tag{8}$$

where A_{Cl} is the amplitude of reflection from the rebar at a given chloride concentration and $A_{Cl,0}$ is the amplitude of reflection from the rebar of the specimen without chlorides at the same degree of saturation.

In addition, the influence of chlorides on the GPR signal is expressed by the amplitude *A*,

$$A = 20\log_{10}(A_{Cl} / A_0)[\text{dB}] \tag{9}$$

where A_{Cl} is the amplitude of reflection from the rebar at a given chloride concentration and A_0 is the amplitude of reflection from the rebar of the same specimen in dry condition.

The summary of the steps performed to obtain the values *A* and A_1 in numerical simulations is shown in Fig. 4.

As already explained, the dielectric permittivity is very often simplified to its real, frequency-independent part. To understand the
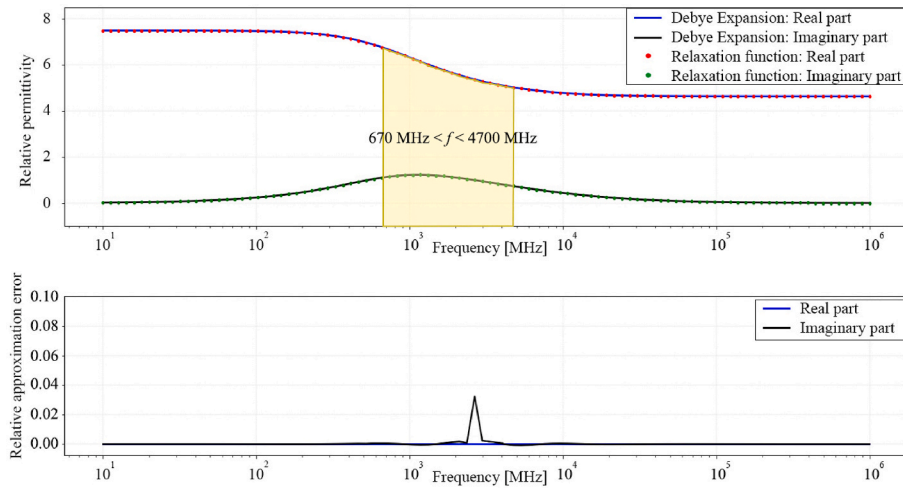
Fig. 3. The fit of the dielectric permittivity of concrete to the multi-Debye model.
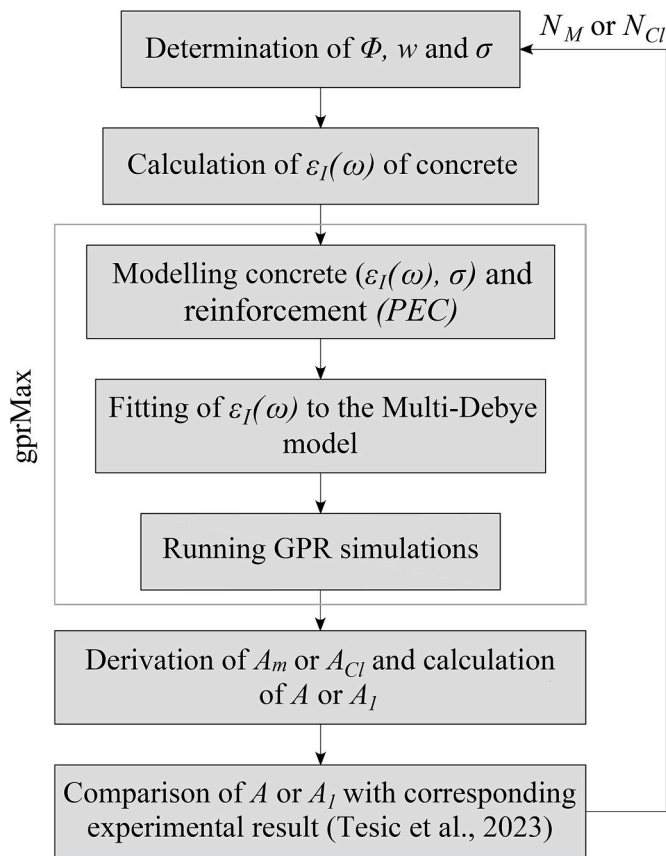

Fig. 4. The steps in numerical simulations for the *M* and *Cl* specimen groups.

impact of such simplification, the specimens in this work were also modelled in this way, whereby the real dielectric permittivity was also calculated with CRIM – $\varepsilon_{I,R}$. The difference to earlier models is that the water is simplified to its real dielectric permittivity $\varepsilon_{3,R} = 81$ (Daniels, 2004). The steps correspond to the flow chart in Fig. 4, except that $\varepsilon_I(\omega)$ is $\varepsilon_{I,R}$, and the step of fitting the dielectric permittivity to the multi-Debye model is excluded.

2.3.2. Modelling properties of the third group – C specimens

Corrosion of concrete reinforcement causes changes in both materials, 1) concrete and 2) metal reinforcement. Both are modelled in the *C*

specimen group.

This paper presents two approaches for modelling concrete whose pores are filled with corrosion products (Fig. 5). The approaches are similar to those in (Cassidy and Millington, 2009) with respect to the uniform and non-uniform layers of concrete filled with corrosion products. However, the height of expansion of the corrosion products *h* and the direction of expansion were taken from the experiments detailly described in (Tesic et al., 2023). It is worth noting that the corrosion products in the concrete reached a height in the order of millimetres from the steel-concrete interface. This is consistent with observations on the transport of corrosion products in natural low current density environments, in carbonated (Stefanoni et al., 2018) and chloride-containing concrete (Furcas et al., 2022). This is because the soluble iron species (Furcas et al., 2022; Korec et al., 2023; Jamali et al., 2013) diffuse through the concrete pores and could be deposited as corrosion products far away from the consumed reinforcement. In the experimental work presented in (Tesic et al., 2023) and considered here as a modelling reference, additional migration as a result of the accelerated corrosion process using the impressed current technique triggered the movement of ions. This led to a distribution of corrosion products in the order of millimetres. As already mentioned, high current density does not lead to the observed phenomena. For the experimental specimens used to create the numerical models, the average current density during the corrosion process was in the range of 3–13.5 μA/cm^2, which can be considered a low current density although impressed current was used during the experiment.

In the first approach, referred to as 'uniform' distribution of corrosion products, it is assumed that the concrete pores in the cross-section radially around the rebar are filled with corrosion products that reach the height *h*. The height of the concrete *h* at which the pores are filled with corrosion products was determined by measurements with a calliper after the specimen was demolished. The dielectric permittivity of the described concrete $\varepsilon_{II}(\omega)$ is determined as follows,

$$\varepsilon_{II}(\omega)^d = f_1^{II} \varepsilon_1^d + f_2^{II} \varepsilon_4(\omega)^d \tag{10}$$

where *d* is the exponent and is equal to 0.5, f_1^{II} is equal to f_1^I, f_2^{II} is equal to the porosity and is determined experimentally, ε_1 is the dielectric permittivity of the solid phase and is equal to 5, and $\varepsilon_4(\omega)$ is the dielectric permittivity of the corrosion products. The dielectric permittivity of the corrosion products is modelled as a complex number and is taken from reference (Cassidy, 2008). The electrical conductivity and magnetic permeability of the corrosion products are not modelled because they are included in the imaginary part of the complex dielectric permittivity, as reported in (Cassidy, 2008). The ε_{II} is then fitted using the multi-Debye function following the procedure described in 2.3.1.
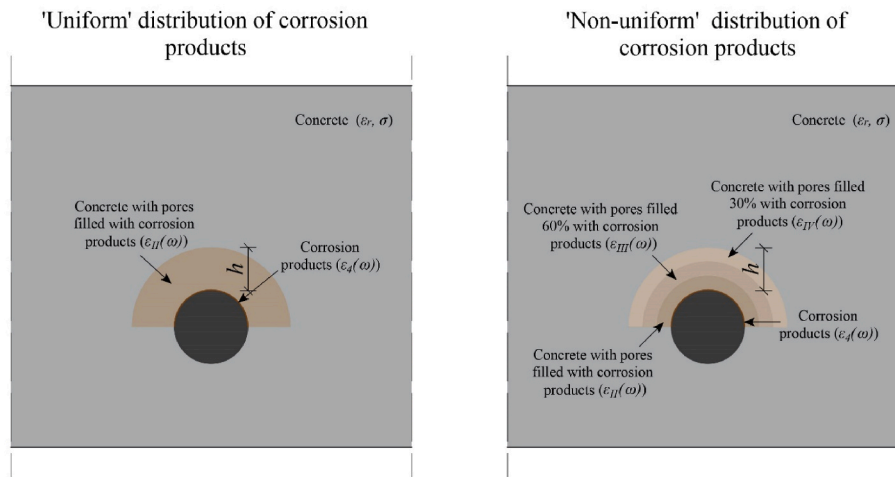
Fig. 5. Concepts for modelling 1) uniformly (left) and 2) non-uniformly distributed corrosion (right).

The second approach, referred to as 'non-uniform' distribution of corrosion products, refers to the case where the corrosion products fill the concrete around the reinforcement in three different layers of $h/3$ thickness. The layer closest to the rebar was 100% filled with corrosion products (ε_{II}), the layer next to it had pores 60% filled with corrosion products (ε_{III}), while the last layer considered was concrete with pores 30% filled (ε_{IV}). The dielectric permittivity $\varepsilon_{III}(\omega)$ and $\varepsilon_{IV}(\omega)$ are determined as follows,

$$\varepsilon_{III}(\omega)^d = f_1^{III}\,\varepsilon_1^d + f_2^{III}\,\varepsilon_2^d + f_3^{III}\,\varepsilon_4(\omega)^d \tag{11}$$

$$\varepsilon_{IV}(\omega)^d = f_1^{IV}\,\varepsilon_1^d + f_2^{IV}\,\varepsilon_2^d + f_3^{IV}\,\varepsilon_4(\omega)^d \tag{12}$$

where d is the exponent and is equal to 0.5, $f_1^{III} - f_3^{IV}$ are the volumetric fractions of the constituents, ε_1 is the dielectric permittivity of the solid phase and is equal to 5, ε_2 is the dielectric permittivity of the air and is equal to 1, and $\varepsilon_4(\omega)$ is the dielectric permittivity of the corrosion products. The f_1^{III} and f_1^{IV} are equal to the f_1^{I}.

The volumetric fractions of constituents are determined as follows,

$$f_2^{III} = 0.4\,\Phi \tag{13}$$

$$f_2^{IV} = 0.7\,\Phi \tag{14}$$

$$f_3^{III} = 0.6\,\Phi \tag{15}$$

$$f_3^{IV} = 0.3\,\Phi \tag{16}$$

The corrosion layer around the reinforcement was modelled according to the experimentally determined mass loss Δm of the reinforcement after the corrosion process. The coefficient of expansion of the corrosion products was assumed to be 3.24 (Zhao et al., 2011) taking into account the environmental conditions.

The concrete containing corrosion products and corrosion layer around the rebar were modelled only from the top of the semicircle of the reinforcement cross-section facing the concrete cover. The experimental setup was suitable to generate this environment, and the phenomenon was confirmed in almost all cases after the laboratory specimens were demolished after the corrosion process (Tesic et al., 2023).

The concrete without corrosion products in the pores is assumed to have the same properties as the concrete before the accelerated corrosion process, so it is modelled using only the real part of the dielectric permittivity, $\varepsilon_r = 6$.

The conductivity of the concrete without corrosion products in the pores was determined experimentally before the accelerated corrosion process.

The laboratory specimen with the highest degree of corrosion ($\Delta m = 2.1\%$) had a 0.95 mm crack at the end of the experiment. Therefore, the crack was modelled as 1 mm wide (because of the elements' dimensions), and in this study, the analysis of the crack filled with I) corrosion products at the height h, and with air for the rest of the crack, II) air, and III) corrosion products. The penetration of corrosion products into cracks depends on the degree of corrosion, current density, crack width, water content, environmental conditions, etc (Stefanoni et al., 2018; Zhu et al., 2023a; Sola et al., 2019). Depending on the parameters mentioned, the proportion of crack filling with corrosion products could vary from empty to completely filled cracks. The borderline cases (empty and completely filled cracks) and the partially filled crack were selected to analyse these characteristics.

The specimens before the corrosion process were modelled without a corrosion layer around the reinforcement and with concrete without corrosion products.

The flow chart on the modelling of the C specimen group is given in Fig. 6.

Furthermore, all specimens were also modelled with real, frequency-independent dielectric permittivity of $\varepsilon_{4,R} = 14.2$, and a conductivity value of $\sigma = 0.007$ S/m (Hong et al., 2022) for corrosion products. The distribution of corrosion products in the concrete cover was modelled uniformly and non-uniformly as previously described, with concrete properties calculated using CRIM.

The amplitude A was determined following the equation:

$$A = 20\log_{10}(A_C\,/\,A_0)\,[\text{dB}] \tag{17}$$

where A_C is the amplitude of reflection from the rebar at a given stage of corrosion and A_0 is the amplitude of reflection from the rebar of the same specimen before corrosion.

3. Results and discussion

3.1. Modelling moisture effect

The normalized amplitude A as a function of the saturation level w, obtained from laboratory tests and numerical simulations is shown in Fig. 7. The numerical models that included modelling of the complex, frequency-dependent dielectric permittivity are marked in magenta as "numerical models (complex)", while those that were modelled using only the real part of the dielectric permittivity are marked in grey as "numerical models (real)". The experimental data are shown in a shaded area bounded by the upper and lower limits of the linear regression line fitted to the experimental results, while their linear regression is shown in black. The limits were obtained by adding/subtracting two standard
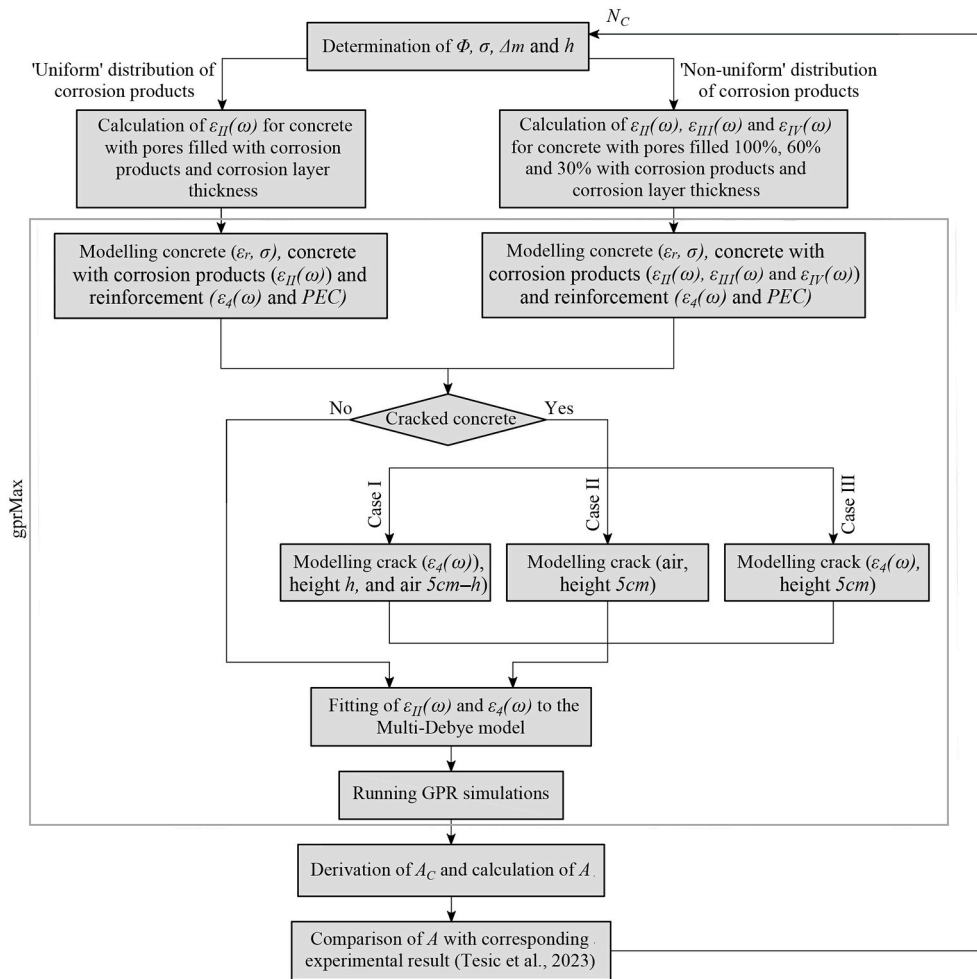
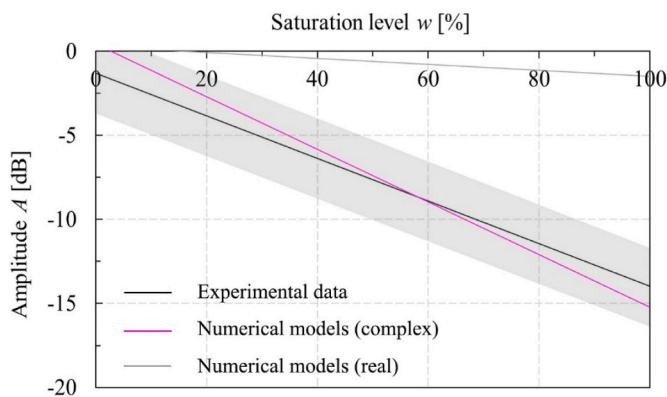**Fig. 6.** Flowchart of the modelling of the *C* specimen group.

Fig. 7. The normalized amplitude *A* as a function of the saturation level *w* (the shaded area corresponds to the prediction interval with 95% confidence for the experimental data).

deviations of the residuals to the fitted regression line of the experimental results, indicating prediction interval with 95% confidence for the experimental data.

When only the real part of the dielectric permittivity was considered, the model significantly underestimated the attenuation of the GPR signal. The results of the models that included the imaginary part of the dielectric permittivity and the frequency dependence are in the range of the experimental data, so that the models can describe the behaviour of the GPR signal in the presence of moisture better than the models that only take into account the real part of the dielectric permittivity.

Comparing the complex numerical models with the experimental data, the *A*-values from the laboratory tests were more negative than those from the numerical simulation in the range from *w* = 0% to *w* = 75–80%, which means that the numerical simulation slightly underestimated the attenuation in this range. A possible reason for this could be lower conductivity values, which were determined experimentally with the Wenner's probe and used as input parameters for the numerical modelling. This is because this non-destructive technique is based on measuring the electrical resistivity of concrete in near-surface areas. In general, the near-surface region may be drier than the inner part of the specimen, leading to higher electrical resistivity/lower conductivity values. The effect is less pronounced as the specimen approaches saturation.

The results of numerical modelling in which complex dielectric permittivity was modelled, agree well with the results of the experimental data. Consequently, the mechanisms that change the signal strength were thoroughly identified and described during modelling. These mechanisms are described in the following text.

To include the influence of relaxation mechanisms in the analysis, it is crucial to initially model the dielectric permittivity as a complex, frequency-dependent function. Among the various relaxation mechanisms, the dipolar polarization of water molecules is the most influential and is modelled in this study using the Debye function. The parameters of the function need to be carefully chosen to account for the effects of the restricted motion of water within the concrete pores. Consequently, the relaxation frequency of the pore water decreases compared to free

water, ensuring that the relaxation frequency of the composite material (i.e., concrete), represented by the peak value of the imaginary component, falls within the GPR operating frequency range (see Fig. 3).

Dipolar polarization, or orientational polarization, occurs when water molecules rotate in response to the applied electromagnetic field. The degree of rotation and polarization depends on frequency, with the inflection point being the relaxation frequency. Below the relaxation frequency, the dipoles follow the incident pulse. As the relaxation frequency is approached, polarization can no longer fully develop, resulting in energy loss in molecular collisions. The peak loss occurs at the resonant relaxation frequency, leading to the highest value of the imaginary component. Above the relaxation frequency, the molecules remain mainly undisturbed in the electromagnetic field. Thus, dipolar polarization becomes the dominant mechanism over other mechanisms (such as atomic or electronic) for the GPR, which operates at a centre frequency of 2.7 GHz. The second mechanism that changes the signal is the increased conductivity of the pore solution as the saturation level increases.

3.2. Modelling chloride effect

Fig. 8 shows the normalized amplitudes A, obtained using equation (9), as a function of saturation level (w) for various mean chloride concentrations in concrete cover, c. The concentrations were determined on concrete powder taken from laboratory specimens and analysed by potentiometric titration, giving the following results: 0.4%, 0.7%, 0.7%, 1.1%, 1.2%, 1.6%, 2%, and 3.1% of m_c.

The conclusion is that the "complex" modelling corresponds much better to the experimental data for the normalized amplitude A than the "real" modelling. For the majority of the specific chloride concentrations, the results of the numerical models (complex) are in the range of the experimental data.

The primary mechanisms responsible for the signal alteration in the presence of chloride ions in the pore water and bound in the cement matrix are dipolar polarization and conduction. The dipolar polarization is primarily due to the rotation of water molecules, and conduction is due to the presence of chloride ions dissolved in the water. Conduction occurs when free charge carriers, such as dissolved chloride ions, are affected by an incident electromagnetic pulse. When the pulse arrives, the charges begin to accelerate and generate currents. When the particles collide, the energy is dissipated and converted into heat.

Fig. 9 shows the functions of the normalized amplitudes A and A_1 as a function of the mean chloride concentration in the concrete cover, c, expressed as a percentage of the cement mass, m_c. The function of A_1 at a saturation level of 15–20 % is very close to the x-axis in the complex models, whereas it falls into the positive range in the real models and is
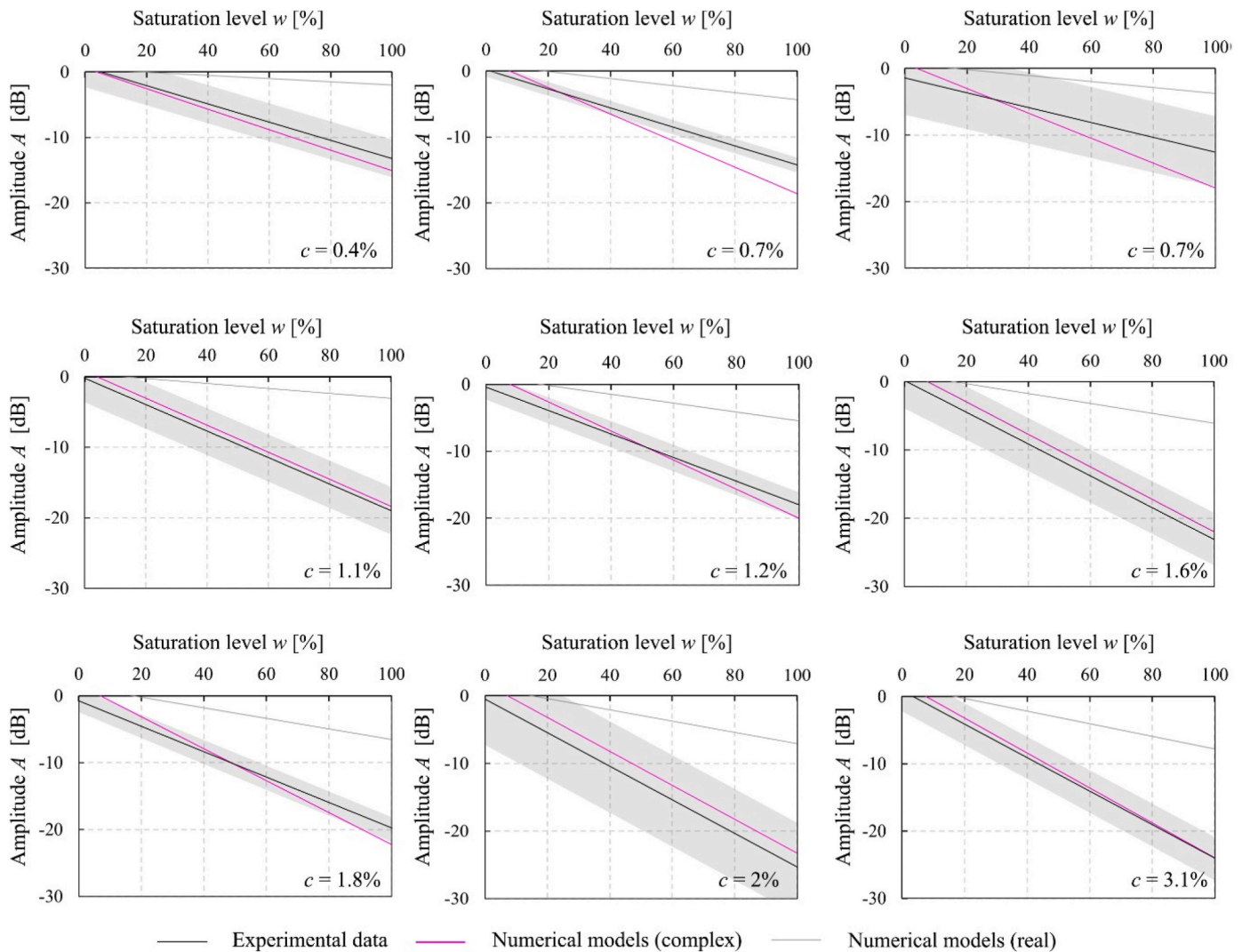

Fig. 8. The normalized amplitude A depending on the saturation level w for various mean chloride concentration in concrete cover (the shaded area corresponds to the prediction interval with 95% confidence for the experimental data).
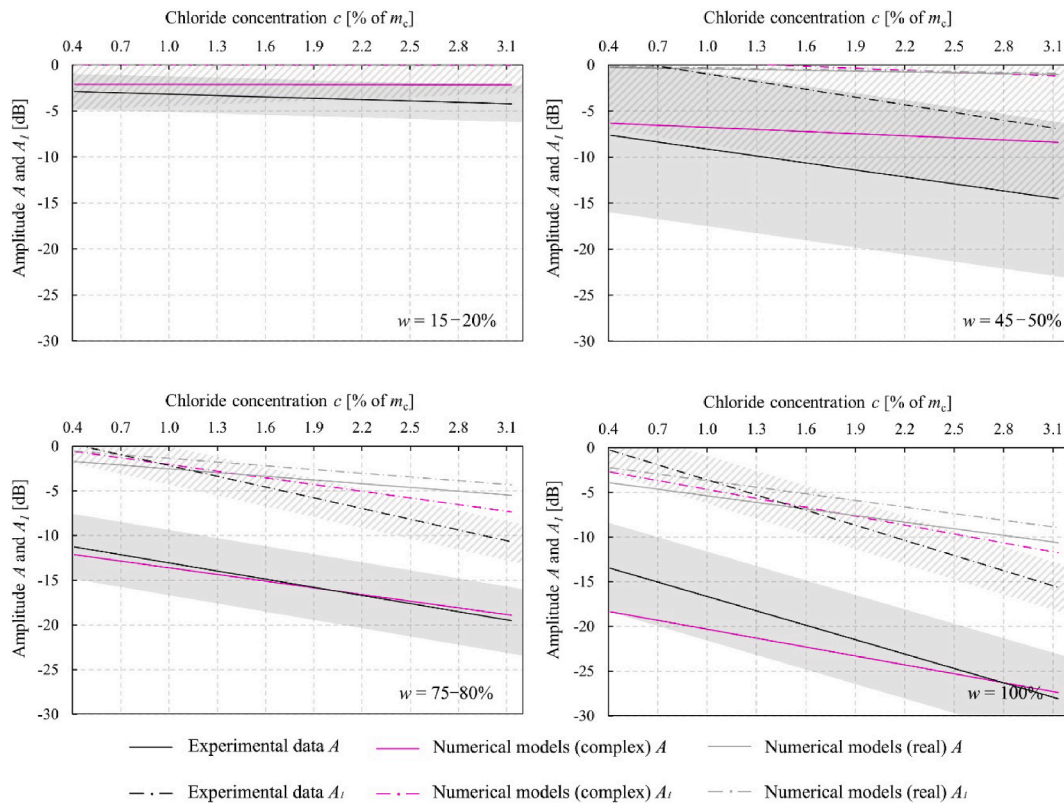
Fig. 9. The normalized amplitudes A and A_1 as a function of the mean chloride concentration in the concrete cover c (in % of m_c) for saturation levels of 15–20%, 45–50%, 75–80 % and 100% (the shaded area corresponds to the prediction interval with 95% confidence for the experimental data).

therefore not visible in the graph.

If the amplitudes are expressed by the normalized amplitude A (normalized to the specimen in the dry state), the combined effect of water and chlorides is quantified. In the numerical models (real), the imaginary part of the dielectric permittivity is not taken into account, so that the effect of water on the GPR amplitude is excluded. On the other hand, if the amplitudes are normalized to the specimens without chloride but with the same saturation level (A_1), the values only show the effect of the chlorides introduced in the modelling with the conductivity value σ. Since the same σ value was used for real and complex models, the A_1 functions for both modelling approaches are close to each other.

The functions for the numerical models (complex) agree well with the experimental data. The normalized amplitude A functions for the 75–80% saturation level showed nearly coincident functions. Although it falls within the range of the experimental results, the deviation of the A-function of the numerical models (complex) from the slope of the experimental data was observed for the saturation levels 15–20% and 45–50%. The deviation is particularly pronounced for specimens with mean chloride concentrations of 1.6% and 2% of m_c at $w = 45$–50%. In contrast, the deviation is not significant for the other specimens. This could be due to the same reason explained in the previous sections and related to the experimentally determined resistivity of the specimens. For the saturation level of 15–20%, the resistivity could not be measured with the Wenner probe because it indicated very high values, i.e. the conductivity went towards zero. Therefore, the input value for conductivity was zero for all numerical models in the saturation range of 15–20 %. Although the conductivity values are low as expected, they probably do not reach zero, so it is assumed that the losses due to conduction effects are omitted in this case. Furthermore, the experimental results showed the largest deviations for $w = 45$–50 %, which can be seen from the wide shaded area of the experimental data.

3.3. Modelling the effect of corrosion products

The normalized amplitude A as a function of corrosion-induced reinforcement mass loss, Δm for the laboratory specimens and for the numerical models is shown in Fig. 10. The numerical models where the corrosion products were modelled only with the respective real part of the dielectric properties are marked in grey as "numerical models (real)", while the models where the magnetic properties of the iron oxides were included are marked in magenta as "numerical models (complex)". The specimens without cracks were modelled with a layer of corrosion products around the reinforcement and concrete with pores filled with corrosion products radially around the reinforcement. In addition to the corrosion layer and the concrete pores with corrosion products, the analysis in the numerical simulations for the specimen with 1 mm crack (i.e., the specimen with the highest degree of corrosion) included three cases: I) crack filled with corrosion products (at height h) and air, II) crack filled with air, III) crack filled with corrosion products. Only the specimen with the highest corrosion degree ($\Delta m = 2.1\%$) showed a crack, Fig. 10. The concrete that did not contain corrosion products was modelled only with the real part of the dielectric permittivity and conductivity measured in the laboratory before the corrosion process. This means that the moisture conditions were not described with the complex dielectric permittivity of the concrete. This is because it is assumed that the moisture conditions have not changed compared to the condition before the corrosion process and that the normalisation procedure (equation (17)) cancels out the contribution of water to the amplitude changes. This section is divided into three sections, the first relating to mechanisms occurring in specimens without cracking, the second to specimens with cracking and the last to the discussion.

3.3.1. Without cracking

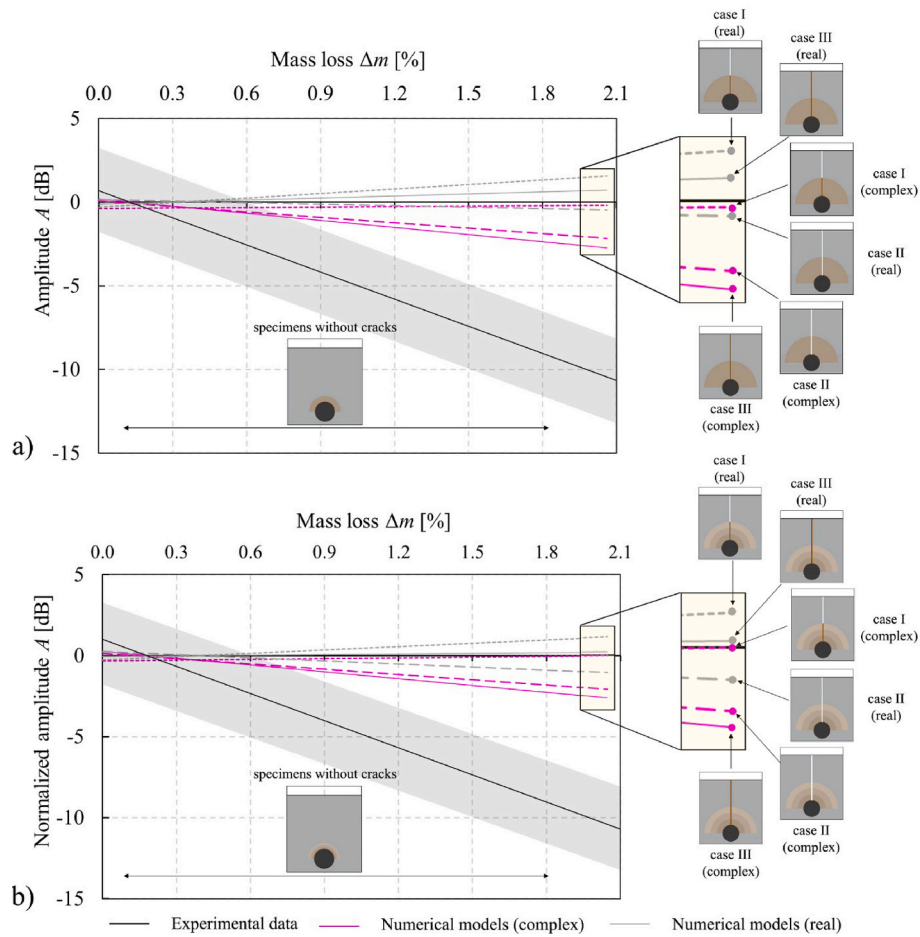The normalized amplitude A where the corrosion products did not

Fig. 10. Normalized amplitude A as a function of mass loss Δm for specimens I) with crack filled with corrosion products and air, II) with crack filled with air, III) with crack filled with corrosion products, for 'uniform' (top) and 'non-uniform' (bottom) distribution of corrosion products (the shaded area corresponds to the prediction interval with 95% confidence for the experimental data).

contain magnetic properties (numerical models (real)), shows predominantly positive values for specimens without crack. However, the A values are very close to zero, indicating that the amplitude does not change significantly with increasing mass loss due to corrosion.

If, on the other hand, the magnetic properties are taken into account, the normalized amplitude A shows a decreasing tendency with an increasing degree of corrosion compared to the initial state for specimens without cracks. The decreasing tendency of amplitude change was also observed from experimental data (Tesic et al., 2023).

Comparing the amplitude change for the specimens without cracks, with respect to uniform and non-uniform pore filling, the losses are higher for the uniform models, as expected, because the larger pore volume is filled with corrosion products. However, the magnitude of change is very comparable for the two different approaches. In fact, the largest difference in amplitude is only 2.7% between the 'uniform' and 'non-uniform' corrosion products propagation around the rebar. This is most likely due to the small volumetric contribution of the corrosion products to the total volume of the concrete, so their volumetric variation does not dramatically change the amplitude. This is more pronounced with low corrosion-induced mass losses and correspondingly low propagation heights h of the corrosion products in the concrete cover.

This reduction in amplitude can be attributed to three different processes.

First, there is a loss of amplitude due to the presence of corrosion products in the concrete pores. These products contribute to a reduction in amplitude and are directly proportional to the imaginary part of the complex dielectric permittivity of the corrosion products. This effect is evident in the specimens modelled in this work, as a transport of corrosion products into the concrete cover was observed. Secondly, the propagation of the wave through the thin layer of corrosion products that form around the rebar also contributes to the reduction in amplitude. Again, the reduction in amplitude is proportional to the imaginary part of the complex dielectric permittivity of the corrosion products.

Finally, additional amplitude loss can occur due to overlapping reflections at two interfaces: 1) between the concrete and the corrosion products and 2) between the corrosion products and the rebar. Since the real part of the dielectric permittivity of the corrosion products has a finite value, the reflection and transmission of the signal occur at the interface between the concrete and the corrosion products. Consequently, a portion of the energy is reflected while the remaining portion penetrates further into the specimen. Similarly, the second reflection occurs at the interface between the corrosion products and the reinforcement. Since the second reflection is delayed compared to the first, this delay results in a reduction of the total amplitude compared to the reflection from a non-corroded rebar.

3.3.2. With cracking

For the specimens with cracks, the value increases in cases I and III, while in case II the A value falls into the negative range of the numerical models (real). However, the tendency of the change does not correspond to the trend observed in the laboratory specimens.

Just like in the specimens without cracks, the 'uniform' and the 'non-uniform' distribution of the corrosion products are very close to each

other in the numerical models (complex) with cracks. Considering the effect of crack on the amplitude losses for the modelled specimens, ordered from lowest to highest loss, are: 1) crack filled with corrosion products and with air, 2) crack filled with air, 3) crack filled with corrosion products.

The normalized amplitude *A* in case I has a positive value. It is more likely that the predominant reflection is the one at the interface between air and corrosion products in the crack, which reduces the effect of reflection from the reinforcement. On the other hand, the losses are lower for the specimens whose crack is filled with corrosion products and air than for the specimens without a crack.

3.3.3. Discussion

From the discussion in the previous sections, it can be concluded that not taking into account the magnetic properties of iron oxides in the numerical modelling leads to insignificant changes in amplitude for the models without crack, while it causes an increasing amplitude in cases I and III and a slight decrease in the case II. This leads to the conclusion that numerical modelling that does not take into account the magnetic properties of iron oxides is not suitable for numerical GPR simulation for corrosion assessment.

In general, the decreasing trend of amplitude measured in concrete specimens with corroded reinforcement agrees with the values measured in the laboratory when the magnetic properties of iron oxides are taken into account. The function of the numerical models that is closest to the experimental results is the one where the crack of the specimen with the highest degree of corrosion was filled with corrosion products. However, the magnitude of change in the numerical simulations is less than in the laboratory specimens, which can be explained as follows.

- the corrosion-related micro-cracks filled with corrosion products contribute to the change in amplitude,
- the dielectric permittivity of the corrosion products is not well described.

In this work, only the corrosion products in the concrete pores and products penetrating into cracks were modelled. However, the corrosion-induced micro-cracks that could interconnect the pores of the concrete occur during corrosion propagation (Robuschi et al., 2021) and should also be modelled. The investigations have shown that the micro-cracks near the steel-concrete interface can be completely filled with corrosion products (Wong et al., 2010). These contribute to the loss of amplitude.

Secondly, the complex dielectric permittivity of the corrosion products used in the numerical models was taken from the literature. However, the composition of the iron oxides formed during laboratory-induced corrosion could be different from the modelled composition.

It should be noted that the distribution of corrosion products in the concrete cover in this work is simplified in terms of geometric distribution and the proportion of pores filled with corrosion products. The further models should be improved, including the more accurate distribution of corrosion products in the modelled specimens.

In this work, the geometry of the cracks was simplified in numerical models to a regular shape perpendicular to the concrete surface. However, the cracks are neither regular nor do they have a constant width through the concrete cover (Zhu et al., 2023b). The existing models should be improved with regard to a more faithful crack geometry, as this could influence the reflections.

When analysing the degree of filling of the corrosion products in the cracks, it was found that the case in which the crack is partially filled with corrosion products leads to the results that deviate the most from the experimental results. The reason for this could lie in the unfavourable distribution of the corrosion products in the crack. The investigations (Zhu et al., 2023a; Sola, 2017) have shown that the corrosion products are deposited at the edges of the cracks instead of

filling the crack to a certain level.

Looking at the two approaches for the distribution of the corrosion products, 'uniform' and 'non-uniform', it is concluded that the differences are small, most likely due to the small volumetric contribution of the corrosion products to the total volume of the concrete.

4. Conclusions

In this work, numerical simulations were carried out on the effects of moisture, chlorides, and corrosion products on the change in the strength of the GPR signal. For this purpose, the complex electrical and magnetic properties of concrete and corrosion products were modelled. The models considering only the real part of the dielectric properties were also included in the analysis. The analysis was based on the observation of the amplitude of the signal reflected from the reinforcement of the concrete specimen, and all the results obtained were compared with identically prepared specimens studied in laboratory experiments.

The following conclusion could be drawn.

- the models in which the dielectric permittivity of the concrete was modelled using the Complex Refractive Index Model, showed good agreement with the results obtained in the laboratory for the specimens where moisture and chlorides were studied.
- when analysing signal losses in wet concrete, the modelling of the imaginary part of the dielectric permittivity, which results from the relaxation mechanisms of water, is the decisive factor for the signal behaviour
- the magnetic properties of corrosion products contribute to the signal losses by migrating into the concrete cover or accumulating around the rebars
- when the corrosion products are modelled with the respective real part of the dielectric permittivity and the conductivity, it was found that the error can be large, also with respect to the trend of the amplitude change.

Three important points can be included in further research to improve the accuracy of models predicting GPR signal behaviour.

1) the microcracks and the corrosion products that penetrated into them should be included
2) the electrical and magnetic properties of the corrosion products should be determined as a function of the specific composition of the iron oxides, which mainly depends on the type of corrosion
3) the more complex geometry of the cracks should be modelled.

Funding

CRediT authorship contribution statement

Ksenija Tesic: Writing – original draft, Visualization, Software, Methodology, Investigation, Data curation, Conceptualization. **Ana Baricevic:** Writing – review & editing, Supervision, Methodology, Conceptualization. **Marijana Serdar:** Writing – review & editing, Project administration, Funding acquisition, Conceptualization. **Nenad Gucunski:** Writing – review & editing, Supervision.

Declaration of competing interest

The authors declare that they have no known competing financial

interests or personal relationships that could have appeared to influence the work reported in this paper.

Data availability

Data will be made available on request.

References

Abu Dabous, S., Yaghi, S., Alkass, S., Moselhi, O., 2017. Concrete bridge deck condition assessment using IR Thermography and Ground Penetrating Radar technologies. Autom. ConStruct. 81, 340–354. https://doi.org/10.1016/j.autcon.2017.04.006.

ACI Committee 228, 1998. Nondestructive Test Methods for Evaluation of Concrete in Structures. American Concrete Institute, Farmington Hills, MI. https://www.concrete.org/publications/internationalconcreteabstractsportal/m/details/id/5119. (Accessed 12 September 2023).

Ahmad, S., 2003. Reinforcement corrosion in concrete structures, its monitoring and service life prediction - a review. Cem. Concr. Compos. 25, 459–471. https://doi.org/10.1016/S0958-9465(02)00086-0.

Ahmed, H., La, H.M, Gucunski, N., 2020. Review of non-destructive civil infrastructure evaluation for bridges: state-of-the-art robotic platforms, sensors and algorithms. Sensors 20, 1–38. https://doi.org/10.3390/s20143954.

Alexander, M., Beushausen, H., 2019. Durability, service life prediction, and modelling for reinforced concrete structures – review and critique. Cement Concr. Res. 122, 17–29. https://doi.org/10.1016/j.cemconres.2019.04.018.

Balanis, C.A., 2012. Advanced Engineering Electromagnetics, second ed. Wiley, Hoboken, NJ, USA https://www.wiley.com/en-cn/Advanced+Engineering+Electromagnetics,+2nd+Edition-p-9781119213483.

Bertolini, L., Elsener, B., Pedeferri, P., Redaelli, E., Polder, R., 2013. Corrosion of Steel in Concrete: Prevention, Diagnosis, Repair, second ed. Wiley-VCH, Singapore. https://doi.org/10.1002/3527603379.

Beushausen, H., Torrent, R., Alexander, M.G., 2019. Performance-based approaches for concrete durability: state of the art and future research needs. Cement Concr. Res. 119, 11–20. https://doi.org/10.1016/j.cemconres.2019.01.003.

Bourdi, T., Rhazi, J.E., Boone, F., Ballivy, G., 2008. Application of Jonscher model for the characterization of the dielectric permittivity of concrete. J. Phys. D Appl. Phys. 41 https://doi.org/10.1088/0022-3727/41/20/205410.

Bourdi, T., Rhazi, J.E., Boone, F., Ballivy, G., 2012. Modelling dielectric-constant values of concrete: an aid to shielding effectiveness prediction and ground-penetrating radar wave technique interpretation. J. Phys. D Appl. Phys. 45 https://doi.org/10.1088/0022-3727/45/40/405401.

Cao, Y., Dong, S., Zheng, D., Wang, J., Zhang, X., Du, R., et al., 2017. Multifunctional inhibition based on layered double hydroxides to comprehensively control corrosion of carbon steel in concrete. Corrosion Sci. 126, 166–179. https://doi.org/10.1016/j.corsci.2017.06.026.

Cao, Q., Abufares, L., Al-Qadi, I., 2022. Development of a simulation-based approach for cold in-place recycled pavement moisture-content prediction using ground-penetrating radar. Transport. Res. Rec. 2676, 682–694. https://doi.org/10.1177/03611981221090933.

Cassidy, N.J., 2007. A review of practical numerical modelling methods for the advanced interpretation of ground-penetrating radar in near-surface environments. Near Surf. Geophys. 5, 5–21. https://doi.org/10.3997/1873-0604.2007003.

Cassidy, N.J., 2008. Frequency-dependent attenuation and velocity characteristics of nano-to-micro scale, lossy, magnetite-rich materials. Near Surf. Geophys. 6, 341–354. https://doi.org/10.3997/1873-0604.2008023.

Cassidy, N.J., 2009. Electrical and magnetic properties of rocks, soils and fluids. In: Jol, H.M. (Ed.), Gr. Penetrating Radar Theory Appl. Elsevier, Amsterdam, pp. 41–72. https://doi.org/10.1016/B978-0-444-53348-7.00002-8.

Cassidy, N.J., Millington, T.M., 2009. The application of finite-difference time-domain modelling for the assessment of GPR in magnetically lossy materials. J. Appl. Geophys. 67, 296–308. https://doi.org/10.1016/j.jappgeo.2008.09.009.

Chahine, K., Ihamouten, A., Baltazart, V., Villain, G., Derobert, X., 2010. On the variants of Jonscher's model for the electromagnetic characterization of concrete. In: Proc. XIII International Conf. Gr. Penetrating Radar. IEEE, pp. 9–14. https://doi.org/10.1109/ICGPR.2010.5550083.

Clem, D.J., Schumacher, T., Deshon, J.P., 2015. A consistent approach for processing and interpretation of data from concrete bridge members collected with a hand-held GPR device. Construct. Build. Mater. 86, 140–148. https://doi.org/10.1016/j.conbuildmat.2015.03.105.

Cole, K.S., Cole, R.H., 1941. Dispersion and absorption in dielectrics I. Alternating current characteristics. J. Chem. Phys. 9, 341–351. https://doi.org/10.1063/1.1750906.

Daniels, D.J., 2004. Ground Penetrating Radar, second ed. The Institution of Electrical Engineers, London, UK. https://doi.org/10.1049/PBRA015E.

Dérobert, X., Iaquinta, J., Klysz, G., Balayssac, J.P., 2008. Use of capacitive and GPR techniques for the non-destructive evaluation of cover concrete. NDT E Int. 41, 44–52. https://doi.org/10.1016/j.ndteint.2007.06.004.

Dérobert, X., Villain, G., Balayssac, J.P., 2018. Influence of concrete carbonation on electromagnetic permittivity measured by GPR and capacitive techniques. J. Environ. Eng. Geophys. 23, 443–456. https://doi.org/10.2113/JEEG23.4.443.

Dinh, K., Gucunski, N., 2021. Factors affecting the detectability of concrete delamination in GPR images. Construct. Build. Mater. 274 https://doi.org/10.1016/j.conbuildmat.2020.121837.

Drobiec, Ł., Jasiński, R., Mazur, W., 2019. Accuracy of eddy-current and radar methods used in reinforcement detection. Materials 12, 1168. https://doi.org/10.3390/ma12071168.

Fan, L., Bao, Y., Meng, W., Chen, G., 2019. In-situ monitoring of corrosion-induced expansion and mass loss of steel bar in steel fiber reinforced concrete using a distributed fiber optic sensor. Compos Part B Eng 165, 679–689. https://doi.org/10.1016/j.compositesb.2019.02.051.

Feng, D., Wang, X., Zhang, B., 2018. Specific evaluation of tunnel lining multi-defects by all-refined GPR simulation method using hybrid algorithm of FETD and FDTD. Construct. Build. Mater. 185, 220–229. https://doi.org/10.1016/j.conbuildmat.2018.07.039.

Furcas, F.E., Lothenbach, B., Isgor, O.B., Mundra, S., Zhang, Z., Angst, U.M., 2022. Solubility and speciation of iron in cementitious systems. Cement Concr. Res. 151, 106620 https://doi.org/10.1016/j.cemconres.2021.106620.

Giannakis, I., Giannopoulos, A., 2014. A novel piecewise linear recursive convolution approach for dispersive media using the finite-difference time-domain method. IEEE Trans. Antenn. Propag. 62, 2669–2678. https://doi.org/10.1109/TAP.2014.2308549.

Giannakis, I., Giannopoulos, A., Davidson, N., 2014. Realistic modelling of ground penetrating radar for landmine detection using FDTD. In: Proc 15th Int Conf Gr Penetrating Radar, GPR 2014. https://doi.org/10.1109/ICGPR.2014.6970568, 954–9.

Giannopoulos, A., 2005. Modelling ground penetrating radar by GprMax. Construct. Build. Mater. 19, 755–762. https://doi.org/10.1016/j.conbuildmat.2005.06.007.

Halabe, U.B., Maser, K., Kausel, E.A., 1989. Propagation characteristics of electromagnetic waves in concrete. In: Massachusetts Institute of Technology, Civil Engineering, Report No.: ARO 2462U.3. EG-UIR.

Halabe, U.B., Sotoodehnia, A., Maser, K.R., Kausel, E.A., 1993. Modeling of the electromagnetic properties of concrete. ACI Mater. J. 90, 552–563. https://doi.org/10.14359/4495.

Hong, S., Lai, W.W.-L., Wilsch, G., Helmerich, R., Helmerich, R., Günther, T., et al., 2014. Periodic mapping of reinforcement corrosion in intrusive chloride contaminated concrete with GPR. Construct. Build. Mater. 66, 671–684. https://doi.org/10.1016/j.conbuildmat.2014.06.019.

Hong, S., Chen, D., Dong, B., 2022. Numerical simulation and mechanism analysis of GPR-based reinforcement corrosion detection. Construct. Build. Mater. 317 https://doi.org/10.1016/j.conbuildmat.2021.125913.

Hugenschmidt, J., Loser, R., 2008. Detection of chlorides and moisture in concrete structures with ground penetrating radar. Mater. Struct. 41, 785–792. https://doi.org/10.1617/s11527-007-9282-5.

Jamali, A., Angst, U., Adey, B., Elsener, B., 2013. Modeling of corrosion-induced concrete cover cracking: a critical analysis. Construct. Build. Mater. 42, 225–237. https://doi.org/10.1016/j.conbuildmat.2013.01.019.

Jaufer, R.M., Ihamouten, A., Goyat, Y., Todkar, S.S., Guilbert, D., Assaf, A., et al., 2022. A preliminary numerical study to compare the physical method and machine learning methods applied to GPR data for underground utility network characterization. Rem. Sens. 14, 1047. https://doi.org/10.3390/rs14041047.

Kaplanvural, İ., Özkap, K., Pekşen, E., 2021. Influence of water content investigation on GPR wave attenuation for early age concrete in natural air-drying condition. Construct. Build. Mater. 297, 123783 https://doi.org/10.1016/j.conbuildmat.2021.123783.

Kim, S., Kang, J., Lee, S.H., Ahn, Y.H., 2016. Effect of chlorides on conductivity and dielectric constant in hardened cement mortar: NDT for durability evaluation. Adv. Mater. Sci. Eng. 2016 https://doi.org/10.1155/2016/6018476.

Klewe, T., Strangfeld, C., Kruschwitz, S., 2021. Review of moisture measurements in civil engineering with ground penetrating radar – applied methods and signal features. Construct. Build. Mater. 278, 122250 https://doi.org/10.1016/j.conbuildmat.2021.122250.

Klysz, G., Balayssac, J.P., Ferrières, X., 2008. Evaluation of dielectric properties of concrete by a numerical FDTD model of a GPR coupled antenna-Parametric study. NDT E Int. 41, 621–631. https://doi.org/10.1016/j.ndteint.2008.03.011.

Koch, G., Brongers, M.P., Thompson, N., Virmani, J., Payer, J., 1998. Corrosion Costs and Preventive Strategies in the United States. U.S. Department of Transport, Houston, TX, USA. http://impact.nace.org/documents/ccsupp.pdf. (Accessed 12 September 2023).

Korec, E., Jirásek, M., Wong, H.S., Martínez-Pañeda, E., 2023. A phase-field chemo-mechanical model for corrosion-induced cracking in reinforced concrete. Construct. Build. Mater. 393, 131964 https://doi.org/10.1016/j.conbuildmat.2023.131964.

Krysiński, L., Hugenschmidt, J, 2015. Effective GPR inspection procedures for construction materials and structures. In: Benedetto, A., Pajewski, L. (Eds.), Civ. Eng. Appl. Gr. Penetrating Radar. Springer, New York, USA, pp. 147–162. https://doi.org/10.1007/978-3-319-04813-0_6.

Lachowicz, J., Rucka, M., 2017. A concept of heterogeneous numerical model of concrete for GPR simulations. In: 2017 9th Int Work Adv Gr Penetrating Radar. IWAGPR 2017 - Proc, pp. 4–7. https://doi.org/10.1109/IWAGPR.2017.7996032.

Lachowicz, J., Rucka, M., 2019. A novel heterogeneous model of concrete for numerical modelling of ground penetrating radar. Construct. Build. Mater. 227, 116703 https://doi.org/10.1016/j.conbuildmat.2019.116703.

Lai, W.L., Kind, T., Wiggenhauser, H., 2011. Frequency-dependent dispersion of high-frequency ground penetrating radar wave in concrete. NDT E Int. 44, 267–273. https://doi.org/10.1016/j.ndteint.2010.12.004.

Lai, W.-L., Kind, T., Stoppel, M., Wiggenhauser, H., 2013. Measurement of accelerated steel corrosion in concrete using ground-penetrating radar and a modified half-cell potential method. J. Infrastruct. Syst. 19, 205–220. https://doi.org/10.1061/(ASCE)IS.1943-555X.0000083.

Lai, W.W.L., Dérobert, X., Annan, P., 2018. A review of ground penetrating radar application in civil engineering: a 30-year journey from locating and testing to imaging and diagnosis. NDT E Int. 96, 58–78. https://doi.org/10.1016/j.ndteint.2017.04.002.

Laurens, S., Balayssac, J.P., Rhazi, J., Arliguie, G., 2002. Influence of concrete relative humidity on the amplitude of Ground-Penetrating radar (GPR) signal. Mater. Struct. 35, 198–203. https://doi.org/10.1007/BF02533080.

Lei, J., Xue, B., Fang, H., Li, Y., Yang, M., 2020. Forward analysis of GPR for underground pipes using CUDA-implemented conformal symplectic euler algorithm. IEEE Access 8, 205590–205599. https://doi.org/10.1109/ACCESS.2020.3037811.

Liu, Y., Guo, L.X., 2016. FDTD investigation on GPR detecting of underground subsurface layers and buried objects. In: 2016 IEEE MTT-S Int Conf Numer Electromagn Multiphysics Model Optim NEMO, p. 2016. https://doi.org/10.1109/NEMO.2016.7561622.

Liu, H., Zhong, J., Ding, F., Meng, X., Liu, C., Cui, J., 2022. Detection of early-stage rebar corrosion using a polarimetric ground penetrating radar system. Construct. Build. Mater. 317, 125768 https://doi.org/10.1016/j.conbuildmat.2021.125768.

Majchrowska, S., Giannakis, I., Warren, C., Giannopoulos, A., 2021. Modelling arbitrary complex dielectric properties – an automated implementation for gprMax. In: 11th Int Work Adv Gr. Penetrating Radar, vol. 10. IWAGPR, Valleta, Malta.

McCann, D.M., Forde, M.C., 2001. Review of NDT methods in the assessment of concrete and masonry structures. NDT E Int. 34, 71–84. https://doi.org/10.1016/S0963-8695(00)00032-3.

Minasny, B., 2006. Microwave Dielectric Behavior of Wet Soils, vol. 133. https://doi.org/10.1016/j.geoderma.2005.08.001.

Núñez-Nieto, X., Solla, M., Novo, A., Lorenzo, H., 2014. Three-dimensional ground-penetrating radar methodologies for the characterization and volumetric reconstruction of underground tunneling. Comput. Chem. Eng. 71, 551–560. https://doi.org/10.1016/j.conbuildmat.2014.08.083.

Nürnberger, U., 2007. Corrosion of metals in contact with mineral building materials. In: Raupach, M., Elsener, B., Polder, R., Mietz, J. (Eds.), Corros. Reinf. Concr. Struct. Mech. Monit. Inhib. Rehabil. Tech. CRC Press LLC, Boca Raton, FL, USA. https://doi.org/10.1533/9781845692285.1.

Ogunsola, A., Reggiani, U., Sandrolini, L., 2006. Modelling shielding properties of concrete. In: 17th Int Zurich Symp Electromagn Compat 2006, pp. 34–37. https://doi.org/10.1109/emczur.2006.214862, 2006.

Omar, T., Nehdi, M.L., Zayed, T., 2017. Performance of NDT techniques in appraising condition of reinforced concrete bridge decks. J. Perform. Constr. Facil. 31 https://doi.org/10.1061/(asce)cf.1943-5509.0001098.

Owusu Twumasi, J., Yu, T., 2015. Forward and inverse dielectric modeling of oven-dried cement paste specimens in the frequency range of 1.02 GHz to 4.50 GHz. In: Proc. SPIE Smart Struct. Mater. + Nondestruct. Eval. Heal. Monit. Society of Photo-Optical Instrumentation Engineers (SPIE), San Diego, California, United States. https://doi.org/10.1117/12.2075672.

Pan, X., Shi, Z., Shi, C., Ling, T.C., Li, N., 2017. A review on concrete surface treatment Part I: types and mechanisms. Construct. Build. Mater. 132, 578–590. https://doi.org/10.1016/j.conbuildmat.2016.12.025.

Pashoutani, S., Zhu, J., 2020. Ground penetrating radar data processing for concrete bridge deck evaluation. J. Bridge Eng. 25 https://doi.org/10.1061/(ASCE)BE.1943-5592.0001566.

Polder, R., Andrade, C., Elsener, B., Vennesland, Ø., Gulikers, J., Weidert, R., et al., 2000. Test methods for on site measurement of resistivity of concrete. Mater. Struct. 33, 603–611. https://doi.org/10.1007/BF02480599.

Rehman, S.K.U., Ibrahim, Z., Memon, S.A., Jameel, M., 2016. Nondestructive test methods for concrete bridges: a review. Construct. Build. Mater. 107, 58–86. https://doi.org/10.1016/j.conbuildmat.2015.12.011.

Robuschi, S., Tengattini, A., Dijkstra, J., Fernandez, I., Lundgren, K., 2021. A closer look at corrosion of steel reinforcement bars in concrete using 3D neutron and X-ray computed tomography. Cement Concr. Res. 144, 106439 https://doi.org/10.1016/j.cemconres.2021.106439.

Sandrolini, L., Reggiani, U., Ogunsola, A., 2007. Modelling the electrical properties of concrete for shielding effectiveness prediction. J. Phys. D Appl. Phys. 40, 5366–5372. https://doi.org/10.1088/0022-3727/40/17/053.

Sbartaï, Z.M., Laurens, S., Balayssac, J.P., Ballivy, G., Arliguie, G., 2006. Effect of concrete moisture on radar signal amplitude. ACI Mater. J. 103, 419–426. https://doi.org/10.14359/18219.

Sbartaï, Z.M., Laurens, S., Rhazi, J., Balayssac, J.P., Arliguie, G., 2007. Using radar direct wave for concrete condition assessment: correlation with electrical resistivity. J. Appl. Geophys. 62, 361–374. https://doi.org/10.1016/j.jappgeo.2007.02.003.

Senin, S.F., Hamid, R., 2016. Ground penetrating radar wave attenuation models for estimation of moisture and chloride content in concrete slab. Construct. Build. Mater. 106, 659–669. https://doi.org/10.1016/j.conbuildmat.2015.12.156.

Sola, E., 2017. Experimental and Numerical Study of Chloride Induced Corrosion in Reinforced Concrete. Ph.D. Thesis. University of Stuttgart, Germany.

Sola, E., Ožbolt, J., Balabanić, G., Mir, Z.M., 2019. Experimental and numerical study of accelerated corrosion of steel reinforcement in concrete: transport of corrosion products. Cement Concr. Res. 120, 119–131. https://doi.org/10.1016/j.cemconres.2018.03.018.

Soldatov, S., Umminger, M., Heinzel, A., Link, G., Lepers, B., Jelonnek, J., 2016. Dielectric characterization of concrete at high temperatures. Cem. Concr. Compos. 73, 54–61. https://doi.org/10.1016/j.cemconcomp.2016.01.006.

Solla, M., Riveiro, B., Arias, P., Lorenzo, H., 2016. Introduction. In: Riveiro, B., Solla, M. (Eds.), Non-Destructive Tech. Eval. Struct. Infrastruct, first ed. CRC Press, London, pp. 3–6. https://doi.org/10.1201/b19024.

Song, H.W., Saraswathy, V., 2007. Corrosion monitoring of reinforced concrete structures - a review. Int. J. Electrochem. Sci. 2, 1–28. https://doi.org/10.1016/S1452-3981(23)17049-0.

Sossa, V., Pérez-Gracia, V., González-Drigo, R., Rasol, M.A., 2019. Lab non destructive test to analyze the effect of corrosion on ground penetrating radar scans. Rem. Sens. 11, 2814. https://doi.org/10.3390/rs11232814.

Stefanoni, M., Zhang, Z., Angst, U., Elsener, B., 2018. The kinetic competition between transport and oxidation of ferrous ions governs precipitation of corrosion products in carbonated concrete. RILEM Tech Lett 3, 8–16. https://doi.org/10.21809/rilemtechlett.2018.57.

Tešić, K., Baričević, A., Serdar, M., 2021a. Non-destructive corrosion inspection of reinforced concrete using ground-penetrating radar: a review. Materials 14, 975. https://doi.org/10.3390/ma14040975.

Tešić, K., Baričević, A., Serdar, M., 2021b. Comparison of cover meter and ground penetrating radar performance in structural health assessment: case studies. Gradjevinar 73, 1131–1144. https://doi.org/10.14256/JCE.3323.2021.

Tesic, K., Baricevic, A., Serdar, M., Gucunski, N., 2022. Characterization of ground penetrating radar signal during simulated corrosion of concrete reinforcement. Autom. ConStruct. 143, 104548 https://doi.org/10.1016/j.autcon.2022.104548.

Tesic, K., Baricevic, A., Serdar, M., Gucunski, N., 2023. Quantifying the impact of parameters of chloride-induced reinforcement corrosion on the GPR signal. Construct. Build. Mater. 399, 132594 https://doi.org/10.1016/j.conbuildmat.2023.132594.

Tsui, F., Matthews, S.L., 1997. Analytical modelling of the dielectric properties of concrete for subsurface radar applications. Construct. Build. Mater. 11, 149–161. https://doi.org/10.1016/S0950-0618(97)00033-0.

Warren, C., Giannopoulos, A., 2018. gprMax User Guide. https://docs.gprmax.com.

Warren, C., Giannopoulos, A., Giannakis, I., 2016. gprMax: open source software to simulate electromagnetic wave propagation for Ground Penetrating Radar. Comput. Phys. Commun. 209, 163–170. https://doi.org/10.1016/j.cpc.2016.08.020.

Wong, P.T.W., Lai, W.W.L., 2022. Characterization of complex dielectric permittivity of concrete by GPR numerical simulation and spectral analysis. J. Nondestr. Eval. 41, 1–15. https://doi.org/10.1007/s10921-021-00836-z.

Wong, H.S., Zhao, Y.X., Karimi, A.R., Buenfeld, N.R., Jin, W.L., 2010. On the penetration of corrosion products from reinforcing steel into concrete due to chloride-induced corrosion. Corrosion Sci. 52, 2469–2480. https://doi.org/10.1016/j.corsci.2010.03.025.

Wong, P.T.W., Lai, W.W.L., Sham, J.F.C., Poon, C., 2019. Hybrid non-destructive evaluation methods for characterizing chloride-induced corrosion in concrete. NDT E Int. 107 https://doi.org/10.1016/j.ndteint.2019.05.008.

Yee, K.S., 1966. Numerical solution of initial boundary value problems involving maxwell's equations in isotropic media. IEEE Trans. Antenn. Propag. 14, 302–307. https://doi.org/10.1109/TAP.1966.1138693.

Zadhoush, H., Giannopoulos, A., Giannakis, I., 2021. Optimising the complex refractive index model for estimating the permittivity of heterogeneous concrete models. Rem. Sens. 13, 723. https://doi.org/10.3390/rs13040723, 1–15.

Zhao, S., Al-Qadi, I., 2017. Pavement drainage pipe condition assessment by GPR image reconstruction using FDTD modeling. Construct. Build. Mater. 154, 1283–1293. https://doi.org/10.1016/j.conbuildmat.2017.06.103.

Zhao, Y., Ren, H., Dai, H., Jin, W., 2011. Composition and expansion coefficient of rust based on X-ray diffraction and thermal analysis. Corrosion Sci. 53, 1646–1658. https://doi.org/10.1016/j.corsci.2011.01.007.

Zhu, W., Yu, Z., Yang, C., Dong, F., Ren, Z., Zhang, K., 2023a. Spatial distribution of corrosion products influenced by the initial defects and corrosion-induced cracking of the concrete. J. Test. Eval. 51 https://doi.org/10.1520/JTE20220455.

Zhu, W., Yang, C., Yu, Z., Xiao, J., Xu, Y., 2023b. Impact of defects in steel-concrete interface on the corrosion-induced cracking propagation of the reinforced concrete. KSCE J. Civ. Eng. 27, 2621–2628. https://doi.org/10.1007/s12205-023-0458-5.